Physics Library
QC
1
.P5812
v.56
no.4

THE PHYSICAL REVIEW

VOLUME 56 | Second Series | NUMBER 4

AUGUST 15, 1939

Published for the

AMERICAN PHYSICAL SOCIETY

by the

AMERICAN INSTITUTE OF PHYSICS
Incorporated

LANCASTER, PA., AND NEW YORK, N. Y.

UNIVERSITY OF MICHIGAN LIBRARIES

THE PHYSICAL REVIEW

A journal of experimental and theoretical physics established by E. L. Nichols in 1893

Published by the American Institute of Physics for the

American Physical Society

OFFICERS

President

JOHN T. TATE
University of Minnesota
Minneapolis, Minnesota

Vice President

JOHN ZELENY
Yale University
New Haven, Connecticut

Secretary

W. L. SEVERINGHAUS
Columbia University
New York, New York

Treasurer

G. B. PEGRAM
Columbia University
New York, New York

Local Secretary for the Pacific Coast

PAUL KIRKPATRICK
Stanford University
California

Editor

JOHN T. TATE
University of Minnesota
Minneapolis, Minnesota

BOARD OF EDITORS

JOHN T. TATE, *Editor* J. W. BUCHTA, *Assistant Editor*

Associate Editors

K. T. BAINBRIDGE	A. L. HUGHES	W. BLEAKNEY
H. P. ROBERTSON	T. H. JOHNSON	G. BRIT
H. B. WAHLIN	F. A. JENKINS	D. M. DENNISON

Manuscripts for publication should be submitted to John T. Tate, University of Minnesota, Minneapolis, Minnesota.

Proof and all correspondence concerning papers in the process of publication, should be addressed to the Publications Manager, American Institute of Physics, 175 Fifth Avenue, New York, New York.

Subscription Price

United States and Possessions and Canada $15.00
Foreign $16.50

Back Numbers

Complete set: Series 2,[1] Vol. 1, 1913–Vol. 54, 1938—$990.00
Yearly rate: $16.50
Single copies: $1.50 each prior to July, 1929; $.75 each after July, 1929.

Subscriptions and orders for back numbers should be addressed to Prince and Lemon Streets, Lancaster, Pennsylvania, or to the American Institute of Physics, 175 Fifth Avenue, New York, New York.

Advertising is not accepted for the *Physical Review* but attention is called to the *Review of Scientific Instruments* and the *Journal of Applied Physics*, companion publications of the Institute, and media through which the field of physics can be reached most effectively. Rates and other information will be furnished on request.

Changes of address and complaints of failure to receive the *Physical Review* in the case of members of the American Physical Society, should be addressed to the Treasurer; in the case of other subscribers, to the Publications Manager. New copies can be sent free in response to complaints of non-delivery only if notice of non-delivery is received within three months of date of issue.

[1] For Series 1 inquire of Physics Department, Cornell University, Ithaca, N. Y.

The Physical Review is published semi-monthly at Prince and Lemon Streets, Lancaster, Pennsylvania.

Entered at the Post Office at Lancaster, Pennsylvania, as second class matter.

Acceptance for mailing at special rate of postage provided for in section 1103, Act of October 3, 1917, authorized September 6, 1926.

Physics
Physics-LSA
Johnson
10-10-63
Replace,

THE
PHYSICAL REVIEW

A Journal of Experimental and Theoretical Physics Established by E. L. Nichols in 1893

VOL. 56, NO. 4 AUGUST 15, 1939 SECOND SERIES

Induced Radioactivity in Cadmium and Indium

J. M. CORK AND J. L. LAWSON
University of Michigan, Ann Arbor, Michigan

(Received June 28, 1939)

The artificial activation of cadmium and indium now yields at least three radioactive isotopes of cadmium and eight radioactive isotopes of indium. The probable masses of several of these isotopes have been determined. In cadmium bombarded with deuterons two chain reactions are observed in which the active cadmium decays to radioactive indium. These are Cd (56 hour) to In (4.5 hour), and Cd (3.75 hour) to In (2.1 hour). Evidence is presented for believing that a new 65-hour gamma-radiation is due to an excited state of a normally stable indium isotope of mass 113. The energies and decay constants of many of the radiations have been accurately measured by means of a magnetic spectrometer of high resolving power.

INTRODUCTION

MANY investigations have now been carried out on the artificial activation of cadmium and indium. As shown in Table I there are eight known stable cadmium isotopes and two known stable isotopes of indium. The early experiments of Fermi[1] showed the production of certain activities by the radiative capture of neutrons. By bombarding these elements with deuterons,[2] fast neutrons,[3] gamma-rays,[4] protons[5] and alpha-particles, many other radioactive products have been observed. It is usually possible to assign each radioactivity to a particular isotope by studying its mode of production and the nature of its radiation.

[1] Amaldi, D'Agostino, Fermi, Pontecorvo, Rasetti and Segrè, Proc. Roy. Soc. **149**, 522 (1935).
[2] J. M. Cork and R. L. Thornton, Phys. Rev. **51**, 608 (1937); J. L. Lawson and J. M. Cork, Phys. Rev. **52**, 531 (1937).
[3] Pool, Cork and Thornton, Phys. Rev. **51**, 890 (1937); F. A. Heyn, Physica **4**, 160 (1937); Goldhaber, Szilard and Hill, Phys. Rev. **55**, 47 (1939).
[4] W. Bothe and W. Gentner, Naturwiss. **25**, 284 (1937); Chang, Goldhaber and Sagane, Nature **139**, 962 (1937).
[5] S. W. Barnes and P. W. Aradine, Phys. Rev. **55**, 50 (1939).

CADMIUM

In an earlier experiment by Cork and Thornton,[2] cadmium bombarded with deuterons was found to yield a cadmium radioactivity of peculiar behavior. The chemically separated cadmium was found to increase in activity for a short time before beginning to decay. This suggested the building up of a second radioactive material by a chain reaction. Subsequent chemical separations of indium from the cadmium showed such a daughter activity with a half-life reported as 2.3 hours building up from a radioactive cadmium parent of 58 hours half-life. Goldhaber[3] showed that if the subsequent indium separations were taken from the cadmium fifty or more hours after bombardment, the indium activity decayed with a half-life of not 2+ hours but 4+ hours. This latter is now a well-known period in indium attributed[6] to an excited state of In^{115*}. A further analysis of the chemically separated cadmium activity is shown in Fig. 1. The small circles along curve *A* are the experi-

[6] M. Goldhaber, Nature **142**, 521 (1938).

TABLE I. *Isotopes of cadmium and indium. Percentages of stable isotopes indicated by vertical figures and half-lives of radioactive isotopes by italic figures. Unassigned activities:* Cd (*3 minute*)? Cd (*40 day*).

At. Wt.	106	107	108	109	110	111	112	113	114	115	116	117	118
$_{47}$Ag		52.5	*2 min.*	47.5	*20 sec.*	*7.5 day*							
$_{48}$Cd	1.5		1.0		15.2	15.2	21.8	14.9	23.7	*56 hr.*	15.9	*3.75 hr.*	
$_{49}$In						*20 min.*	*72 sec.*	*65 hr.* 4.5	*56 day*	*4.5 hr.* 95.5	*13 sec.* *54 min.*	*2.1 hr.*	
$_{50}$Sn							1.1		0.8	0.4	15.5	9.1	22.5

mental points of the composite decay of the cadmium precipitate. If indium separations are made from the cadmium during the first few hours an activity of 2.1 hours half-life is predominant. After 20 hours such separations yield almost no 2.1-hour activity but a fairly pure activity of 4.5 hours half-life. This suggests a double chain reaction in which two active indium isotopes are built up from two active isotopes of cadmium.

The cadmium activity after many days shows a half-life of 40 days. If this 40-day period is subtracted from the composite activity an end-period of 56 hours half-life is observed. Now if it is assumed that this 56-hour cadmium is a parent activity in equilibrium with a 4.5-hour daughter indium, the activity of the former can be evaluated as shown in curve *B*, Fig. 1. The computed build-up of the 4.5-hour activity is shown in curve *C*, Fig. 1. These are both calculated on the assumption that the electrometer is equally sensitive to the radiations from both activities. If curves *B* and *C* are now subtracted, there is left the parent cadmium and daughter indium for the second chain reaction together with any other short period cadmium activity. Since the half-life of the daughter indium is known to be 2.1 hours it is possible by trial to find the half-life of the parent cadmium. The best value has been observed to be 3.75 ± 0.2 hours. Curves *D* and *E* of Fig. 1 show these components. If these resolved curves *B*, *C*, *D* and *E* are added to form curve *A*, a remarkably good agreement is obtained with the observed experimental points except at the very beginning. There is probably an additional cadmium activity of less than three minutes half-life. Since the chemical separation requires a minimum time of about 15 minutes this activity is very difficult to observe.

INDIUM

There are two stable isotopes of indium, their relative abundance being 4.5 percent and 95.5 percent for isotopes of mass 113 and 115, respectively. By various types of bombardment at least eight radioactive isotopes of indium have now been produced. There seems little question regarding the correctness of the assignment of certain of these activities to particular indium isotopes as previously reported.[2, 3] These are as follows: 20-minute positron to In^{111}, 72-second to In^{112}, 13-second and 54-minute to In^{116}, 50-day to In^{114} and 4.5-hour to In^{115*}. Recently the 4.5-hour activity has been studied in a magnetic spectrometer of high resolution.[7] Two monochromatic groups of electrons were observed. Since the experimental difference in energy of these groups corresponds to the difference between the *K* and *L* shell atomic binding energies in indium they were believed to be the internal conversion electrons ejected from the indium atoms by the passage of nuclear gamma-rays through the outer electrons. The energy of this gamma-radiation has thus been found to be very precisely 0.336 ± 0.001 Mev. This indium activity apparently is composed only of this internally converted gamma-ray, as no background of electrons having a continuous spectrum could be detected. The intensity of the sample was sufficiently strong that it is possible to assume at least twenty times as many gamma-ray transitions as beta-ray transitions from the 4.5-hour level. However there also appears to be an indium activity of several days half-life accompanying the 4.5-hour period. Apparently this activity is either built up from the decay of cadmium as a third chain reaction or from the

[7] J. L. Lawson, Phys. Rev. **56**, 131 (1939).

4.5-hour gamma-ray decay of the activated indium. The nature of its radiation has not yet been determined and it is impossible to assign it to a particular isotope.

The first indium precipitate from cadmium bombarded with deuterons shows an activity of 65 hours half-life. This was first revealed on the beta-ray spectrometer, since this activity seems to consist almost entirely of electrons due to internally converted gamma-rays. The spectral distribution is shown in Fig. 2. Perhaps not much faith can be placed in the smaller peaks, but the large ones have been substantiated by other sources. They indicate K and L electrons from converted gamma-rays of energies 0.170 and 0.245 Mev. The energy differences between these K and L electrons for the two gamma-rays are 24.0 and 23.4 kev, which agree well with values predicted from x-ray data for indium (23.6 kev). The general background of electrons having a continuous distribution is little more than would be expected from the 50-day activity which is always present. The 65-hour activity is also produced weakly in indium which is exposed to neutrons from lithium bombarded with deuterons. Because there seems to be no beta-radiation connected with the gamma-ray emission, and because the gamma-ray emission probably takes place in indium itself as revealed by the K and L conversion electron energy difference, it seems

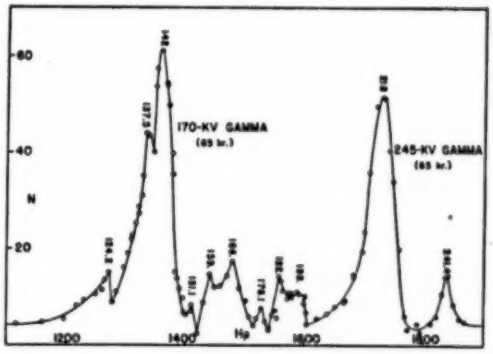

FIG. 2. Long period indium spectrum.

reasonable to assign the 65-hour activity to an excited state of a normally stable indium isotope, either In^{113*} or In^{115*}. S. W. Barnes[8] reports the production of this activity by a proton-neutron reaction, which would thus rule out the possibility of In^{115*}. The multiplicity of the gamma-rays may be due to various possible transitions from the excited state to the normal state.

A collection of the observed radioactivities produced in indium and cadmium is shown in Table II. The type of radiation, energy, method of observation and the mass of the most probable isotope responsible for the radiation has been included. In several cases the latter cannot be uniquely determined. Since in the first Cd-In-Sn

[8] S. W. Barnes, private communication.

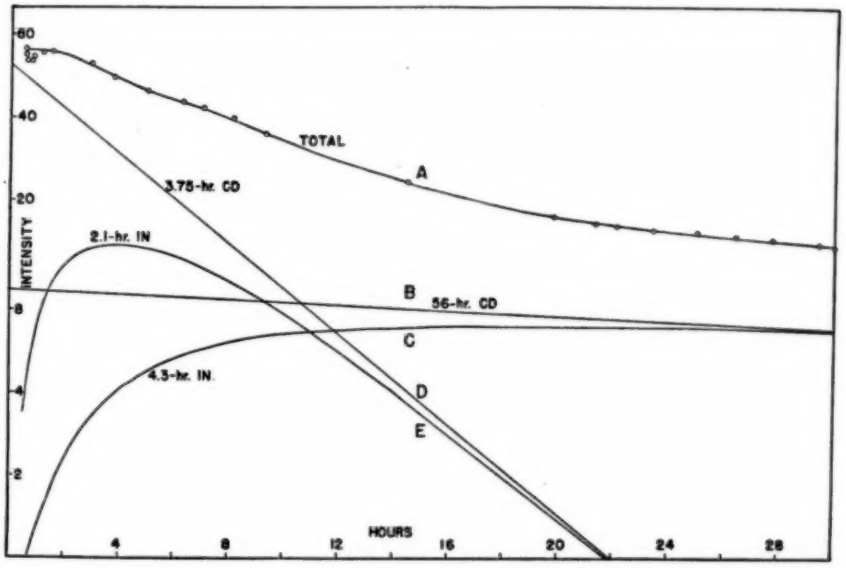

FIG. 1. Resolution of cadmium decay showing growth of two indium activities.

TABLE II. *Radioactive periods in cadmium and indium.*

ELEMENT	ACTIVITY	EMISSION	ENERGY Mv	PROBABLE ISOTOPE	METHOD
	3 min.(?)				
	3.75 hr.	Electron		117	
$_{48}$Cd	56 hr.	Electron Gamma	1.11 0.8	115	Mag. Spect. Cl. Cham.
	40 day	Electron Gamma	0.95		Cl. Cham.
	13 sec.	Electron Gamma	2.8	116	Cl. Cham.
	72 sec.	Electron		112	
	20 min.	Positron	2.15	111	Cl. Cham.
	54 min.	Electron Gamma	0.85 1.0, 1.3, 1.8	116	Mag. Spect. Cl. Cham.
$_{49}$In	2.1 hr.	Electron Gamma	1.73 0.388	117	Mag. Spect. Mag. Spect.
	4.5 hr.	Gamma	0.336	115	Mag. Spect.
	65 hr.	Gamma	0.170 0.245	113	Mag. Spect. Mag. Spect.
	56 day	Electron	1.75	114	Cl. Cham.

chain reaction the indium is associated with In^{115}, the 56-hour cadmium activity must be due to Cd^{115}. It would seem reasonable then to place the second chain reaction as due to isobars of mass 117, for there are no stable isotopes of either cadmium or indium having this mass. However, S. W. Barnes[8] has recovered from a radioactive tin of 100-day half-life, attributed to Sn^{113}, an active indium of 110-minute half-life. In this activity he observes the same gamma-ray as measured on our beta-ray spectrometer. Unless there are two activities in indium of half-lives nearly two hours, the parent cadmium in the second chain reaction of 3.75-hour half-life must be due to Cd^{113*}, that is, an excited state of normal stable cadmium of mass 113. Further tests on samples produced in other ways can answer this. The long period cadmium activity of

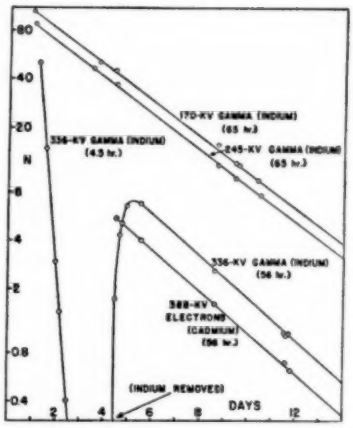

FIG. 3. Spectrometer decay curves.

40-day half-life emits negative electrons and hence might reasonably be due to an isomer of either 115 or 117.

The beta-ray spectrometer is a valuable instrument in determining half-life periods as well as energies of radiations. In Fig. 3 are shown certain decay curves taken with the spectrometer. The half-life of the 0.336-Mev gamma-radiation is shown to be 4.5 hours. The growth and subsequent decay of this same gamma-ray in equilibrium with the 56-hour cadmium activity definitely proves this chain reaction. The half-life for the decay of the two gamma-rays previously mentioned is also shown to be 65 hours. Because of the resolution of the spectrometer it has been possible to separate and study this activity whereas it is nearly impossible to make a good analysis by means of only an ionization chamber.

The chemical separations in this investigation have been performed by Mr. W. H. Sullivan. The work has been made possible by a grant from the Horace H. Rackham fund.

X-Ray Resonance Absorption Lines in the Argon *K* Spectrum

LYMAN G. PARRATT
Physics Department, Cornell University, Ithaca, New York
(Received June 23, 1939)

Recorded with a two-crystal vacuum spectrometer, the absorption curve for argon gas near the *K* absorption edge, 3866 x.u., is analyzed in terms of the main edge and the $1S \rightarrow nP$ $(n>3)$ series of resonance absorption lines. The main edge is determined uniquely as follows: the wave-length position is taken as at the series limit; the width is obtained from the measured width of the most intense absorption line; and the shape is given by the theoretical arctangent curve. The wave-length positions of all the resonance absorption lines are taken from the optical terms of potassium, and, with the width and shape of each line known, the various members of the series $1S \rightarrow nP$ are determined uniquely. The relative intensities of these lines are 100 : 34 : 18 : 8.5, etc. This analysis illustrates the type and completeness of the analysis we should like to make for solid absorbers, but, unfortunately, the definition and meaning of the main edge of a solid absorber are rather obscure.

THE existence of fine structure accompanying x-ray absorption edges has been known for some twenty years. The interpretation of this structure is that the electron may be removed to some one of the many outer energy levels. Each of these transitions has a characteristic probability and, of course, satisfies Bohr's frequency condition.

Most investigations of fine structure have been concerned with absorption edges of solid absorbers. Studies of the distribution of outer levels and the transition probabilities for a solid absorber are very complex. Considerable but somewhat limited progress has been made in these studies.[1] In the present note we shall interpret an absorption curve for the simplest type of absorber, a monatomic gas, and discuss the type of analysis that we should like to make for solid absorbers.

In a monatomic gaseous absorber the electron transition may be to any one of the unfilled atomic optical levels,[2] the transition obeying the usual selection rules,[3] or, with sufficient absorbed energy, the transfer may be to infinity. According to this interpretation, one expects fine structure on the long wave-length side of the main absorption edge for a monatomic gas and one expects the structure to consist of true resonance absorption lines of frequency separations and relative intensities predictable from spectral theory. Generally, the overlapping of absorption lines with themselves and with the main edge makes impossible an unambiguous recognition of the expected component structure. The experimental curve of the *K* absorption region for argon gas, however, is amenable to analysis. A study of the argon *K* edge was made in 1926 by Coster and van der Tuuk[4] with similar but less definitive conclusions than those of the present study.

With a two-crystal vacuum spectrometer[5] several absorption curves of the argon *K* region, wave-lengths near 3866 x.u., were recorded for each of several values of mass per unit area of the absorbing gas. For the precise study of each section of the curve between mass absorption coefficients μ_1 and μ_2, the optimal value of mass per unit area is

$$\rho x = \log_e (\mu_2/\mu_1)/(\mu_2-\mu_1),$$

where ρ is the density and x is the thickness for the maximum relative change in transmitted intensity. The average of these several curves is reproduced, the solid dots, in Fig. 1.

The first step in the analysis of the observed curve is a correction for the finite resolving power of the spectrometer. The calcite crystals used in the present work were perfect specimens

[1] For example, see A. E. Lindh, *Handbuch der Experimental Physik* (1930), XXIV 2. Teil, Chapter X; R. de L. Kronig, Zeits. f. Physik **75**, 191 (1932); and Beeman and Friedman, Phys. Rev. **55**, 1115(A) (1939).
[2] W. Kossel, Zeits. f. Physik **1**, 119 (1920).
[3] M. Siegbahn, Zeits. f. Physik **67**, 567 (1931).
[4] D. Coster and J. H. van der Tuuk, Zeits. f. Physik **37**, 367 (1926).
[5] This spectrometer has been previously described: L. G. Parratt, Phys. Rev. **54**, 99 (1938).

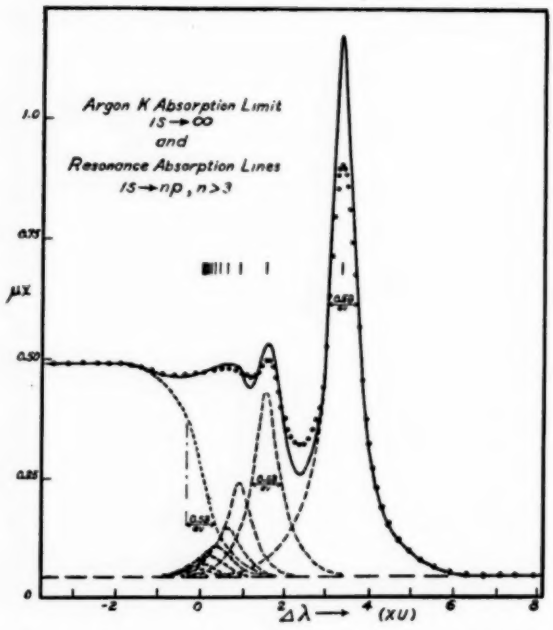

FIG. 1. Microscopic analysis of the absorption curve near the K edge for argon gas. The dots are observed values of absorption coefficients; the solid curve is corrected for finite resolving power; the broken curves represent the component structure: the main edge and resonance absorption lines.

of Class I,[6] and with such crystals the uncertainty in the correction is perhaps a minimum. We know that the observed width of the first sharp resonance absorption line is greater than the true width by the approximate amount[7] $2.9\times(0.34)^{1.7}=0.45$ x.u. This corrected width and the fact that the observed and corrected curves are not much different where the slope is constant or nearly constant serve as guides in our sketching of the corrected absorption curve, the solid line in Fig. 1. The most certain part of the somewhat arbitrarily corrected curve is the width of the most intense absorption line, 0.58 electron volt.

The electronic configuration of argon, $1s^2 2s^2 2p^6 3s^2 3p^6$, is altered in the absorption act by the removal of one of the $1s^2$ electrons to infinity or, with less absorbed energy, to an outer optical P level (if we neglect possible jj coupling between this electron and the inner electron hole). P levels are the only final levels allowed by the selection rules. (The distinction between the $P_{1/2}$ and $P_{3/2}$ levels is not significant because of their negligible separation.) So far as the outer levels are concerned the argon atom with a missing inner electron behaves approximately as a potassium atom. From the optical terms of potassium,[8] the various P level separations are: $4P\rightarrow 5P=1.44$ ev; $5P\rightarrow 6P=0.53$ ev; $6P\rightarrow 7P=0.25$ ev; etc., with the series limit at 2.71 ev from the $4P$ level. If we identify the first resonance line in the absorption curve with the transition $1S\rightarrow 4P$, the first transition allowed by the selection rules, we may represent the wave-length positions of the other absorption lines of the series $1S\rightarrow nP$ $(n>3)$ and of the series limit by the short vertical lines in the center of Fig. 1.

Before we attempt the resolution into component lines we must determine the background or the main absorption edge. By definition for a monatomic gaseous absorber, the center of the main K edge coincides in wave-length with the $1S\rightarrow nP$ series limit. The width of the main edge is equal to the width of the $1S\rightarrow 4P$ line, 0.58 ev, minus the width of the $4P$ state, according to an interpretation[9] of the theory of Weisskopf and Wigner.[10] Since the width of the $4P$ state is negligible compared with the $1S$ width we conclude that the width of the main edge is 0.58 ev. Furthermore, the theoretical shape of the main edge is given by an arctangent curve.[9] Then, with the position, width and shape known, the main edge is readily drawn as in Fig. 1. This analysis places the main edge at a wave-length position somewhat less, 3.5 to 4 x.u. in the present case, than its usually accepted measured value. In this connection we note that most measured wave-lengths of absorption edges are obtained with instruments of resolving power insufficient to reveal the absorption lines or to allow their proper interpretation.

Having thus determined the background, we proceed with the resolution into component resonance lines. By the same arguments as above, all these lines have the same shape and the same width, 0.58 ev. The component lines would be determined uniquely if their wave-length positions were known. The separations between the

[6] L. G. Parratt, Rev. Sci. Inst. **6**, 387 (1935).
[7] From Eq. (7) of reference 6.
[8] R. F. Bacher and S. Goudsmit, *Atomic Energy States* (McGraw-Hill, 1932), p. 245.
[9] Richtmyer, Barnes and Ramberg, Phys. Rev. **46**, 834 (1934).
[10] V. Weisskopf and E. Wigner, Zeits. f. Physik **63**, 54 (1930).

three most intense lines whose resolution is more or less obvious agree within experimental error with the predictions from the potassium term values: we conclude that our interpretation is correct and that the wave-length positions of all the lines are known. The components are readily sketched in the figure with the obvious additional criterion that the sum of the component ordinates at a given wave-length must equal the observed intensity. It is gratifying that all of the observed intensity is accounted for satisfactorily by component lines whose relative intensities decrease gradually to zero. The relative intensities of these lines are 100 : 34 : 18 : 8.5, etc.

It is of interest to note that the corrected width of an absorption line gives directly the width of the initial state if the final state width is negligible. Many solid absorbers have prominent and easily measurable absorption lines (sometimes called "white lines" in photographic studies) and, when applicable, this direct method of determining the width of a K or an L state may be very convenient.

In the absorption curve of a solid absorber we expect to find on the short wave-length side of the main edge resonance absorption lines more or less perturbed by overlapping wave functions from neighboring atoms. We also expect to find resonance absorption bands due to transitions to the allowed Brillouin energy bands.[11] The resolution of these resonance lines and bands into the component structure, which would yield very significant information about the solid, demands first a determination of the contour of the main edge. It is evident from the analysis of the argon curve and from the additional complications of the solid structure that the meaning of the main edge for a solid absorber is rather obscure.

[11] A typical absorption curve for a solid absorber, the L_{III} region for silver, is reproduced in Fig. 5 of reference 5.

AUGUST 15, 1939 PHYSICAL REVIEW VOLUME 56

Nuclear Energy Levels in B^{10} [1]

P. GERALD KRUGER, F. W. STALLMANN AND W. E. SHOUPP[2]
Department of Physics, University of Illinois, Urbana, Illinois.

(Received June 16, 1939)

Five thousand stereoscopic pictures of electron tracks in a cloud chamber yielded six hundred sixty-five Compton electrons from a thin mica foil and seventy-six ± electron pairs formed in the gas in the chamber. These data indicate thirty-one lines in the γ-ray spectrum of B^{10}. Nine energy levels account for the observed lines in a satisfactory manner, and are not in disagreement with the neutron spectrum from the same reaction. An attempt to correlate the observed energy levels with those predicted by theory leads to the following suggested classification: $^3S_1$ as the ground state (relative energy zero); $^3D_{123}$ at 0.26, 0.50 and 0.61 Mev; ^1S at 1.44 Mev; ^1D at 1.93 Mev; ^3D at 2.92 Mev; ^1D at 3.64 Mev; and ^3F at 4.73 Mev.

A PREVIOUS[3] examination of the γ-rays from B^{10} showed the presence of six γ-ray lines which could be correlated with the neutron data of Bonner and Brubaker.[4] However, the probable error in the lines reported was of the order of 0.1 Mev and the resolution of the method poor, so that it was impossible to say if more than six γ-ray lines were present. For that reason the experiment has been repeated under conditions which give better resolution and higher accuracy of the measurement of γ-ray energies.

There are two convenient ways of measuring γ-ray energies: the Compton recoil electron method and the ± electron pair production

[1] A preliminary report of part of these data was given at the Washington meeting of the American Physical Society, Phys. Rev. **55**, 1129(*A*) (1939).

[2] Fellow at the Westinghouse Research Laboratory since September 1938.

[3] P. G. Kruger and G. K. Green, Phys. Rev. **52**, 773 (1937).

[4] T. W. Bonner and W. M. Brubaker, Phys. Rev. **50**, 308 (1936).

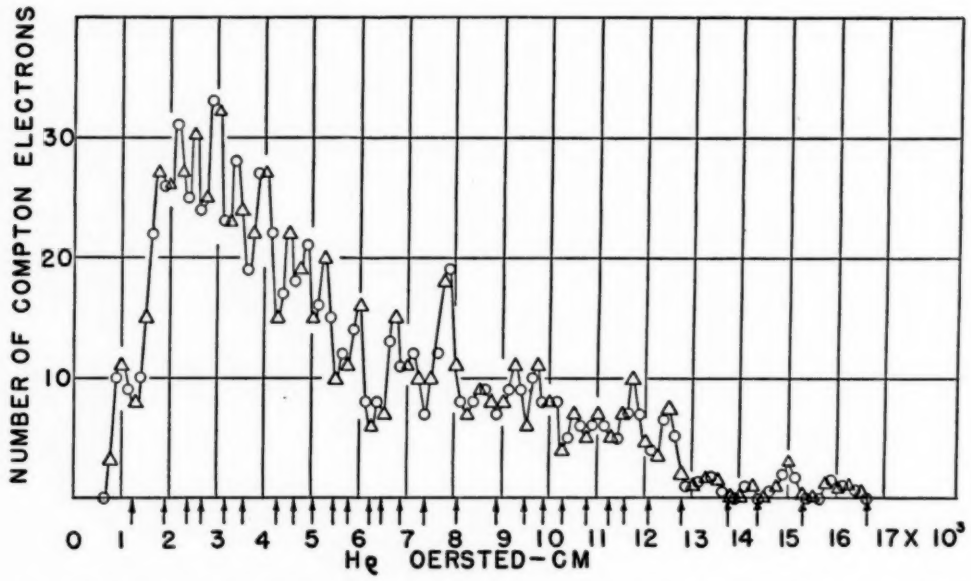

FIG. 1. Momentum distribution for Compton electrons ejected from a 50-mg/cm² mica foil by γ-rays from B^{10}.

method. Both have disadvantages. The Compton recoil method has the inherent disadvantage of straggling effects in the conversion foil, but must be used for γ-ray energies below 2 mc^2, and is best below 1.5 Mev unless the γ-ray lines are very intense. If a thin foil of material of large atomic number is used for ± electron pair production, there exists the same disadvantage of straggling. However, ± pair electrons produced in a gas do not suffer straggling and thus, a study of their energies will yield the most accurate results for γ-ray energies above 2 mc^2. With these ideas in mind both methods have been used to study the γ-rays of B^{10}. Below 1.16 Mev the Compton electron method has been used, whereas above 1.16 Mev the ± electron pair data are considered best, though the Compton data in that region agree with the ± electron pair data as well as can be expected.

Increased accuracy has been attained by taking stereoscopic pictures of the electron tracks and by carefully collimating the γ-ray beam. Stereoscopic pictures enable a more rigid selection of tracks, so that, in the case of Compton recoil electrons one can be sure that the electrons emerge in the forward direction within ±10° to the direction of the incident γ-rays and that both Compton electrons and ± pair electrons lie in the plane of the cloud chamber i.e., that the plane of the track is perpendicular to the magnetic field.

The collimation of the γ-ray beam was affected by placing a lead block six inches thick between the beryllium target and the cloud chamber and aligning a suitable hole in the lead block in such a way that the hole allowed free passage only to γ-rays which filled the solid angle subtended by the cloud chamber at the target. This prevents, to a large extent, the entrance of scattered γ-rays into the cloud chamber and together with the more rigid selection of tracks made possible by stereoscopic pictures, has greatly increased the resolving power of the method.

A rough consideration of the effects of small angle scattering on the path of an electron through a gas led to the conclusion that air was approximately the best gas to use in the chamber for the ± electron pair production method. Though the probability of ± electron pair production increases with Z^2 so does the small angle scattering. Thus the choice of a suitable gas must be made on the basis of selecting the gas which will give a satisfactory yield and not too much error due to scattering. Air meets these conditions well, the predicted probable error in the γ-ray energy from one ± electron pair measurement being about ±5 percent. Thus only a few pairs per γ-ray line must be observed in order to have γ-ray energies accurate to plus-

minus a few hundredths of a million electron volts.

The beryllium target, which was bombarded with 0.96 Mev deuterons, was placed in the end of the beam exit tube of the cyclotron. The cloud chamber was positioned so that its center was on a line perpendicular to the direction of incident deuterons. This allowed room to place a $2\frac{1}{2}''$ thick lead shield between the cloud chamber and the cyclotron chamber to reduce the background radiation from the cyclotron. The cloud chamber was 20 cm in diameter, 2.5 cm deep and was filled with air and alcohol vapor at atmospheric pressure. The Helmholtz coils gave a magnetic field of about 1500 oersteds which was constant over the sensitive volume of the cloud chamber to ± 0.5 percent. The Helmholtz coil current was read for every expansion and the magnetic field calculated for each track measured.

The Compton electrons were ejected from a 50-mg/cm^2 mica foil placed in the cloud chamber perpendicular to the line connecting the Be target and the chamber center.

For measuring the tracks, their stereoscopic images were projected, by the optical system used during photography, on a fine ground glass screen which could be clamped in place once the track images were in coincidence. The radii of curvature were measured by a special measuring engine built for the purpose. The engine was built so that three points could be brought in coincidence with the circular track and the length of the chord defined by the two end-points as well as the sagitta read off directly. From these data the radius is readily calculated. The accuracy of measurement of the engine was checked by measuring circles of known radii of curvature. The result showed that the readings are reliable to less than ± 0.5 percent.

The momentum distribution of the six hundred sixty-five Compton recoil electrons is shown in Fig. 1. There each circle represents the number of electrons observed in $H\rho$ intervals of 250 oersted-cm. The triangles represent the number of electrons in $H\rho$ intervals of the same size but overlapping the first set by $H\rho = 125$ oersted-cm.

TABLE I. *Gamma-ray lines in the* B^{10} *spectrum.*

$H\rho$ oersted cm	E_C Mev	E_p Mev	Relative Intensity	E_{calc} Mev	Transition		
1,250	0.25		60	0.24 & 0.26	B_2-B_1	B_1-A	
1,900	0.41		120	0.49 & 0.35		$D-C$	B_3-B_1
2,400	0.55		160	0.50		B_2-A	
2,700	0.63		130	0.61		B_3-A	
3,200	0.77		160	0.72		$F-E$	
3,600	0.89		140	0.94		$C-B_2$	
4,300	1.08		170	1.09 & 0.99		$G-F$	$E-D$
4,650	1.19	1.16	120	1.18		$C-B_1$	
5,050	1.31	1.33	120	1.32		$D-B_3$	
5,500	1.44	1.43	100	1.48, 1.43 & 1.44	$E-C$	$D-B_2$	$C-A$
5,800	1.52	1.57	35				
6,250	1.66	1.68	70	1.67		$D-B_1$	
6,500 6,900	1.74 1.85	1.80	70	1.81 & 1.71		$G-E$	$F-D$
7,400	1.99	1.91 2.11	25 20	1.93		$D-A$	
8,100	2.20	2.24	8	2.20		$F-C$	
		2.31	20	2.31		$E-B_3$	
8,900	2.44	2.45	40	2.42		$E-B_2$	
9,500	2.63	2.64	40	2.66		$E-B_1$	
9,900	2.74	2.78	30	2.80		$G-D$	
10,300	2.89	2.91	30	2.92		$E-A$	
10,800	3.01	3.00	22	3.03		$F-B_3$	
11,300	3.15		20	3.14		$F-B_2$	
11,600	3.25	3.25	4	3.29		$G-C$	
12,100	3.40	3.38	50	3.38		$F-B_1$	
12,800	3.62	3.66	40	3.64		$F-A$	
13,800	3.92	3.90	10				
14,400	4.12	4.15	4	4.12		$G-B_3$	
		4.24	1	4.23		$G-B_2$	
15,300	4.35	4.46	12	4.47		$G-B_1$	
16,600	4.74	4.71	7	4.73		$G-A$	

TABLE II. *Gamma-ray energies as deduced from the measurements on ± electron pairs formed in an air-filled cloud chamber.*

Below are listed the $h\nu$ values in Mev corresponding to each pair observed.

	1.120	1.307	1.427	1.545	1.639	1.792	1.911	2.134	2.242	2.320	2.424	2.613	2.770
	1.157	1.339	1.420	1.584	1.679	1.826	1.903	2.078		2.316	2.480	2.671	2.786
	1.190	1.308	1.446	1.596	1.685	1.848				2.283		2.626	
	1.145	1.273	1.467	1.538	1.674	1.749				2.300			
	1.124	1.350	1.402		1.704					2.343			
	1.191	1.378	1.417										
	1.164	1.339	1.413										
	1.176	1.355											
		1.313											
		1.320											
No of pr. per line	8	10	7	4	5	4	2	2	1	5	2	3	2
Average value of $h\nu$	1.158	1.328	1.427	1.566	1.676	1.804	1.907	2.106	2.242	2.312	2.452	2.637	2.778
Diff. between extreme $h\nu$ values per line	0.071	0.105	0.065	0.058	0.065	0.099	0.008	0.056		0.060	0.056	0.058	0.016
	2.910	3.004	3.263	3.355	3.622	3.864	4.127	4.238	4.395	4.648	5.478	6.064	6.481
	2.918		3.241	3.412	3.700	3.930	4.175		4.513	4.704			
							4.139		4.481	4.770			
No. of pr. per line	2	1	2	2	2	2	3	1	3	3			
Average value of $h\nu$	2.914	3.004	3.252	3.383	3.661	3.897	4.147	4.238	4.463	4.707			
Diff. between extreme $h\nu$ values per line	0.008		0.022	0.057	0.078	0.066	0.048		0.118	0.122			

The minima[3] between peaks give the $H\rho$ values for the γ-ray lines and are indicated in Fig. 1 with arrows. The corresponding values are listed in Table I, column one, and are used to calculate the γ-ray energies with the formula:

$$h\nu_\gamma = mc^2\left[\frac{1+(1+A^2)^{\frac{1}{2}}}{2A} - \frac{1}{2}\right],$$

where $$A = mc^2/eH\rho.$$

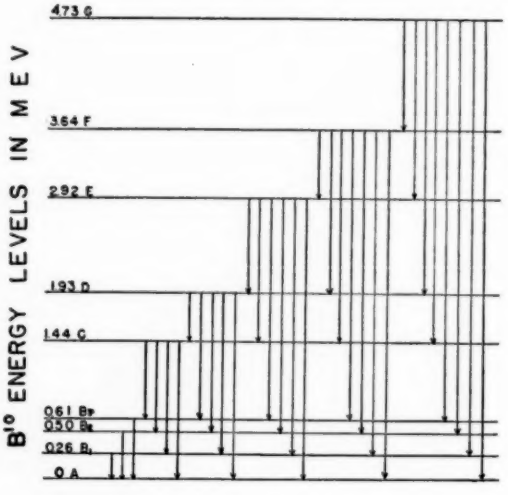

FIG. 2. Nuclear energy levels in B^{10}. Gamma-ray energies used in developing this term system have been obtained from measurements on ± pair electrons for gamma-ray energies larger than 1.16 Mev. Below 1.16 Mev the measurements from Compton electron have been used.

The energies of the γ-rays, thus calculated, are given in column two (E_C) of Table I.

The energy of a γ-ray which produces a ± electron pair is given by $h\nu_\gamma = 2mc^2 + KE^- + KE^+$, where

$$KE^\pm = mc^2[(B^2+1)^{\frac{1}{2}} - 1]$$

and

$$B = H\rho e/mc^2.$$

The γ-ray energies corresponding to the seventy-six observed pairs which represent twenty-three γ-rays of energy above 1.16 Mev are given in Table II. As the tabulation shows, the energy spread for any one γ-ray line is approximately 0.06 Mev. In most cases this is less than the expected spread of ±5 percent due to small angle scattering. The discrepancy may be explained partly by the careful selection of tracks. The average values of the γ-ray lines in Table II are listed for comparison in column three (E_p) of Table I.

From the observed thirty-one γ-ray lines the energy level system shown in Fig. 2 has been deduced. For comparison with the observed γ-ray energies, the differences between the energy levels are tabulated in column five of Table I. Four lines have been used twice and one line three times but this represents no difficulty since the lines calculated from the term system are so nearly alike that they could not be resolved by the present method. This is particularly true in

the low energy region where the energy values depend on Compton electrons. Line 1.80 Mev may be double with values 1.77 Mev and 1.84 Mev as can be seen by examining the pair energies for this line in Table II. Arbitrary term designations A, B_1, B_2, B_3, C, D, E, F, G, have been given the energy levels in Fig. 2. The corresponding transitions for the lines are given in column six of Table I.

All but three lines (1.57, 2.11, and 3.90 Mev) of Table I have been used. Here it is to be noted that lines 1.57 Mev and 2.11 Mev have a sum equal to 3.68 Mev which is near the term value 3.64 Mev. This may indicate another level at 1.57 Mev or 2.11 Mev. There is no indication of a possible place for the line 3.90 Mev.

The intensities of the lines given in column four of Table I are the average of the intensities as deduced from the Compton electrons and the $\pm$ pair electron. To get the intensities from the Compton electrons the curve in Fig. 1 was reduced according to the process previously described.[3] The relative intensity of the lines as deduced from $\pm$ electron pairs was obtained by taking into account the probability of pair production at various energies.

If the term system in Fig. 2 is correct there should be evidence for more neutron groups from this reaction

$$\left[\begin{array}{l} {}_4Be^9+{}_1D^2\rightarrow{}_5B^{11}\rightarrow{}_5B^{*10}+{}_0n^1 \\ \qquad\qquad {}_5B^{*10}\rightarrow{}_5B^{10}+\gamma \end{array}\right]$$

than were reported by Bonner and Brubaker.[4]

TABLE III. *Intensity correlation between the neutron spectrum and the γ-ray spectrum.*

TERM	*A* Σ γ-RAY INTENSITY OUT OF LEVEL	*B* Σ γ-RAY INTENSITY INTO LEVEL	*C* NEUTRON POPULATION	$\frac{B+C}{A}$
F	335	85	320	$\frac{405}{335}=1.2$
E	225	195	55	$\frac{250}{225}=1.1$
D	405	150	170	$\frac{320}{405}=0.8$
C	280	140	120	$\frac{260}{280}=0.9$
B	350	770	640	$\frac{1410}{350}=4.0$

Such evidence is found in the excellent results of Staub and Stephens.[5] Their curves* (Figs. 1 and 2) are shown in Fig. 3 after being redrawn slightly.

By assuming $Q=4.18$ Mev and the values of the energy levels as deduced from our γ-rays (Fig. 2), the energy of the neutron groups which should be observed for Staub and Stephens' energy of incident deuterons, can be calculated. The position of these neutron groups is shown by the arrows along the energy axis in Fig. 3. It is seen that all of the predicted groups which can be resolved are present, though the position of the groups does not agree well with the predicted

[5] H. Staub and W. E. Stephens, Phys. Rev. **55**, 131 (1939).

* The authors wish to express their thanks to Dr. W. E. Stephens for making the original data for these curves available to them.

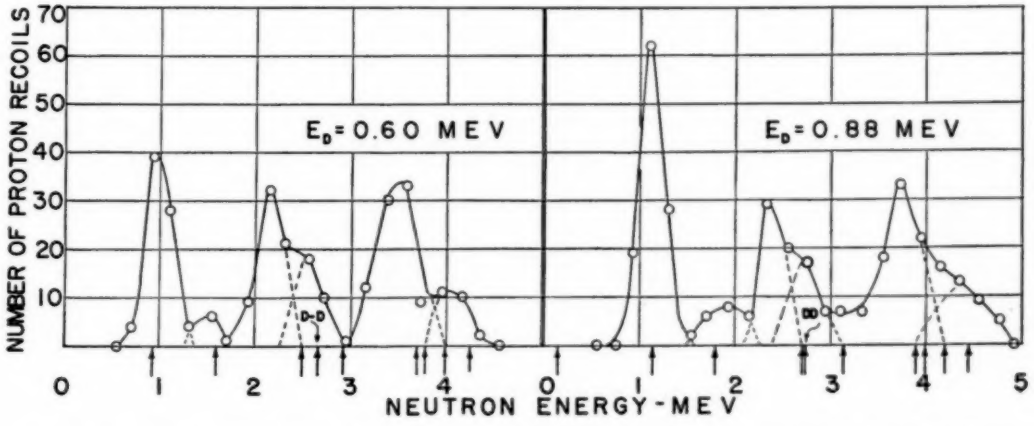

FIG. 3. Neutron spectrum from the reaction ${}_4Be^9+{}_1D^2\rightarrow{}_5B^{10}+{}_0n'$ for two energies of incident deuterons (0.60 and 0.88 Mev). Data from Staub and Stephens.

position. This may be due to errors in the range energy curve, stopping power values, or inadequate corrections.

Staub and Stephens expressed the view that the neutron group at approximately 3.00 Mev was due to D−D contamination neutrons. This can hardly be true in view of the fact that the intensity ratio of the two neutron peaks at approximately 2.50 Mev and 3.00 Mev for the two energies of incident deuterons (0.6 and 0.88 Mev) remains nearly constant whereas the excitation functions for the two reactions vary greatly for the two energies. Moreover, the position of the D−D neutron group, indicated by the arrows marked D−D in Fig. 3, and calculated for their energy of incident deuteron does not fit the 3.00 Mev peak. Thus, it seems clear that the D−D contamination neutrons cannot be present in their experiment in large numbers, and that the 3.00 Mev peak really corresponds to neutrons leaving the B^{10} nucleus in the 1.44 Mev level.

Now it is possible to obtain the areas under the neutron peaks and thus get an idea of the initial neutron population of the levels and to compare that with the observed γ-ray intensities. The intensity check which should be observed is

$$\frac{(\Sigma\gamma\text{-ray intensities}+\Sigma\text{ neutron population})_{in}}{(\Sigma\gamma\text{-ray intensities})_{out}}=1.$$

The results are shown in Table III. The agreement is good except for the B level and the discrepancy there is due to the low intensity of lines 0.63, 0.55 and 0.25 Mev. It is possible that these lines obtained much too low an intensity due to successive subtraction of straggling tails from the peaks at higher energy during the reduction process of the curve in Fig. 1.

Feenberg and Wigner,[6] and Feenberg and Phillips[7] have made theoretical calculations concerning the type and position of terms in the B^{10} nucleus. An attempted correlation between the theoretical levels and the observed levels leads to the following: A, B_1, B_2, B_3, C, D, E, F, G are, respectively, $^3S_1$; $^3D_1$, $^3D_2$, $^3D_3$, $^1S_0$; $^1D_2$; ^3D; ^1D and ^3F. This gives a ratio

$$\frac{\text{calculated sing.-trip. splitting}}{\text{observed sing.-trip. splitting}}\cong 2.3,$$

which is fairly constant for the suggested classification.

It is impossible to make a further check on the classification at this time by using the intensities of the various lines. Many more pairs and Compton electrons will need to be observed before the intensities are sufficiently accurate for such a check.

The authors wish to express their thanks to Professor R. Serber for many helpful discussions.

[6] E. Feenberg and E. Wigner, Phys. Rev. **51**, 95 (1937).
[7] E. Feenberg and M. Phillips, Phys. Rev. **51**, 597 (1937).

Nuclear Spin and Magnetic Moment of $_{13}Al^{27}$*

S. MILLMAN AND P. KUSCH
Columbia University, New York, New York

(Received June 19, 1939)

The molecular beam magnetic resonance method has been applied to a determination of the gyromagnetic properties of the Al^{27} nucleus. The observed gyromagnetic ratio is 1.451 ± 0.004 in units of $e/2Mc$. A comparison of this ratio with that obtained from the hyperfine splitting of several aluminum lines for various assumed values of the spin of Al^{27} fixes the spin of this nucleus as 5/2. The value of the magnetic moment is then found to be 3.628 ± 0.010 nuclear magnetons. The sign of the moment is experimentally determined to be positive.

THE h.f.s. of aluminum has been the subject of several investigations which lead to discordant values for the nuclear spin of Al^{27} but yield values for the nuclear magnetic moment which are in agreement within the capabilities of the Goudsmit, Fermi-Segrè (G. F. S.) formula. Jackson and Kuhn[1] have investigated the h.f.s. of the resonance lines of Al I in absorption. From measurements of the relative intensities of the two resolved components of the line $3^2P_{1/2}-3^2D_{3/2}$ they conclude that the spin of Al^{27} is 9/2. From an analysis of the three resolved h.f.s. components of the $3^2P_{1/2}-4^2S_{1/2}$ line the same investigators obtain the hyperfine splitting of the $3^2P_{1/2}$ and $4^2S_{1/2}$ states. For an assumed spin of 9/2 the Goudsmit formula yields 3.6 and 4.1 nuclear magnetons as the magnetic moment of Al^{27}, when applied to the two observed splittings, respectively. Heyden and Ritschl[2] have observed the h.f.s. of several lines of Al II and by use of the interval rule find the spin of Al^{27} to be 5/2. Their data also furnish a measure of the h.f.s. of the $3s\ ^2S_{1/2}$ state of Al III from which they deduce a moment of 3.7 nuclear magnetons by use of the Fermi-Segrè formula.

We have applied the molecular beam magnetic resonance method[3] to a study of the nuclear gyromagnetic properties of Al^{27}. In order to obtain a molecular beam containing aluminum and detectable by the surface ionization method it is necessary that the molecule issuing from the oven contain an alkali atom as well as aluminum. The double salts $NaCl\cdot AlCl_3$ and $KCl\cdot AlCl_3$ were found to be suitable for our purposes. At temperatures of about 600°K these molecules show practically no dissociation and have vapor pressures sufficiently high to give workable beams.

Following the procedure discussed in earlier papers[3] three resonance curves were observed common to the two compounds used. Two of the curves are due to Cl^{35} and Cl^{37}, whose nuclear g's have already been reported[4] and are the same as those observed in such simple compounds as LiCl and RbCl. Since aluminum is the only other common constituent of the two molecules investigated and since the observed effect is much too large to be attributed to any impurities in the compounds used, the third resonance minimum must be attributed to the Al^{27} nucleus. A typical aluminum resonance curve is shown in Fig. 1. The nuclear g value, obtained from the ratio of the oscillating frequency to the magnetic field at resonance, is 1.451 ± 0.004 in units of $e/2Mc$, when referred to the nuclear g of Li^7 as standard.[3]

In order to obtain the nuclear magnetic moment from the observed g value it is necessary to know the nuclear spin. Our method does not measure spin directly. However, in cases where the total hyperfine splitting of an atomic energy state is known our independent g measurements may serve as a deciding factor in fixing the nuclear spin.

When a nuclear moment is calculated by means of the G. F. S. formula from the experimentally determined splitting of an atomic energy state the result is not particularly sensitive to the

* Publication assisted by the Ernest Kempton Adams Fund for Physical Research of Columbia University.

[1] D. A. Jackson and H. Kuhn, Proc. Roy. Soc. **A164**, 48 (1938).

[2] M. Heyden and R. Ritschl, Zeits. f. Physik **108**, 739 (1938).

[3] I. I. Rabi, S. Millman, P. Kusch and J. R. Zacharias, Phys. Rev. **55**, 526 (1939).

[4] P. Kusch and S. Millman, Phys. Rev. **55**, 680 (1939).

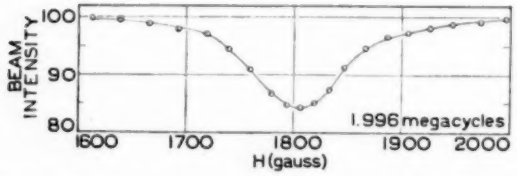

FIG. 1. Resonance curve of Al^{27} observed in $KCl \cdot AlCl_3$ with a current of 13 amp. in the wires producing the oscillating field.

assumed value of the nuclear spin, since the moment is proportional to $i/(i+\frac{1}{2})$. The gyromagnetic ratio, on the other hand, is proportional to $1/(i+\frac{1}{2})$ and is quite sensitive to the assumed value of the spin. Hence a comparison of this ratio, calculated from an observed hyperfine splitting of an energy level for various assumed values of i, with that independently measured furnishes a criterion for fixing the nuclear spin. For this it is necessary to assume only the approximate validity of the G. F. S. formula. Nuclear g calculations[5] for cases similar to those under consideration, the $^2S_{1/2}$ state of the alkalis and the $^2P_{1/2}$ state of indium, have not differed from the g values measured directly by more than ten percent.

Table I lists the observed hyperfine splitting, the quantity $(i+\frac{1}{2})g$ calculated by means of the G. F. S. formula and the resulting g values for various assumed values of the nuclear spin. Our observed g value of 1.451 agrees best in each of the three cases with that obtained by assuming a spin of 5/2. It is noteworthy that in the last two cases, where the agreement for an assumed spin of 5/2 is particularly good, the calculations are based on the h.f.s. of S states. In the first case the nuclear g is calculated from the h.f.s. of a P state. Goudsmit[6] states that it is to be expected that g values calculated from the h.f.s. of a P state will be somewhat low.

TABLE I. *Nuclear g values calculated from the h.f.s. of* Al^{27} *by use of the G.F.S. formula. The hyperfine splittings in columns 2 and 3 are those observed by Jackson and Kuhn*[1] *and that in column 4 is based on the work of Heyden and Ritschl.*[2]

STATE	$3s^23p\ ^2P_{\frac{1}{2}}$	$3s^24s\ ^2S_{\frac{1}{2}}$	$3s\ ^2S_{\frac{1}{2}}$
$\Delta\nu$ (cm^{-1})	0.048	0.048	0.516
$(i+\frac{1}{2})g$	3.90	4.48	4.41
g for $i=3/2$	1.95	2.22	2.20
$i=5/2$	1.30	1.48	1.47
$i=7/2$	0.98	1.11	1.10
$i=9/2$	0.78	0.89	0.88

The nuclear spin is thus found to be 5/2, in agreement with the result of Heyden and Ritschl. The magnetic moment, μ, is the product of the spin and the observed g and has the value 3.628 ± 0.010 nuclear magnetons. The sign of the moment is found to be positive by a method previously described.[7]

This research has been aided by a grant from the Research Corporation.

[5] P. Kusch, S. Millman and I. I. Rabi, Phys. Rev. **55**, 1176 (1939); S. Millman, I. I. Rabi and J. R. Zacharias, Phys. Rev. **53**, 484 (1938).

[6] S. Goudsmit, Phys. Rev. **43**, 636 (1933).

[7] S. Millman, Phys. Rev. **55**, 628 (1939).

The Absorption Spectrum of Aluminum Fluoride (AlF)

GEORGE D. ROCHESTER
Department of Physics, University of Manchester, Manchester, England

(Received May 22, 1939)

A new band system attributed to the molecule AlF is described. Nearly all the observed bands can be placed into one system, with the following vibrational constants, in cm^{-1}:

STATE	PROBABLE TYPE	ν_e	ω_e	$x_e\omega_e$	$y_e\omega_e$
X	$^1\Sigma$	0	814.5	8.1	—
A	$^1\Pi$	43935	822.9	8.5	0.187

INTRODUCTION

THIS investigation was undertaken as part of a series of investigations of the ultraviolet absorption of metallic halides under high dispersion. Up to the present analyses of the spectra of the diatomic molecules SnF, PbF and AgCl have been published.[1-3]

A weak band system, lying in the spectral region λλ3200–4200A, and attributed to the molecule AlF has been reported recently by Yuasa.[4] The spectrum was excited by a Geissler-tube discharge through the vapor of aluminum fluoride and nearly all the observed bands could be placed in one system with $\nu_e \sim 29{,}500$ cm^{-1}, $\omega_e'' \sim 700$ cm^{-1} and $\omega_e' \sim 710$ cm^{-1}.

The spectrum described in the present paper lies in the region λλ2200–2350A and does not appear to have been observed before. What are probably the analogous spectra of the molecules AlCl and AlBr, have, however, been observed by numerous workers.[5] The vibrational constants of these molecules, are given in Table I, in cm^{-1}. Both spectra consist of sequences of double-headed bands degraded mainly to the red end of the spectrum.

EXPERIMENTAL

The spectrum was photographed in the first order of a 30,000 lines per inch, Al-coated, concave grating, the property of the Department of Physics, the University of California, Berkeley. AlF vapor was produced by heating a few grams of aluminum fluoride (AlF_3) in a carbon-tube furnace to temperatures varying from 1300 to 1700°C. Details of the furnace and the source of continuum were as given in a former paper.[1]

A preliminary survey from λ2000–6000A with a Hilger small quartz spectrograph showed a spectrum confined to the region λλ2150–2400A with very intense absorption at λ2270A and no other bands in the spectrum which could be attributed to AlF. The spectrum was then photographed with large dispersion on Hilger Schumann plates. Suitably exposed plates were obtained with exposure times of half an hour. Four sets of plates were taken at furnace temperatures of 1300, 1400, 1600 and 1700°C.

Measurements of all band-heads were made with a comparator and reduced to wave-lengths from iron-arc wave-length standards. The accuracy of measurement of the band-heads, which were very sharp, was approximately 1 cm^{-1}. Wave numbers given in the tables are the mean of several measurements from different plates.

TABLE I. *Vibrational constants of* AlCl *and* AlBr.

MOLECULE	ν_e	ω_e''	ω_e'	ELECTRONIC TRANSITION
AlCl	38,254	450	481	$^1\Pi \rightleftharpoons {}^1\Sigma$
AlBr	35,883	299	379	do

[1] F. A. Jenkins and G. D. Rochester, Phys. Rev. **52**, 1135 (1937).
[2] G. D. Rochester, Proc. Roy. Soc. **A167**, 567 (1938).
[3] F. A. Jenkins and G. D. Rochester, Phys. Rev. **52**, 1141 (1937).
[4] T. Yuasa, Soc. Reports Tokyo Bunrika Daigaku **3**, 239 (1938).
[5] F. H. Crawford and C. F. Frolliott, Phys. Rev. **44**, 953 (1933); E. Miescher, Helv. Phys. Acta **7**, 462 (1934); P. C. Mahanti, Zeits. f. Physik **88**, 550 (1934); W. Holst, Zeits. f. Physik **89**, 40 (1934); B. N. Badhuri and A. Fowler, Proc. Roy. Soc. **A145**, 321 (1934); H. G. Howell, Proc. Roy. Soc. **A148**, 696 (1935).

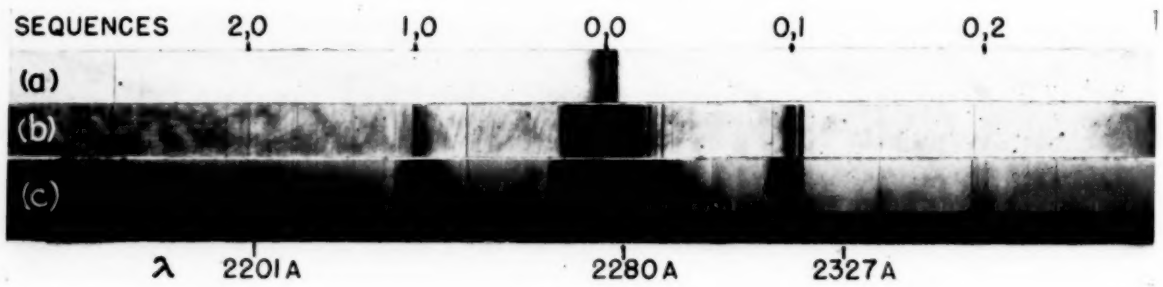

FIG. 1. The band spectrum of AlF at (a) 1300, (b) 1400 and (c) 1700°C.

Description of the spectrum

Photographs of the spectrum taken with the concave grating are reproduced in Fig. 1. Strips (a), (b) and (c), show the spectrum at furnace temperatures of 1300, 1400 and 1700°C. At a temperature of 1300°C the absorption is intense over a narrow region of the spectrum. As the temperature is raised this region increases in width and intensity and other regions of absorption make their appearance on the long and short wave sides. These regions of absorption are all so narrow that with small dispersion the spectrum has the appearance of five wide absorption lines. With large dispersion each region of absorption is seen to be a sequence of closely spaced lines and bands. In the main sequence, at λ2275A, most bands degrade to the red as do the bands in the 1,0 sequence, at λ2230A, and the 2,0 sequence, at λ2200A. Bands in the 0,1 sequence, at λ2320A, and the 0,2 sequence at λ2360A degrade to shorter wave-lengths.

Because of the narrowness of the bands estimates of their individual intensities have not been made. The relative intensities of the sequences have, however, been estimated and are as follows:

Sequence	2,0	1,0	0,0	0,1	0,2
Intensity	1	10	100	10	1

In all sequences the most intense bands are those nearest the system origin.

Vibrational analysis

The occurrence of five regions of absorption, three consisting of bands degraded to longer wave-lengths and two of bands degraded to shorter wave-lengths, suggests—as has been assumed in the previous section—that the five regions are five sequences of one system, and that the B values of the upper and lower electronic states are so nearly equal that "crossing over" occurs. Examples of such "crossing" have already been found in the spectra of the molecules, CN (the "tail-bands"), and AlCl[5] (see Table II, after Holst[6]). The same explanation must hold in the case of AlF. Of some sixty bands forty have been placed in one large system which is given in Table III. It is seen that the five regions of absorption prove to be five sequences. Quantum numbers have been allocated by a study of the intensity distribution. To within a fair degree of accuracy the wave numbers of the band-heads can be represented by the formula,

$$\nu = 43935 + 822.9(v'+\tfrac{1}{2}) - 8.5(v'+\tfrac{1}{2})^2 - 0.187(v'+\tfrac{1}{2})^3 - 814.5(v''+\tfrac{1}{2}) + 8.1(v''+\tfrac{1}{2})^2.$$

Vibrational constants for the lower state were derived in the usual way by graphing $\Delta G(v+\frac{1}{2})$ against $(v+1)$ while those of the upper state were found by the method of least squares. Though the formula does not represent the bandheads to within the accuracy of measurement it seems to be the best that can be obtained without undue complication. There seems to be some evidence for a perturbation of the level $v'=9$.

Classified bands are given in Table IV and unclassified bands in Table V. It is assumed that the band-heads which can be represented by the formula are Q heads and that the unclassified bands, which must belong to the same system, are R or P heads. The absence of an

TABLE II. *Rotational constants of* AlCl.

	$v=0$	1	2	3	4	5	6	7
B_v'	0.256	0.250	0.244	0.238	0.232	0.226	0.220	0.214
B_v''	0.241	0.240	0.238	0.236	0.234	0.232	0.230	0.228

[6] W. Holst, *Spectroskopische Untersuchungen über einige Aluminium-Verbindungen* (Stockholm, 1935), p. 54.

TABLE III. AlF *Bands.*

v' \ v''	=0	1	2	3	4	5	6	7	8	9	10	11	ΔG'
0	43937 797 804	43140 779 805	42361 806										805.0
1	44741 796 787	43945 778 783	43167 767 781	42400									783.7
2	45528 800	44728 780 767	43948 763		42437								765.0
3		75495 784	44711 766 749	43945 746									747.5
4			45460 769	44691 754 728	43937 730								729.0
5				45419 752	44667 736 706	43931 716 708	43215 712						708.7
6					45373 734	44639 712 684	43927 678						681.0
7						45323 718	44605 704 637	43901 686 642	43215				639.5
8							45242 699	44543					
9									44465 665	43800 643 604	43157 598		601.0
10										44404 649	43755 626 576	43129 573	574.5
11											44331 629	43702	
ΔG''	797.7	780.2	767.3	753.0	735.0	715.3	701.5	686.0	665.0	646.0	627.5		

isotope effect makes it impossible to associate any of the unclassified with the classified bands.

TABLE IV. *Classified bands.*

ν (CM⁻¹)	O−C (CM⁻¹)	CLASS (v', v'')	DEGRADATION
42361	4	0, 2 Q	Line
42400	4	1, 3 Q	"
42437	4	2, 4 Q	V
43129	5	10, 11 Q	V
43140	1	0, 1 Q	V
43157	−7	9, 10 Qp	V
43167	5	1, 2 Q	V
43215	−6	5, 6 Q	Line
	3	7, 8 Q	"
43702	10	11, 11 Q	R
43755	−6	10, 10 Q	R
43800	−16	9, 9 Q?	R
43901	6	7, 7 Q	Line
43927	8	6, 6 Q	"
43931	−5	5, 5 Q	"
43937	−9	4, 4 Q	"
	0	0, 0 Q	"
43945	1	1, 1 Q	V
	−4	3, 3 Q	V
43948	−1	2, 2 Q	V
44331	2	11, 10 Q	R
44404	−11	10, 9 Qp	R
44465	−20	9, 8 Qp	Line?
44543	−3	8, 7 Q	R
44605	9	7, 6 Q	R
44639	2	6, 5 Q	R
44667	−2	5, 4 Q	R
44691	−4	4, 3 Q	R
44711	−4	3, 2 Q	R
44728	−3	2, 1 Q	R
44741	−1	1, 0 Q	R
45242	−5	8, 6 Q	Line?
45323	10	7, 5 Q	R
45373	3	6, 4 Q	R
45419	0	5, 3 Q	R
45460	−1	4, 2 Q	R
45495	−2	3, 1 Q	R
45528	−1	2, 0 Q	R

p, perturbed.

DISCUSSION

It has been pointed out by several workers that the halide spectra of a given element are closely analogous. Thus all the spectra lie in the same spectral region and are due to similar electronic transitions. Further, as the mass of the halogen increases the corresponding systems occur at longer wave-lengths and the vibrational constants progressively increase.

Examination of the spectra of the halides of aluminum in the light of these considerations suggests that the system described in this paper is analogous to the strongest systems in the spectra of AlCl and AlBr. It is therefore probable that the system is due to a transition between an upper state of the electronic type $^1\Pi$ and the ground state which is a $^1\Sigma$ state.[6] The vibrational constants show that the system reported by Yuasa[4] does not involve the ground state of AlF.

I wish to express my thanks to Dr. E. Olsson for help with this analysis.

TABLE V. *Unclassified bands. Frequencies (cm⁻¹) of unclassified bands.*

SEQUENCE 0,2	0,1	0,0	2,0
42369V	43122V	43384R	45303R
42383V	43165V	43478R	45345R
42393V	43489R	43565R	45394R
42406V		43639R	45431R
42418V		43718R	45559R
		43724R	
		43783R	
		43867R	
		43892R	

On Diffraction and Radiation of Electromagnetic Waves

S. A. SCHELKUNOFF
Bell Telephone Laboratories, New York, New York

(Received June 28, 1939)

Inasmuch as it is rarely possible to treat diffraction of electromagnetic waves exactly, the Kirchhoff formulation of Huygens' Principle has been frequently used in approximate calculations. If the Kirchhoff formula is applied directly to the field intensities of the incident wave over the aperture, the diffracted field is found to be inconsistent with Maxwell's equations. If, on the other hand, this formula is applied to some auxiliary vector potential from which the diffracted field is subsequently deduced by differentiation, the result (although consistent with Maxwell's equations) depends on the particular choice of the auxiliary vector and in some instances, at least, is obviously unreasonable (Appendix III). The calculations of diffracted fields and radiation fields, based either on the Equivalence Principle or on the more general Induction Theorem, depend upon *a priori verifiable* approximations to the actual fields in the neighborhoods of the sources of the diffracted and radiated waves. For this reason we feel that these methods are preferable to those based on the Kirchhoff formula.

THE purpose of this paper is to describe several methods for dealing with diffraction and radiation of electromagnetic waves, which are believed to have certain advantages over the methods based on the Kirchhoff formula. These methods arise out of certain "induction" and "equivalence" theorems. At present, it is rarely possible to solve diffraction and radiation problems exactly. Either the usual methods or the methods to be described in this paper require approximations. The point in favor of the latter methods is our ability to use physical intuition and available knowledge, theoretical and experimental, as a guide in making the necessary approximations.

The essential feature of the following theorems is *identification of certain portions of given electromagnetic fields as the fields of appropriate fictitious electric and magnetic current sheets*.

THE INDUCTION THEOREM

It is not easy to state the Induction Theorem in its most general form and it is more expedient to formulate its variants to fit special conditions. In one form, the theorem was enunciated in a previous paper.[1] We shall now state it in the form directly applicable to the problem of radiation from an open end of a perfectly conducting metal pipe.

Let E^0, H^0 be the field which would exist over the surface of the aperture if the pipe were continued to infinity; let E', H' be the "reflected" field, that is, the field which has to be added to the "impressed" field E^0, H^0 in order to obtain the actual field in region (1) just within the pipe when it is terminated; and, finally, let E'', H'' be the "transmitted" or the actual field in region (2) just beyond the end of the pipe. Consider the field $\bar{E}$, $\bar{H}$ composed of E', H' in region (1) and of E'', H'' in region (2). We assert that the field $\bar{E}$, $\bar{H}$ could be produced, in the presence of the pipe, by electric and magnetic current sheets over the aperture and that the densities of the sheets are

$$J^0 = n \times H^0, \quad M^0 = -n \times E^0, \tag{1}$$

J being the density of the electric current sheet, M the density of the magnetic current sheet and n the unit normal to the sheets pointing into region (2). Evidently E^0 and H^0 could be replaced by their components tangential to the surface of the sheets.

While a formal proof of this theorem will be discussed in Appendix I, a few details will be given here in the belief that they will elucidate the meaning of this theorem and the manner in which it can be modified to suit different conditions. The electric and magnetic intensities of the total field around the pipe, under actual conditions, must be continuous across the aperture; thus over the aperture we have

$$E^0 + E' = E'', \quad H^0 + H' = H'';$$

or

$$E'' - E' = E^0, \quad H'' - H' = H^0. \tag{2}$$

By our assumptions the field $\bar{E}$, $\bar{H}$ satisfies

[1] S. A. Schelkunoff, Bell Syst. Tech. J., pp. 92–112, January, 1936.

Maxwell's equations everywhere except over the aperture and the surface of the pipe. This field also satisfies the proper boundary conditions over the surface of the pipe. Over the aperture of the pipe, the field $\bar{E}$, $\bar{H}$ and, in particular, its tangential components are discontinuous. It follows from the integral form of Maxwell's equations (or directly from the laws of Ampère and Faraday) that discontinuities in the components of magnetic and electric intensities, tangential to a surface S, exist if and only if there are corresponding superficial electric and magnetic current sheets over S. The density of the electric current sheet is equal to the discontinuity in the tangential component of the magnetic intensity and the density of the magnetic current sheet is equal to the discontinuity in the tangential component of the electric intensity.[2]

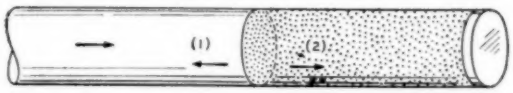

FIG. 1. Pipe enclosing two different dielectric media.

Therefore, if we start with the current sheets (1) and wish to determine the field produced by them in the presence of the pipe, we must regard the field $\bar{E}$, $\bar{H}$ as a possible solution. If we accept for the moment that any solution of Maxwell's equations which satisfies given boundary conditions and behaves in the proper manner at infinity is unique, then $\bar{E}$, $\bar{H}$ is the field which we would calculate from the current sheets (1) no matter what particular method of calculation we are likely to adopt.

Let us consider another situation. Let a perfectly conducting metal pipe enclose two different dielectric media which are separated by a plane boundary (Fig. 1) and let a progressive wave E^0, H^0 move from left to right in region (1). By the Induction Theorem, the wave reflected from the interface between the two media and the wave transmitted into region (2) could be produced by electric and magnetic current sheets over the interface, whose densities are given by (1). In this instance, the exact solution can be obtained directly as well as from the Induction Theorem, thus affording a verification of the theorem.

Consider now a system with one degree of freedom. An example of such a system is an ordinary transmission line terminated in some impedance (Fig. 2). Let $V^0(x)$, $I^0(x)$ be the voltage and the current that would exist in the progressive wave moving from left to right if the line were terminated in its characteristic impedance instead of the actual impedance. Choose some particular point x_0 on the actual terminated line. If $V'''(x)$, $I'''(x)$ is the actual voltage and current to the right of this section and $V'(x)$, $I'(x)$ is the voltage and the current which must be added to $V^0(x)$, $I^0(x)$ in order to obtain the actual voltage and current to the left of the section, then the continuity conditions at $x=x_0$ require

$$V^0(x_0)+V'(x_0)=V'''(x_0), \qquad I^0(x_0)+I'(x_0)=I'''(x_0);$$

or

$$V'''(x_0)-V'(x_0)=V^0(x_0), \qquad I'''(x_0)-I'(x_0)=I^0(x_0). \quad (3)$$

In this case, the Induction Theorem consists in asserting that the wave $\bar{V}(x)$, $\bar{I}(x)$, equal to V'', I' on the left of $x=x_0$ and to V''', I'' on the right of it, *could be produced by a zero impedance generator in series with the line and an infinite impedance generator (constant current generator) in shunt with the line, the voltage of the series generator and the current through the shunt generator being, respectively, $V^0(x_0)$ and $I^0(x_0)$.*

EQUIVALENCE THEOREMS

Broadly speaking, the equivalence theorems differ from the corresponding induction theorems in that the latter specify the current sheets capable of producing both the reflected field E', H' and the transmitted field E'', H'' while the former specify the current sheets capable of producing only the transmitted field. Thus, if in

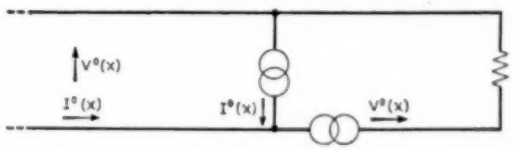

FIG. 2. Transmission line terminated in an impedance.

[2] It also follows from the integral form of Maxwell's equations that the discontinuities in the *normal* components of electric and magnetic *current densities* are determined by the discontinuity in the tangential field *intensities*.

region (1), we postulate a zero field in place of the reflected field E', H' and two current sheets (over the surface of the aperture) defined by

$$J''=n\times H'', \quad M''=-n\times E'', \qquad (4)$$

to take care of the discontinuities in the total field E, H comprised of the zero field in region (1) and the actual transmitted field E'', H'' in region (2). It should be noted that in equivalence formula (4) the densities of the current sheets are not known in advance as is the case in the corresponding Induction Formula (1).

Another equivalence theorem may be obtained by choosing a closed surface S comprised of the surface of the aperture and the outer surface of a horn, postulating a zero field inside the surface and E'', H'' outside, and introducing electric and magnetic current sheets over S of densities given by (4). We assert, then, that these sheets will produce the postulated field. This theorem may be called the "free-space" equivalence theorem in order to emphasize that in carrying out the calculations, the horn must be ignored and the response must be calculated by the "free-space" retarded potentials in contrast with the previous equivalence theorem according to which the response to the current sheets had to be calculated subject to the boundary conditions at the surface of the horn. On the other hand, the current sheets required by the free-space equivalence theorem extend over the outer surface of the horn as well as over the aperture while in the other theorem they extend only over the aperture. In a previous paper[1] the "free-space" equivalence theorem has been named the Equivalence Principle[3] in the belief that it is a precise expression and a generalization of a physical principle enunciated by Huygens.

Huygens' principle is commonly stated as follows:[4] Each element of any wave front acts as a new source of disturbance, sending out secondary waves, and these secondary waves combine to form the new wave front. I am inclined to believe that if with the aid of a hypothetical perfectly absorbing screen we could isolate the disturbance produced by an individual secondary source, we should find this disturbance identical with that produced by the elementary source (4). It is impossible to prove this contention any more than to prove that the energy flow per unit area in an electromagnetic field is expressed by $E\times H$. Just as in the latter case, it can be proved only that the *total flow* of energy across a *closed* surface can be obtained by integrating the Poynting vector, in the former case it can be proved only that when we integrate a certain expression over a closed surface we obtain the correct field. In either case it is possible to modify the integrand and still obtain the same results *when the integration is performed over the closed surface*. The choice of a particular integrand must necessarily be made on other than mathematical grounds.

Let us now consider a perfectly conducting metal tube and a progressive wave moving from left to right (Fig. 3). The actual field at some point P to the right of some cross section S_1 could be produced by electric and magnetic current sheets given by (4), or by (1) since in this case $E''=E^0$ and $H''=H^0$. The action of these current sheets must be calculated subject to the boundary conditions at the surface of the pipe. This field could also be calculated by the free-space equivalence principle by using the current sheets spread over a *closed* surface S_2 surrounding point P and whose densities are still given by (1).

Radiation from Horns

Preceding theorems can be used for the approximate calculation of the power radiated by horns and the radiation patterns of those horns. Three methods of approach present themselves:

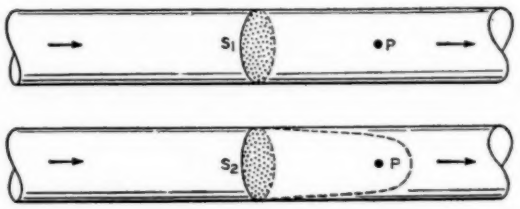

FIG. 3. Perfectly conducting metal tube; progressive wave moving from left to right.

[3] The Equivalence Principle was originally discovered by A. E. H. Love [Phil. Trans. Roy. Soc. **A197**, 1–45 (1901)] and subsequently by H. M. MacDonald [*Electric Waves* (1902), p. 16]. The latter supplied two proofs [MacDonald, *Electric Waves* (1902), p. 16; MacDonald, Proc. London Math. Soc. Series E, **10**, 91–95 (1911)] of the theorem, of which only the second is valid. A few years ago, the theorem was rediscovered by the present author as one of a group of theorems treated in a previous paper (reference 1) and here.

[4] A. E. Caswell, *An Outline of Physics* (1929), p. 544.

1. In accordance with the free-space equivalence principle the sources within the horn *and* the horn itself[5] are replaced by electric and magnetic current sheets, surrounding the horn, with densities given by (4); then, the free-space field of these sources is calculated by means of the following formulae.

$$E = -i\omega\mu A + \frac{1}{i\omega\epsilon}\,\text{grad. (div. } A) - \text{curl } F,$$
$$H = -i\omega\epsilon F + \frac{1}{i\omega\mu}\,\text{grad. (div. } F) + \text{curl } A, \tag{5}$$

where the magnetic vector potential A and the electric vector potential F are given by

$$A = \int_{(S)} \frac{J'' e^{-i\beta r}}{4\pi r} dS, \quad F = \int_{(S)} \frac{M'' e^{-i\beta r}}{4\pi r} dS. \tag{6}$$

These formulae become much simpler if we are interested only in the field at great distances from the horn.[6]

In practical applications neither J'' nor M'' are known exactly and suitable approximations must be made, with available theoretical and experimental knowledge as a guide. The situation is similar to that in which we find ourselves when calculating the power radiated by antennas and by transmission lines from the electric current distribution. The latter is not known exactly but available evidence points to the fact that it is nearly sinusoidal.

If the aperture of the horn is so large that the cut-off frequency of the horn is appreciably below the operating frequency, practically all energy reaching the aperture passes into the outer medium. In this case, it is reasonable to suppose that the field over the aperture will be substantially the same, except near the edges, as if the horn were infinitely long. Thus, we can assume that over the aperture J'' and M'' are approximately equal to the *known* quantities J^0 and M^0. Over the surface of the horn M'' is *known* to be very small (it would vanish for perfectly conducting horns) and J'' is *assumed* to be small.

[5] That is, the sources induced in the horn.

[6] S. A. Schelkunoff, *A General Radiation Formula* (to be published).

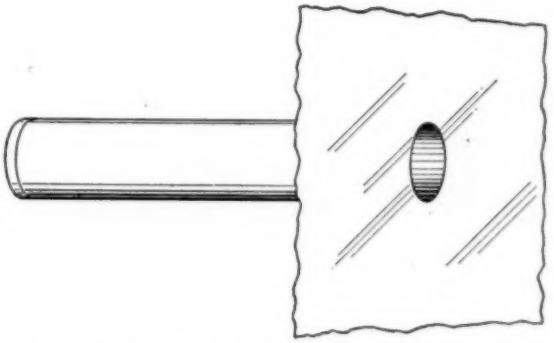

FIG. 4. Pipe ending in a perfectly conducting plane.

It may be pointed out that in theory it is possible to calculate the radiation pattern and the radiated power from the conduction current in the horn. In practice, however, no basis has been found for making a reliable *a priori* assumption with regard to this current distribution.

2. The second method of approach consists in replacing the sources within the horn by electric and magnetic current sheets with the same densities (4) as in the preceding case but extending only over the aperture. These current sheets are supposed to act in the presence of the horn as a reflecting surface. Thus, A and F are given by

$$A = \int_{(S_a)} J'' \cdot \psi_1(x, y, z; x', y', z') dS,$$
$$F = \int_{(S_a)} M'' \cdot \psi_2(x, y, z; x', y', z') dS, \tag{7}$$

where ψ_1 and ψ_2 are two diadics and the integration is extended over the surface S_a of the aperture. The scalar product of the moment of an electric current element and diadic ψ_1 is the magnetic vector potential of the electric current element and, similarly, the scalar product of the moment of the magnetic current element and diadic ψ_2 is the electric vector potential of the element.

In applying (7) we no longer need approximate estimates of the field over the outer surface of the horn; instead we have to approximate ψ_1 and ψ_2. In the case of the horn considered above, we would say that the effect of the horn, as a reflecting surface, on the radiation field is probably small and that we could replace ψ_1 and ψ_2 by the free-space transmission factors. In this case we

obtain the same result whether we follow the first or the second method of approach.

The second method may, however, be more valuable than the first in other situations. For example; consider a pipe and an infinite perfectly conducting plane (Fig. 4). The first method will give us the same result as if the plane were absent since, not knowing *a priori* J'' in the plane, we should be forced to ignore it. The second method will supply us with a better result since we shall deal with electric and magnetic current sheets over a perfectly conducting plane.[7] This problem can be solved by the free-space retarded potentials. The image of the electric current sheet in the plane is negative and will cancel the effect of the sheet itself. The image of the magnetic current sheet is positive and will double the effect of the sheet. In other words, instead of (6) we now have

$$F=\int_{(S_a)} \frac{M''e^{-i\beta r}}{2\pi r}dS, \quad A=0. \tag{8}$$

Since M'' is determined by the tangential components (E_x'', E_y'') of the electric intensity, we can obtain from (5) and (8)

$$\begin{aligned}
E_x&=\frac{1}{2\pi}\int_{(S_a)} E_x''\left(i\beta+\frac{1}{r}\right)\frac{e^{-i\beta r}}{r}\cos\theta dS,\\
E_y&=\frac{1}{2\pi}\int_{(S_a)} E_y''\left(i\beta+\frac{1}{r}\right)\frac{e^{-i\beta r}}{r}\cos\theta dS,\\
E_z&=-\frac{1}{2\pi}\int_{(S_a)} (E_x''\cos\varphi+E_y''\sin\varphi)\\
&\qquad\times\left(i\beta+\frac{1}{r}\right)\frac{e^{-i\beta r}}{r}\sin\theta dS.
\end{aligned} \tag{9}$$

These results agree with Sommerfeld's modification of the Kirchhoff formula.[8]

3. By the Induction Theorem the field $\bar{E}$, $\bar{H}$ consisting of the reflected field E', H' inside the horn and the transmitted field E'', H'' outside the horn can be produced by electric and magnetic current sheets with densities given by (1). Thus, we have

$$A=\int_{(S_a)} J^0\cdot\psi_1 dS, \quad F=\int_{(S_a)} M^0\cdot\psi_2 dS, \tag{10}$$

where ψ_1 and ψ_2 are the same diadics as in (7).

In theory, this theorem is more powerful than either of the two preceding theorems. It does not require any approximations to the field over the surface of integration and it gives both the reflected and the transmitted field. In practice, however, the major value of this theorem is to furnish a basis for approximating the field over the aperture. In transmission systems admitting of only one transmission mode, the Induction Theorem leads to a definite solution (see Appendix II). We then assume that the known results in the simple case may be taken as a first approximation in more complex cases.

The Kirchhoff Formula

It is only fitting that we should not pass in silence the well-known Kirchhoff formula which has been universally used for solving diffraction problems and recently has been applied to problems of radiation.[9, 10, 11] This formula is

$$V=\int_{(S)}\left[\left(i\beta+\frac{1}{r}\right)V\cos(n,r)-\frac{\partial V}{\partial n}\right]\frac{e^{-i\beta r}}{4\pi r}dS, \tag{11}$$

where V is a wave function, S any closed surface surrounding a source-free region, and n is the normal to S looking into this region.

When applying (11) to electromagnetic problems, we are confronted with greater difficulties than we were when applying previous methods. In either case, we have to make approximations to the integrand over the surface of integration but while before we were aided in making the necessary approximations by physical intuition and experience, we have nothing to guide us, at least at present, in the case of the Kirchhoff formula. We could interpret, for example, V as a cartesian component of the magnetic vector potential, but we have no knowledge of its

[7] While the actual plane has a hole in it, in applying the second method we are permitted to plug the hole with a perfectly conducting disk since the field due to the postulated current sheets is known to be identically zero on the side of the pipe.

[8] A. Sommerfeld, Göttinger Nachr. 1894, Nr. 4.

[9] R. Darbord, L'Onde Elec. **11**, 53–82 (1932).

[10] H. Diamond and F. W. Dunmore, Nat. Bur. Stand. J. Research **19**, 1–19 (1937). (Paper RP1006.) Proc. I. R. E. **25**, 1542–1560 (1937).

[11] W. L. Barrow and F. M. Greene, Proc. I. R. E., **26**, 1498–1519 (1938).

behavior over the outer surface of the horn. We can expect no help from the experiment since we cannot measure the magnetic vector potential either directly or indirectly. Likewise, we could apply (11) to the electric vector potential but with no better success. If we simply ignore the contributions coming from the outer surface of the horn, we get different radiation patterns, depending upon the choice of V. If we apply (11) directly to cartesian components of E and H and ignore the contributions of the outer surface of the horn, we obtain a result which is inconsistent with Maxwell's equations. In other words, while (11) is correct when applied to a *closed* surface, there seems to be no way to adapt it to practical needs when we are forced to make approximations. An interesting example of the difficulties which may confront us is given in Appendix III.

At this point a few words must be said about the comparison made by Barrow and Greene[11] between experimental radiation patterns and those calculated with the aid of the Kirchhoff formula from the magnetic vector potential. As the authors point out the agreement is satisfactory only in the horizontal plane (in the plane perpendicular to the electric vector). The agreement would have been satisfactory in the vertical plane (but not in the horizontal) if (11) were applied to the electric vector potential. In the case considered by Barrow and Greene formula (6) agrees satisfactorily with experimental results in both planes. Fig. 5 represents a comparison between an experimental vertical radiation pattern and patterns calculated by different methods.

Conclusion

It is hardly necessary to emphasize that the proposed methods of dealing with radiation and diffraction problems are based, at least in the important practical cases, on certain approximations. Fortunately these approximations are susceptible of direct experimental verification. It is hoped that this paper will stimulate such experiments.

These experiments should be made preferably on fairly small apertures. As the aperture becomes larger, the difference (but not the ratio) of the radiation intensities obtained from the Equivalence Principle on one side, and from the Kirchhoff formula on the other, becomes small; this is because the "space factor" of the array of secondary sources over the aperture becomes the dominant factor and the precise nature of the secondary sources loses its importance. In fact, one could make almost arbitrary assumptions with regard to the secondary sources and obtain the radiation patterns, for large apertures, which would differ but little.

Appendix I

The essential parts of our proofs of induction and equivalence theorems are the appropriate uniqueness theorems, that is, theorems asserting the uniqueness of the field defined by a given set of conditions. If the given set of conditions is known to lead to a unique solution, we are assured of obtaining the same solution no matter what method we happen to use even if we were simply to guess the solution and then to verify it. For instance, in dealing with free oscillations inside a perfectly conducting spherical sheet we may obtain a certain solution subject to the condition that the tangential component of the electric intensity vanishes at the surface of the

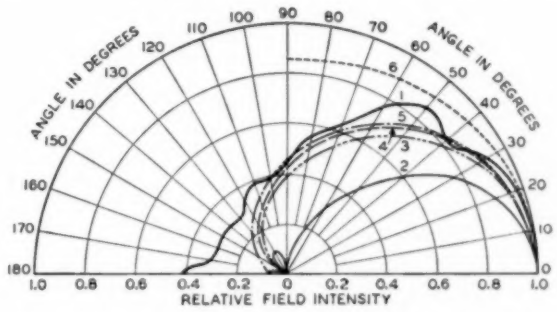

Fig. 5. (1) The experimental vertical radiation pattern obtained by Barrow and Greene for the open end of a rectangular tube; this curve is taken from Fig. 10*B* of reference 11; (2) the preferred theoretical curve calculated by Barrow and Greene by applying the Kirchhoff formula to a Hertzian vector; (3) the theoretical curve calculated by Barrow and Greene by applying the Kirchhoff formula directly to the electric vector and disapproved by them because the direction of the electric vector in the radiation field is wrong; (4) the theoretical curve obtained from the Equivalence Principle on the assumption that the ratio of E to H over the aperture is the same as for plane waves in free space; (5) the theoretical curve obtained from the Equivalence Principle on the assumption that the field over the aperture is the same as would have been over the same surface in case the tube were continued indefinitely; (6) the theoretical curve for the case in which a perfectly conducting infinite flange is added to the open end of the tube.

spherical sheet. The field outside the sphere may be taken equal to zero. Having obtained the solution, we find that the tangential component of the magnetic intensity is discontinuous across the sphere. In accordance with Maxwell's equations, this discontinuity implies electric current in the sphere, the density of this current being equal to the above-mentioned discontinuity. If we were to calculate the field of this current sheet by the retarded potential method, we expect to obtain the field from which we started.

An exhaustive analysis of uniqueness theorems of electromagnetics would require considerable space and could properly be regarded as a subject in itself. We shall restrict ourselves to the simplest case of monochromatic waves in dissipative media. This case is really sufficient for our purposes since we can assume the conductivity of the medium to be so slight that its effect is negligibly small and yet be sure that the needed theorems are applicable.

We shall write Maxwell's equations in the following form

$$\begin{aligned} \text{curl } E &= -i\omega\mu H - M, \\ \text{curl } H &= (g+i\omega\epsilon)E + J, \end{aligned} \tag{12}$$

where J and M are the densities of the applied electric and magnetic currents. Let us multiply scalarly the first equation by the conjugate of H, the conjugate of the second equation by E, and subtract; thus we obtain

$$\begin{aligned} H^*\cdot\text{curl } E - E\cdot\text{curl } H^* = &-M\cdot H^* - E\cdot J^* \\ &- gE\cdot E^* + i\omega\epsilon E\cdot E^* - i\omega\mu H\cdot H^*, \end{aligned} \tag{13}$$

where the asterisks designate the conjugate complex numbers. Integrating over a volume enclosed by a surface S and taking into account that

$$H^*\cdot\text{curl } E - E\cdot\text{curl } H^* = \text{div. } E\times H^*, \tag{14}$$

$$\int_{(v)} \text{div. } E\times H^* dv = \int_{(S)} (E\times H^*)_n dS,$$

we obtain

$$\begin{aligned} -\int_{(v)} (E\cdot J^* + M\cdot H^*)dv &= g\int_{(v)} E\cdot E^* dv \\ + i\omega\int_{(v)} (\mu H\cdot H^* - \epsilon E\cdot E^*)dv &+ \int_{(S)} (E\times H^*)_n dS, \end{aligned} \tag{15}$$

where n is the normal to S pointing away from the volume under consideration. In (15) the region v may be a multiply connected region enclosed by surface S_0 externally and by surfaces S_1, S_2, etc. internally; in this case, S consists of S_0, S_1, S_2, etc.

In dissipative media the field at great distances from the sources vanishes as an exponential function of the distance; hence, the last term in (15) vanishes in the limit as S_0 recedes to infinity. If there are no impressed currents or if in the regions occupied by impressed currents, the components of the field in the directions of these currents vanish, then the left member of (15) is equal identically to zero. The first term on the right is real and the second is a pure imaginary; therefore, in absence of impressed currents these terms must vanish separately. Since $E\cdot E^*$ is essentially positive, the volume integral can vanish only if E vanishes everywhere; then H also vanishes everywhere and the electromagnetic field is identically zero.

Let us now prove with the aid of the above result the free-space equivalence principle (4). The assertion is that the current sheets (4) over a surface S enclosing given sources produce the field $\bar{E}$, $\bar{H}$ which is equal to the field E'', H'' on the source-free side of S and to the field 0, 0 on the other side of S. This synthetically obtained field is certainly one solution of Maxwell's equations subject to the proper boundary conditions across S and behaving in the appropriate manner at infinity. The question is whether it is the only one. In other words, shall we obtain the same field $\bar{E}$, $\bar{H}$ if we solve (12) by the retarded potential method or shall we obtain a different field $\bar{E}_1$, $\bar{H}_1$? Let us suppose that the latter is the case. Then we have

$$\begin{aligned} \text{curl } \bar{E} &= -i\omega\mu\bar{H} - M'', \\ \text{curl } \bar{E}_1 &= -i\omega\mu\bar{H}_1 - M'', \\ \text{curl } \bar{H} &= (g+i\omega\epsilon)\bar{E} + J'', \\ \text{curl } \bar{H}_1 &= (g+i\omega\epsilon)\bar{E}_1 + J''. \end{aligned} \tag{16}$$

On subtracting these equations we find that the difference field $\bar{E}-\bar{E}_1$, $\bar{H}-\bar{H}_1$ satisfies the homogeneous form of (12), that is, the form in which $M=J=0$. Therefore, this field vanishes identically throughout the entire space and $\bar{E}_1=\bar{E}$, $\bar{H}_1=\bar{H}$.

Similarly we can prove an equivalence

theorem for the case in which the horn is retained and the impressed current sheets (4) extend only over the mouth of the horn. The Induction Theorem (1) is also proved in the same manner.

In connection with the above theorems, the reader has undoubtedly noted an interesting paradox. The electric and magnetic current sheets on S imply only *discontinuities* in the magnetic and electric intensities across the surface. How is it that in accordance with the above theorems we know the actual intensities on either side of the sheet and not only their differences? The explanation lies in the fact that in these theorems the densities of the superficial current sheets *are not independent*, these densities are obtained from functions satisfying the homogeneous Maxwell's equations and theoretically either the electric field alone or the magnetic field alone suffice for defining *both* current sheets.

Appendix II

In the case of a simple transmission line,[12] a direct verification of the Induction Theorem is possible and the results are useful as an aid to the study of more complex cases. As before we shall designate by a single prime the reflected voltage and current and by a double prime the transmitted voltage and current. The subscript $_1$ will be used to designate those parts of the voltage and the current which are produced by the impressed series voltage V^0 and the subscript $_2$ will refer to the voltage and current produced by the shunt current I^0.

We shall consider the case of a semi-infinite transmission line, with characteristic impedance Z_0, terminated in the impedance Z at some point $x=x_0$. Carrying out the calculations in accordance with the Induction Theorem, we obtain

$$\begin{aligned}
I_1'(x_0) &= V^0/(Z_0+Z),\\
I_2'(x_0) &= -ZI^0/(Z_0+Z),\\
I_1''(x_0) &= V^0/(Z_0+Z),\\
I_2''(x_0) &= Z_0I^0/(Z_0+Z),\\
V_1'(x_0) &= -Z_0V^0/(Z_0+Z),\\
V_2'(x_0) &= Z_0ZI^0/(Z_0+Z),\\
V_1''(x_0) &= ZV^0/(Z_0+Z),\\
V_2''(x_0) &= Z_0ZI^0/(Z_0+Z).
\end{aligned} \tag{17}$$

Thus, the total reflected voltage and current and the total transmitted voltage and current are

$$\begin{aligned}
I'(x_0) &= \frac{Z_0-Z}{Z_0+Z}I^0, \quad V'(x_0) = \frac{Z-Z_0}{Z+Z_0}V^0,\\
I''(x_0) &= \frac{2Z_0}{Z_0+Z}I^0, \quad V''(x_0) = \frac{2Z}{Z_0+Z}V^0.
\end{aligned} \tag{18}$$

These expressions are precisely the same as would be obtained directly from the boundary conditions at point $x=x_0$.

If Z is nearly equal to Z_0, V' and I' are small while V'' and I'' are nearly equal to V^0 and I^0. This is the case when practically all power carried by the wave V^0, I^0 is transmitted beyond $x=x_0$. Similarly we expect that in the case of a horn with a large mouth, when practically all power delivered to the mouth passes on into the outer medium, E'' and H'' are substantially equal to E^0 and H^0 as we have previously assumed in our applications of the equivalence theorems.

On the other hand, if Z is either very small compared with Z_0 or very large, then the reflection is nearly complete and one of the quantities V'', I'' nearly vanishes while the other is nearly doubled. In this case the effect across the impedance Z is produced largely either by the series generator alone or the shunt generator alone. In the corresponding three-dimensional case (which occurs when the frequency is near the cut-off frequency) we expect, therefore, that as a first approximation we can calculate the radiation patterns by assuming only one current sheet over the mouth of the aperture. The corresponding radiation patterns will be symmetrical about the plane of the aperture of the horn. The departure from symmetry will be caused by the incomplete reflection.

Appendix III

Consider a perfectly conducting semi-infinite coaxial pair with an open end. Let the radii a and $b(b>a)$ be very small compared with the wavelength. The field inside the coaxial pair is approximately

$$E_\rho = \frac{60I}{\rho}\cos\beta z, \quad H_\varphi = -\frac{iI}{2\pi\rho}\sin\beta z, \quad \beta = \frac{2\pi}{\lambda}, \tag{1}$$

where: I is the maximum amplitude of the

[12] A transmission line admitting of only one transmission mode.

current, λ the wave-length, ρ the distance from the axis and z the distance along the axis. The open end is in the plane $z=0$.

The field can be obtained from a vector potential whose components are

$$A_\rho = A_\varphi = 0, \quad A_z = \frac{iI}{2\pi} \log \frac{\rho}{\rho_0} \sin \beta z. \tag{2}$$

This can be verified by substitution in

$$H_\varphi = -\frac{\partial A_z}{\partial \rho}, \quad E_\rho = \frac{1}{i\omega\epsilon} \frac{\partial^2 A_z}{\partial \rho \partial z}. \tag{3}$$

The values of the above wave function and its normal derivative over the aperture are

$$A_z = 0, \quad \frac{\partial A_z}{\partial n} = \frac{i\beta}{2\pi} I \log \frac{\rho}{\rho_0}. \tag{4}$$

Using the Kirchhoff formula in the customary manner (i.e., by applying it to the aperture) we find that at great distances from the aperture the approximate value of A_z is

$$A_z = -\frac{iI}{4\lambda}\left[\left(b^2 \log \frac{b}{\rho_0} - a^2 \log \frac{a}{\rho_0}\right) - \tfrac{1}{2}(b^2 - a^2)\right] \frac{e^{-i\beta r}}{r}. \tag{5}$$

From this we calculate the field and then the radiated power; thus we obtain

$$W = \frac{40\pi^4}{\lambda^4}\left[\left(b^2 \log \frac{b}{\rho_0} - a^2 \log \frac{a}{\rho_0}\right) - \tfrac{1}{2}(b^2 - a^2)\right]^2 I^2. \tag{6}$$

By choosing ρ_0 properly we can make the radiated power W equal to anything from zero to infinity. The approximate value for W found with the aid of the Equivalence Principle corresponds to ρ_0 satisfying

$$b^2 \log \frac{b}{\rho_0} - a^2 \log \frac{a}{\rho_0} = 0. \tag{7}$$

Note: On Diffraction and Radiation of Electromagnetic Waves

J. A. Stratton and L. J. Chu
Massachusetts Institute of Technology, Cambridge, Massachusetts

Dr. Schelkunoff has kindly shown us the manuscript of the preceding paper which is closely allied to ours.[13] Since our formulation of the problem differs somewhat from that of Dr. Schelkunoff in "Some Equivalence Theorems of Electromagnetics and Their Application to Radiation Problems,"[14] and in the preceding paper, it appears worth while to point out that the results obtained by the Equivalence Principle are identical with ours. If the field of the equivalent surface currents is calculated from the vector potential or the Hertz vector, the contour charges need not be introduced explicitly. The contour charges simply ensure the self-consistency of the assumed field on the surface.

[13] J. A. Stratton and L. J. Chu, "Diffraction Theory of Electromagnetic Waves," Phys. Rev. **56**, 99–107 (1939).
[14] S. A. Schelkunoff, Bell Sys. Tech. J. **15**, 92–112 (1936).

On the Surface States Associated with a Periodic Potential

WILLIAM SHOCKLEY
Bell Telephone Laboratories, New York, New York

(Received June 19, 1939)

The wave functions and energy levels associated with a finite one-dimensional periodic potential field are investigated. In a plot of the energy spectrum *versus* interatomic distance the surface levels appear only at lattice constants so small that the boundary curves for the allowed energy bands have crossed. The levels appear in the "forbidden" region between allowed bands in pairs one coming from each of the adjoining bands. In three dimensions these surface levels give rise to surface bands. The surface bands probably exist and are half-filled for diamond. They exist for all metals and are entirely unoccupied only for the monovalent metals.

IN dealing with wave functions in solids, the problem is simplified by considering an infinite crystal or else a part of an infinite crystal. This is done so as to deal with wave functions which satisfy simple boundary conditions. However, the simplifications so introduced obscure certain features of interest associated with the surface of the crystal. This defect was apparent to Tamm,[1] who considered the wave functions for an idealized one-dimensional crystal in which the atomic fields were represented by square potential wells (the model of Kronig and Penney[2]).

Tamm found in this case that it was possible to have energy levels whose wave functions were localized at the surface of the crystal. In this treatment a semi-infinite crystal was used, and Tamm found that one surface level was possible for each energy gap between the ordinary allowed bands of energies. In a later paper Fowler[3] discussed Tamm's levels for a finite crystal and pointed out that the levels should occur in pairs because of the two faces of the crystal. They have since been discussed by Rijanow[4] and Maue[5] and most recently by Goodwin.[6] In none of these papers, however, was it found how the surface levels originate from the atomic levels as the crystal is conceived of as being formed by varying the lattice constant from infinity to a finite value.

In the present paper we shall discuss the solution of this problem for a general one-dimensional crystal, Fig. 1(a), containing a finite number of atoms each of which is represented by a potential well whose shape is symmetrical about the center of the atom but is otherwise arbitrary. (This restriction considerably simplifies the mathematical work but is probably not essential.) The particular behavior of the potential beyond the edges of the end cells does not affect our results so long as it stays positive. We shall find that the surface levels exist only under certain particular conditions and shall see how they arise from the bands of allowed levels.

The results may be best understood in terms of a plot of energy *versus* lattice constant. In Fig. 2 such a plot is shown in a qualitative fashion. We see that at large lattice constants we have narrow energy bands such as are to be expected from small overlapping between the atoms. Furthermore, all the wave functions of the band are of the "penetrating type" rather than the surface type. The surface states first appear after the boundary curves of the energy bands have crossed. Postponing for the moment the origin of these boundary curves, we note that after they have crossed, two energy levels have separated, one from each of the bands. These energies correspond to wave functions of the surface type while the other energies correspond to penetrating wave functions. The energy difference between the two surface functions decreases exponentially as the number of atoms increases. The wave functions themselves are of the Tamm type near each surface—that is, they decay exponentially in both directions away

[1] I. Tamm, Physik. Zeits. Sowjetunion **1**, 733 (1932).
[2] R. de L. Kronig and W. G. Penney, Proc. Roy. Soc. **A130**, 499 (1931).
[3] R. H. Fowler, Proc. Roy. Soc. **A141**, 56 (1933).
[4] S. Rijanow, Zeits. f. Physik **89**, 806 (1934).
[5] A. W. Maue, Zeits. f. Physik **94**, 717 (1935).
[6] E. T. Goodwin, Proc. Camb. Phil. Soc. **35**, 205, 221, 232 (1939).

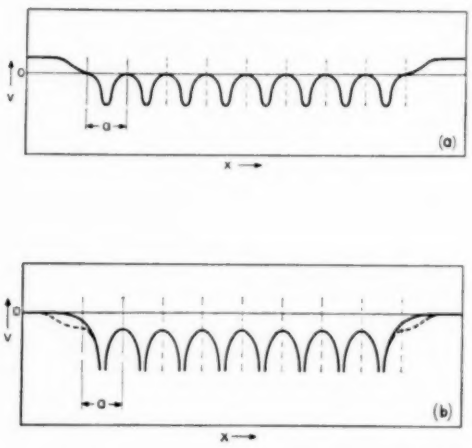

FIG. 1. The potential in the one-dimensional lattice. (*a*) A periodic potential. (*b*) The potential corresponding to Goodwin's "tight binding" approximation.

from the surface. The difference between the two surface waves is one of symmetry: The type of crystal envisaged here possesses a center of symmetry and the wave functions are therefore either symmetrical or antisymmetrical, depending upon whether they have the same or opposite signs on the two edges of the crystal.

The equations for the boundary curves of Fig. 2 are similar to those met with by applying Slater's method of finding three-dimensional wave functions.[7] The wave function in an individual cell is expanded in terms of two functions g and u which are symmetrical and antisymmetrical about the center of the cell. If the wave function is required to be of the form $\psi = \exp(ikx)v(x)$ where $v(x)$ has the period "a" of the lattice, one finds by a familiar process that

$$\tan^2(ka/2) = -(g'/g)/(u'/u),$$

where g and u are the values at the edge of the cell of the functions g and u and g' and u' are corresponding derivatives. The allowed bands of energies occur where only one of the ratios (g'/g) and (u'/u) is negative; the forbidden regions occur where neither or both are negative. Certain crossings of the curves of Fig. 1 are possible; these may occur between $g'/g = \infty$ and $u'/u = 0$ and between $g'/g = 0$ and $u'/u = \infty$; no other crossings are possible. It is, therefore, seen that all possibilities for the occurrence of surface states are represented in Fig. 2.

[7] J. C. Slater, Phys. Rev. **45**, 794 (1934).

In Goodwin's work surface states have been found to occur for the case of "tight binding"—that is, the case of large lattice constant and uncrossed bands. Goodwin's states arise from his use of a potential which is more realistic than ours; his potential is shown in Fig. 1(b). We see that it is periodic except for the outer edges of the end cells, where it is somewhat higher than in the other cells. If we make his potential periodic as indicated by the dotted lines, then the diagram for the states will be as in Fig. 2. If we now correct the energies of these wave functions by taking as a perturbation the difference between the periodic potential and Goodwin's, we find that two of the wave functions acquire energies above the boundary curves. These two functions will be surface states having wave functions damped towards the interior of the crystal. The origin of these states is essentially different from the origin of the states occurring after the bands have crossed. They will always lie near the band from which they originate. If we had used Goodwin's potential, we should have found these surface states lying just above each energy band in both the case of uncrossed and crossed bands. In the case of crossed bands there would then be four surface states. Goodwin, following the treatment of Maue, has also considered the case of almost free electrons. He uses a periodic potential without edge effects in the end cells. The surface states he obtains in this way are of the same type as ours, and in Appendix 5 we show that the conditions under which he obtains them are equivalent to the crossing of

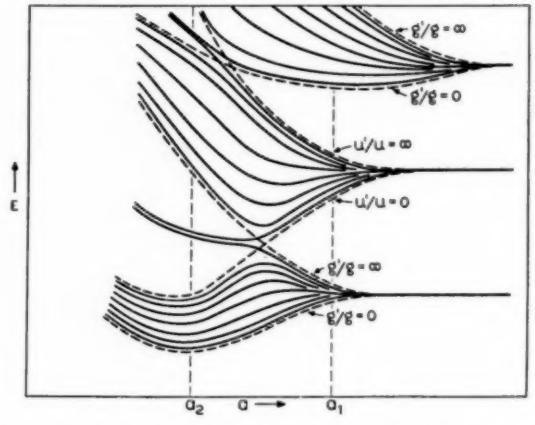

FIG. 2. Energy spectrum for a one-dimensional lattice with eight atoms.

the energy bands. In the remainder of this paper we shall be concerned only with the type of surface states represented in Fig. 2, which arise from the periodic potential.

If we suppose that there is one electron with each spin per atom then before the crossing of the boundary curves there are just enough states to accommodate all the electrons in the lowest band. After the crossing, however, there are one too few states in the lowest band and one electron is forced into a surface state. Hence after the crossing has occurred, the surface states will be half-occupied.

Extension to Three Dimensions

We can visualize to some extent how this last result would be modified in three dimensions by considering a potential equal to the sum of three one-dimensional potentials. For the case where the boundary curves have crossed so much that there is a complete gap in energy between the first and second allowed bands (this occurs when the energy gap in the one-dimensional Fig. 2 is more than twice the width of the lowest band), there are roughly half as many electrons left over as there are surface atoms. This may be seen as follows: For this case the wave functions are the products of three one-dimensional wave functions. For states in the lowest band each factor may run through $(N-1)$ values; hence there are $(N-1)^3$ states in the lowest band. Since there are N^3 electrons there are $N^3-(N-1)^3 = 3N^2-3N+1 \leqq 3N^2$ electrons left over. For the surface states, two possible values are available for one factor and $(N-1)$ for each of the other two. Thus there will be $2(N-1)^2$ surface states for the x faces or $6(N-1)^2$ for all six faces or $6N^2-12N+6 \leqq 6N^2$ in all, the same as the number of surface atoms. These surface states form a band corresponding to the variations in energy of the two penetrating factors. Our reasoning indicates that $3N^2$ or half of these states will be occupied and we should therefore expect the surface band to be conducting in two dimensions just as a partially filled three-dimensional band is conducting.

The suppositions upon which the above considerations rest seem to be fulfilled for diamond. The work of Kimball[8] has shown that for diamond the $2s$ and $2p$ boundary curves have crossed to such an extent that there is a wide region of forbidden energies making diamond an insulator. We should, therefore, expect that there would be half-filled surface bands and surface conductivity in diamond. Such a conductivity has not been observed and this may possibly be due to the presence of adsorbed atoms. If a layer of adsorbed atoms is attached to the surface by losing electrons to the vacant levels in the surface band,[9] so many electrons might be added that the surface band would be completely filled and thus rendered nonconducting. The surface levels can enter into conduction in yet another way by acting as "impurity levels." Electrons in the normally filled states can be excited optically or thermally to the surface levels thus leaving a partially filled and therefore conducting band; similarly electrons can be excited from the surface levels to higher bands and thus enter into the conduction. The number of electrons involved in processes of this sort would depend upon the surface area of cracks in the crystal and would therefore lead to a structure sensitive behavior of the properties of semi-conductors. Considerations of this sort are not new in their general features; however, the fact that the surface levels will normally be half-occupied has not been shown before.

The forbidden regions between the x-ray levels do not arise from the crossing of the energy bands and our theory predicts no surface levels for them. There will be surface states of Goodwin's "tight binding" type in these energy gaps; they will lie very close to the allowed bands from which they originate. A similar situation exists between the highest occupied and lowest unoccupied bands of the alkali halide crystals (calculations for NaCl[10] and LiF[11] show that these gaps correspond to uncrossed bands). Even where there are no surface states of the type considered here, it is, of course, still possible for electrons to be trapped on the surface because of polarization forces and resulting distortion of the lattice. However, this is a rather different type of process from the one we have been considering, which is more directly connected with the energy levels of the periodic potential.

[8] G. E. Kimball, J. Chem. Phys. **3**, 560 (1935).

[9] See, for example W. G. Pollard, Phys. Rev. **55**, 1147(A) (1939) and also **56**, 324 (1939).

[10] W. Shockley, Phys. Rev. **50**, 754 (1936).

[11] D. H. Ewing and F. Seitz, Phys. Rev. **50**, 760 (1936).

The surface states should occur for a number of metals. In the metals there is always a large degree of overlapping of the atomic level boundary curves but not in such a way as to result in a separation of the bands. Instead the bands overlap considerably. For a particular direction of the propagation vector k, for example normal to a 110 crystal face of a body-centered lattice, there will be allowed and forbidden values of energy. In the forbidden regions there will be wave functions corresponding to complex values of k and, since the boundary curves have crossed, these will give rise to surface states. Fig. 3(a) shows the dependence of energy upon k for the 100 plane in k space for sodium.[7] The surface states correspond to values of k having real components corresponding to the edge of the Brillouin zone and an imaginary component perpendicular to the plane of the surface—the 110 plane in our example. The energy lies in the energy discontinuity at the edge of the zone. Fig. 3(b) shows qualitatively how the energy varies in the surface of the zone for the states of the first zone, the surface states, and the states of the second zone. We see that the lowest energy for the surface states is lower than the lowest energy in the second zone and higher than the lowest energy on the surface of the first zone. For the monovalent elements the first zone is only partially filled and all the electrons occupy states in the interior of the zone;[12] hence none have high enough energies to occupy surface states. In the divalent metals, however, some electrons occupy states in the second zone and therefore have energies higher than the lowest surface levels. On the basis of this reasoning we should expect that all metals save the monovalent ones to have some electrons occupying surface levels. These surface states will affect the charge distribution near the surface of the metal and their contributions must be considered when calculations of work function and contact potential are carried out for polyvalent metals.

The writer would like to express his gratitude to his colleague Mr. R. O. Grisdale and to Professor W. G. Pollard for several stimulating discussions upon the nature of the surface states.

[12] See, for example, N. F. Mott and H. Jones, *The Theory of the Properties of Metals and Alloys* (Oxford, 1936), Chapter V.

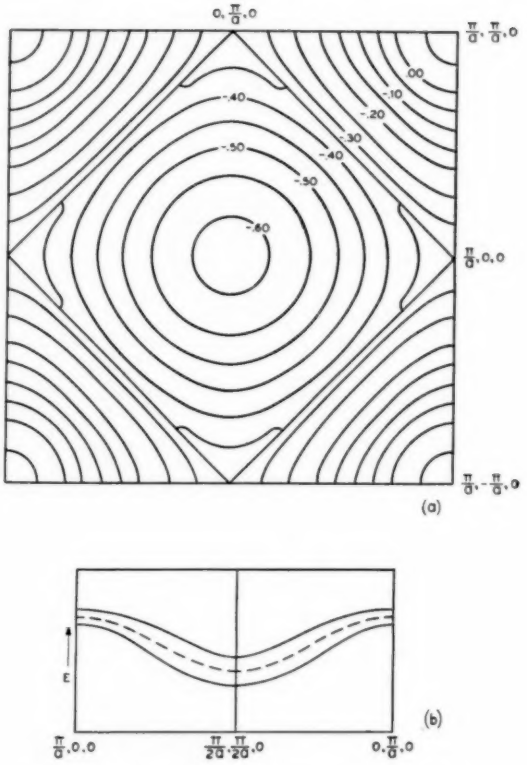

FIG. 3. Energies for surface states and penetrating states.

APPENDIX: MATHEMATICAL ANALYSIS

1. Expressions for the lattice functions

Let the center of the left-hand cell of Fig. 1(a) be $x=0$; then its edges are $x=\pm a/2$. For a given energy E there are only two linearly independent solutions of Schroedinger's equation in the field of this cell; since the potential is symmetrical about $x=0$, these may conveniently be chosen as $g(x)$ and $u(x)$ where g and u are, respectively, even and odd functions of x, i.e., symmetrical and antisymmetrical about $x=0$.

We shall require that the wave function be of the form $\psi_k=\exp(ikx)v(x)$ where $v(x+a)=v(x)$. If the function in the cell at $x=0$ is expanded in the form $\psi_k=ag(x)+ibu(x)$, then in the second cell it is $\psi=\exp(ika)(ag(x-a)+ibu(x-a))$ and the conditions that ψ and its derivative be continuous at the cell boundary $x=a/2$ are

$$ag+ibu=e^{ika}(ag-ibu), \tag{1}$$

$$ag'+ibu'=e^{ika}(-ag'+ibu'), \tag{2}$$

where

$$g=g(a/2), \qquad u=u(a/2),$$
$$g'=(dg(x)/dx)_{x=a/2}, \quad u'=(du(x)/dx)_{x=a/2}.$$

These equations can be solved only if their determinant vanishes. This gives the equation

$$\tan^2 ka/2=-\gamma/\mu, \tag{3}$$

where

$$\gamma=g'/g \quad \text{and} \quad \mu=u'/u.$$

This equation determines k as a function of γ and μ which in turn depend upon the energy. The wave function is multiplied in going from cell to cell by the factor

$$f=\exp 2i\theta \quad \text{where} \quad \theta=ka/2. \tag{4}$$

2. The value of ψ'/ψ for the running waves

We shall next find the value of

$$\frac{\psi_k'(a/2)}{\psi_k(a/2)}=\rho_k \tag{5}$$

for the resulting solution of Eq. (3). This ratio is

$$\frac{ag'+ibu'}{ag+ibu}=i\mu\tan\theta=\rho_k \tag{6}$$

as may be verified by noting that from (1) $b/a=(g/u)\tan\theta$ and by using (3).

3. The boundary conditions for the entire crystal

If $\psi_k(x)$ is a solution in the lattice field then

$$\psi_{-k}(x)=\psi_k(-x) \tag{7}$$

is also a solution for the same energy and, therefore, ψ_k and ψ_{-k} represent a complete set of linearly independent solutions (the pathological case of $\psi_k(-x)/\psi_k(x)=$constant occurs only for energies of the boundary curves; it introduces no new features and is formally included in the equations given below.) The general solution in the crystal is

$$\psi=A\psi_k+B\psi_{-k}. \tag{8}$$

This function must join continuously to wave functions for the outside region. These outside wave functions must, of course, be damped exponential waves as we proceed away from the surface. This means that the ratio of $\psi'/\psi=\sigma$ evaluated at $x=-a/2$ (the left edge of the crystal) is a definite single valued function of the energy. For the symmetrical array of n atoms the value of ψ'/ψ at $x=na+a/2$ (the right edge) must be $-\sigma$. For negative energies in Fig. 1, σ must be positive.

We must therefore satisfy the equations

$$\sigma=\frac{A\psi_k'(-a/2)+B\psi_{-k}'(-a/2)}{A\psi_k(-a/2)+B\psi_{-k}(-a/2)} \tag{9}$$

and

$$-\sigma=\frac{A\psi_k'(na+a/2)+B\psi'_{-k}(na+a/2)}{A\psi_k(na+a/2)+B\psi_{-k}(na+a/2)}. \tag{10}$$

Some algebraic manipulation leads to the result that these equations possess solutions if

$$\sigma=\mu\tan\theta\tan n\theta \quad (S), \tag{11}$$

$$\sigma=-\mu\tan\theta\cot n\theta \quad (A), \tag{12}$$

where the expressions (S) and (A) mean that the corresponding solutions are either symmetrical or antisymmetrical functions, i.e., even or odd, about the midpoint of the crystal. The odd and even character can be established by computing the ratio of the denominators of Eqs. (9) and (10). If Eq. (11) is satisfied, this ratio is $+1$; for (12) it is -1.

4. Determining the allowed solutions

In order to justify all the statements made in the first part of this paper, it is necessary to investigate the solutions of these equations for eight different types of allowed bands and four different types of forbidden bands and to carry this out twice; once for n even and once for n odd. For the purposes of this paper we shall consider only the cases represented by the lattice constants a_1 and a_2 in Fig. 2 and these only for n even. In Fig. 4(a) and (b) are shown the general trend of the γ and μ curves for these two lattice constants. The energy scales have been distorted so that the allowed and forbidden bands correspond for the two cases.

Three ranges of values for γ/μ must be considered I $\gamma/\mu<0$, II $0<\gamma/\mu<1$, III $1<\gamma/\mu$. For the first of these $\tan^2\theta$ is positive and θ lies between zero and $\pi/2$. The value of $\gamma/\mu=1$ cannot occur since it implies that g and u are not linearly independent. For II and III $\tan^2\theta$ is negative and we write θ in the form

$$\theta=\alpha-i\beta. \tag{13}$$

In Table I we have tabulated the expressions associated

TABLE I.

	I	
$\gamma/\mu<0$, $\beta=0$,		$\tan\alpha=\lvert(\gamma/\mu)^{\frac{1}{2}}\rvert$
$\tan\theta=\tan\alpha$		$f=e^{2i\alpha}$
$\tan n\theta=\tan n\alpha$		$\cot n\theta=\cot n\alpha$
	II	
$0<\gamma/\mu<1$, $\alpha=0$,		$\tanh\beta=\lvert(\gamma/\mu)^{\frac{1}{2}}\rvert$
$\tan\theta=-i\tanh\beta$		$f=e^{2\beta}$
$\tan n\theta=-i\tanh n\beta$		$\cot n\theta=i\coth n\beta$
	III	
$1<\gamma/\mu$, $\alpha=\pi/2$,		$\coth\beta=\lvert(\gamma/\mu)^{\frac{1}{2}}\rvert$
$\tan\theta=-i\coth\beta$		$f=-e^{2\beta}$
	n even	
$\tan n\theta=-i\tanh n\beta$		$\cot n\theta=i\coth n\beta$
	n odd	
$\tan n\theta=-i\coth n\beta$		$\cot n\theta=i\tanh n\beta$

with these three cases. The equations have been so written that positive values will be obtained for α and β; there is no loss in generality in this since both positive and negative values of k occur in (8). In Table II we give the values to

TABLE II.

	I	
$\sigma/\mu=\tan\alpha\tan n\alpha$		(S)
$\sigma/\mu=-\tan\alpha\cot n\alpha$		(A)
	II	
$\sigma/\mu=-\tanh\beta\tanh n\beta$		(S)
$\sigma/\mu=-\tanh\beta\coth n\beta$		(A)
	III	
	n even	
$\sigma/\mu=-\coth\beta\tanh n\beta$		(S)
$\sigma/\mu=-\coth\beta\coth n\beta$		(A)
	n odd	
$\sigma/\mu=-\coth\beta\coth n\beta$		(S)
$\sigma/\mu=-\coth\beta\tanh n\beta$		(A)

which $\tan\theta\tan n\theta$ and $-\tan\theta\cot n\theta$ reduce for these ranges.

The method employed in finding the solutions is a qualitative graphical one. Fig. 4(c) represents the variations

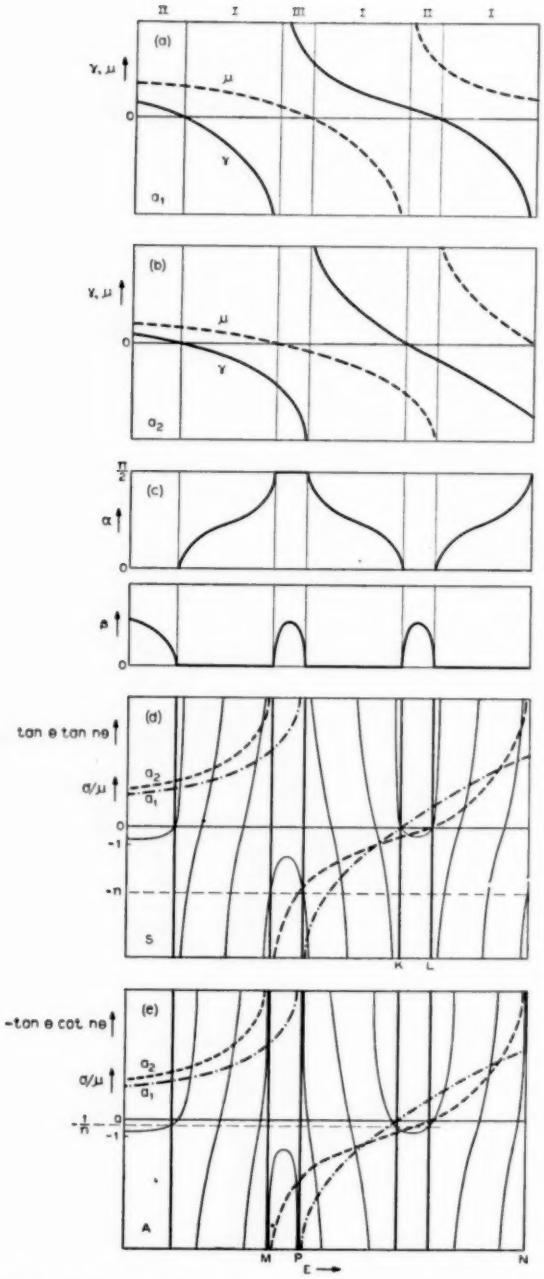

FIG. 4. Graphical results of the analysis. (*a*) γ and μ *vs.* E for $a=a_1$. (*b*) γ and μ *vs.* E for $a=a_2$. (*c*) α and β *vs.* E for $a=a_1$ and $a=a_2$. (*d*) Plot corresponding to Eq. (11). (*e*) Plot corresponding to Eq. (12).

of α and β which are qualitatively the same for Fig. 4(*a*) and (*b*). In Fig. 4(*d*) is plotted $\tan\theta \tan n\theta$ for the (S) type functions for the case of six atoms. Also on this figure are shown curves of σ/μ for both a_1 and a_2 lattice constants. For energies below zero on Fig, 1, σ will be a monotonically decreasing positive function of the energy and the variations in σ/μ will arise chiefly from those of μ. Inersections of σ/μ and $\tan\theta \tan n\theta$ on Fig. 4(*d*) correspond to solutions of (11) except for two indeterminate cases occurring at the energies marked K and L in Fig. 4(*d*); these correspond to $\mu=\infty$ and a study of Eq. (11) for them shows that the right side is proportional to $1/n$ and hence that 1 and 2 are not solutions of (11). In Fig. 4(*e*) are similar curves for the A functions. The curve for a_1 at M and N and the curve for a_2 at P in the figure can be shown to give no solutions of Eq. (12). It is not practical to draw figures corresponding to large values of n as some of the significant features of Fig. 4 would not be apparent. However, in reaching the conclusions given in this paper, it has been supposed that n is very large; this means that $|1/n|$ and $|n|$ are surely lesser and greater than $|\sigma/\mu|$ in Fig. 4(*e*) and (*d*), respectively.

From consideration of the significant intersections on Fig. 4(*d*) and (*e*), one can establish the results portrayed in Fig. 2 and similar considerations for other values of n render these conclusions general.

The result that no surface states exist for the energy gap at a_1 can be established without recourse to the mathematical methods leading to Eqs. (11) and (12). Since this proof gives a more intuitive notion of the condition for the existence of surface states, it is given here: For any given energy value in the gap between bands in Fig. 2, γ and μ are positive and only damped waves are possible (this follows from Eq. (3)). The two solutions for the crystal are damped waves, one damped to the right and one to the left. Furthermore these waves can be taken as real as may be seen from the equation $b/a=(g/u)\tan\theta$. (Also if the waves could not be made real by multiplying by a constant factor, the real and imaginary parts would be linearly independent and our one-dimensional Schroedinger equation in the lattice would have four linearly independent solutions—an impossibility.) Consider the right edge of the crystal and choose $g(x)$ and $u(x)$ so that $g=u=1$, then $g'=\gamma$, $u'=\mu$. In order to have a surface state at the right edge, the wave function must consist predominantly of a wave damped to the left: if the crystal is large, the wave damped to the right is negligible at the right edge. Hence the wave function must be larger on the right edge than on the left edge of each cell. These various statements together mean that it must be of the form $Ag(x)+Bu(x)$ in the cell where A and B have the same sign (positive for simplicity) so that on the right edge the value $A+B$ is larger in absolute value than $A-B$ on the left edge. This requirement means that the slope on the right edge, $A\gamma+B\mu$, is also positive (since in the gap at a_1, γ and μ are positive). The above reasoning shows that if a surface state exists on the right edge of the crystal and has a positive value on the right edge of the last cell it has also a positive slope, i.e., $d\psi/dx>0$ at $x=(n+\frac{1}{2})a$. This wave function must join a wave function from the outside and if the energy is below zero the slope to value ratio for this outside wave function, denoted by $-\sigma$, is certainly negative. It is, therefore, impossible to join the two wave functions with continuous values and slopes and hence no surface states can exist for this energy gap. The situation is different for the gap at a_2 because there γ and μ are both negative and hence the ratio of slope to value for the wave function in the lattice

is negative at the right edge and a solution is possible. In order to prove that solutions actually do occur, considerations like those of Fig. 4 are needed.

5. Comparison with the case of almost free electrons

For the case of free electrons all the boundary curves have just crossed. This must be true because otherwise one would have the absurd result of forbidden energy ranges for free electrons; it can also be seen by considering the g and u wave functions corresponding to the boundary curves of Fig. 2. In the notation of section 1 of the appendix these are

$$g_m(x)=\cos \pi mx/a, \quad u_m(x)=\sin \pi mx/a. \tag{14}$$

Even values of m including zero give the bottoms of g bands and, except for $m=0$, the tops of u bands; odd values of m give the tops of g bands and bottoms of u bands. For free electrons the energy depends only on the value of m and we see that the bands are just crossed.

Goodwin, following the work of Maue, finds that if a potential of the form

$$V=-V_m(-)^m \cos 2\pi mx/a \tag{15}$$

is present, there will be surface states in the energy gap which appears at the energy corresponding to the unperturbed g_m and u_m if V_m is positive but not if V_m is negative. A first-order perturbation calculation shows that for V_m positive this potential raises the energy of g_m and lowers that of u_m if m is odd; for m odd g_m is the top of a g band and u_m the bottom of a u band. Hence the perturbation causes the bands to cross. A similar crossing occurs for m even. For V_n negative the bands are uncrossed and we have no surface states. Hence the findings of Maue and Goodwin for the case of almost free electrons are in keeping with the results of Fig. 2.

6. Comparison with Tamm's potential

In Fig. 5(a) we show the potential which Tamm used in his original paper on surface states. The heavy lines represent δ-function potentials. Tamm's potential is not periodic for the last cell is incomplete. In Fig. 5(a) we have constructed a periodic potential from Tamm's potential by attributing one-half a δ-function to each edge of each cell. There is a negative half of a δ-function left over at the left edge of the crystal. Now a first-order perturbation calculation using the wave function of Section 4 shows that this potential corresponds to uncrossed bands. The Tamm states arise because of the negative δ-function which is left over. For the case of uncrossed bands we found a negative value of ψ'/ψ at the left edge of the crystal for a wave function which decayed exponentially into the crystal. Since the value of ψ'/ψ was positive for the exponential outside and to the left of the crystal, no surface state could occur. The role of left-over δ-function is to reverse the value of ψ'/ψ before it reaches the edge of the cell and thus permit the existence of a surface state.

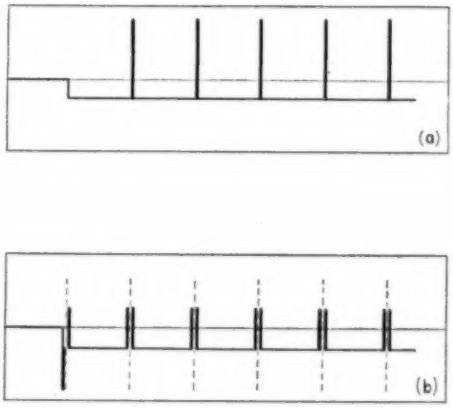

FIG. 5. (a) Tamm's potential. (b) The periodic and symmetrical potential equivalent to Tamm's.

Use of Surface States to Explain Activated Adsorption

W. G. POLLARD
University of Tennessee, Knoxville, Tennessee

(Received June 26, 1939)

A theory is advanced connecting activated adsorption with electron surface states in solids. The theory is constructed for H_2 but the suggested mechanism would work equally well for other molecules. It is supposed that H atoms interact with surface electron states of the solid when the atom gets close enough to make the latter stable. The stability condition for surface states and its relation to the position of the visiting H atom is investigated in some detail. If the energy of the surface state is low enough, the atom will on reaching the critical distance for stability transfer its electron to the surface state with considerable reduction in total energy. At close distances, exchange sets in. The energy of the various interactions is calculated approximately on the basis of a simplified model of the surface potential field and the surface state wave function. By using a reasonable form for the repulsion between the H nucleus and the positive cores in the metal, total energy curves whose minima lie at depths up to 2.5 volts are obtained. An H_2 molecule with sufficient energy may get close enough to the surface to come into the range of interaction of the H atoms with surface states. When this happens the molecule can split into atoms and be bound as such to the surface. The present theory of this interaction seems to be capable of properly accounting for the observed heats of activated adsorption of H_2.

A TENTATIVE theory of activated adsorption has been proposed by Lennard-Jones.[1] It is assumed that the adsorption of systems with unsaturated valencies is accomplished through a lowering of the surface potential of the solid in the immediate neighborhood of the visiting atom. This would give rise to a localized potential hole in which electrons would be caught and enter into normal exchange binding with the visitor. The forces involved would be large and the binding energy of the same order as in diatomic molecules. For molecules with completed bonds an activation energy is involved. The process in the case of H_2 on a metal is best described in terms of Fig. 1 (which is very similar to Fig. 3 in Lennard-Jones' paper[1]). The curve (m) represents qualitatively the normal interaction through van der Waals or polarization forces of an H_2 molecule with a metal M. The other curve (a) represents the much stronger interaction discussed above between two H atoms and the metal. The separation of the two curves at infinity is the dissociation energy D of the molecule. Consider a molecule approaching the metal with total energy W. If W is sufficient for it to reach the intersection G of the curves (m) and (a) (i.e., $W=A$), it can dissociate without changing its total energy. The individual H atoms would then follow the atomic curve (a) to their respective minima where they take up vibrational energy W'. The observed heat of adsorption will be $E=Q+W-W'$ or simply $Q+A$ when the vibrational energy W' is neglected. The combined binding of the two H atoms must be $Q+D$. In order to give a satisfactory explanation of activated adsorption, therefore, any theory of the interaction between the atom and the surface must account for a binding of the order of $\frac{1}{2}(D+E-A)$. The mechanism by which the H_2 bond is broken and bonds between the separate H atoms and the surface are substituted for it has been discussed by Sherman and Eyring[2] from the standpoint of the latter's theory of activation energy in chemical reactions.

It is the purpose of this paper to investigate the nature of possible interactions between monatomic hydrogen and metal surfaces with a view to determining the mechanism which gives rise to the curve (a) in Fig. 1. We begin with a general consideration of electronic surface states in solids.

In the periodic potential field of a crystal lattice the solutions of Schroedinger's equation for an electron are the well-known Bloch functions

$$\psi(\mathbf{r})=u(\mathfrak{y},\mathbf{r})\exp[\mathfrak{y}\cdot\mathbf{r}], \qquad (1)$$

where $\mathfrak{y}$ is in general complex and $u(\mathfrak{y},\mathbf{r})$ is periodic with the lattice period. The total energy of the electron with this wave function is a function of $\mathfrak{y}$. For an infinite crystal there are a number of ranges or bands of the total energy

[1] J. E. Lennard-Jones, Trans. Faraday Soc. **28**, 341 (1932).

[2] A. Sherman and H. Eyring, J. Am. Chem. Soc. **54**, 2661 (1932).

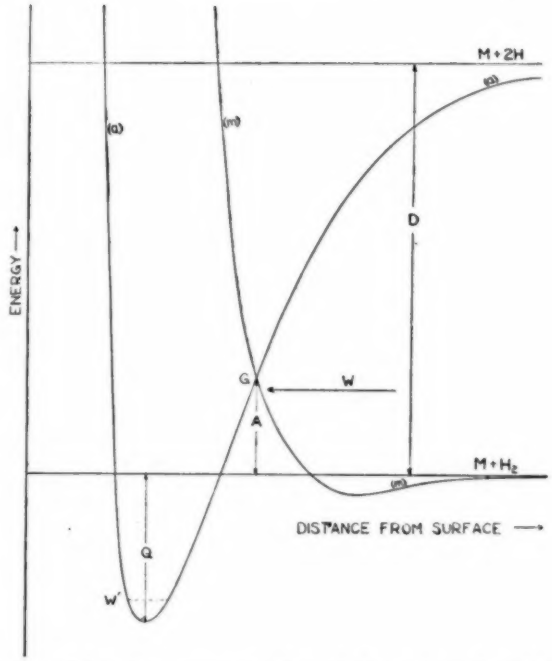

FIG. 1. Schematic representation of the proposed mechanism of activated adsorption.

for which all three components of $\mathfrak{y}$ are pure imaginary so that $\mathfrak{y}=i\mathbf{k}$ with $\mathbf{k}$ real. In these solutions the function $u(\mathbf{k}, \mathbf{r})$ represents the atomic wave function of the electron around each lattice point and goes into the corresponding isolated atom wave function upon infinite separation of the lattice points. The function $\exp[i\mathbf{k}\cdot\mathbf{r}]$ represents a modulation of the function $u(\mathbf{k}, \mathbf{r})$ and is associated with the continual transfer of electrons from one lattice point to another. These solutions make up the totality of stationary states in the interior of crystalline solids.

When, however, the crystal is regarded as being of finite size and its surface is taken into account, stationary solutions involving one real component of $\mathfrak{y}$ are possible. This was first pointed out by Tamm.[3] These solutions represent a state of motion in which the electron is confined to the surface with its wave function exponentially damped both into and out from the surface but free to move over it. They are obtained from the family of solutions (1) by choosing the component of $\mathfrak{y}$ normal to the surface real, taking the other two pure imaginary, and fitting the resulting function smoothly across the boundary to the exterior solution.

[3] Ig. Tamm, Physik. Zeits. Sowjetunion **1**, 733 (1932).

Tamm employed a semi-infinite periodic potential of the Kronig and Penny type. Let E be the energy of the surface state, V_s the rise in potential at the surface, and p the Kronig and Penny parameter measuring the magnitude of potential fluctuations in the lattice. The essential features of his solution may be stated as follows: (a) Surface states exist only for those values of the energy which satisfy

$$E \gtrless V_s - \hbar^2 p^2 / 2ma^2, \qquad (2)$$

where a is the lattice period. (b) For all energies satisfying (2), there exists one and only one surface state in each "forbidden" region or energy gap between allowed bands of the interior states.

These states have since been studied by several investigators,[4] and it has been shown that the second property (b) above has to be altered for a finite lattice with a surface at each end to make the surface states occur in pairs. Recently Shockley[5] has made quite a detailed study of these states, and has described the manner in which they originate from the atomic levels of the isolated atoms as the lattice distance is continuously decreased from very large values. The energy minimum (a) imposed on the surface states is formulated in a much more general and precise way. As the atoms composing the lattice approach each other, the isolated atom levels broaden and finally intersect. The electronic bands on either side of the intersection are separated with forbidden regions between. The levels associated with surface states, however, can originate only after the point of intersection has been reached. In actual crystals at their equilibrium configuration the bands above a certain energy will have intersected and all below will not. This energy corresponds to the minimum imposed by condition (2).

In the application to adsorption with which this paper is concerned, the condition (2) is of considerable importance, and it is desirable to associate it as closely as possible with actual

[4] R. H. Fowler, Proc. Roy. Soc. **A141**, 56 (1933); S. Rijanow, Zeits. f. Physik **89**, 806 (1934); A. W. Maue, Helv. Phys. Acta **7**, supp. 2, 68 (1934), Zeits. f. Physik **94**, 717 (1935); E. T. Goodwin, Proc. Camb. Phil. Soc. **35**, 205 (1939). The reader is referred to the accompanying paper of Shockley's for a discussion of this work.

[5] W. Shockley, Phys. Rev. This issue. The author is greatly indebted to Dr. Shockley for the privilege of seeing his paper before publication.

solids. For this purpose the treatment presented in the appendix to this paper is useful. An approximate solution for the surface state wave functions is obtained there in the form

$$\psi(\kappa, \gamma; \mathbf{r}) = u(\kappa, \gamma; \mathbf{r}) \exp[i\kappa\cdot\varrho+\gamma z] \quad \text{inside the lattice } (z \leqslant 0)$$
$$= \sum_n c_n(\gamma) f_n(z) Q_n(\kappa, \varrho) \quad \text{outside the lattice } (z \geqslant 0) \tag{3}$$

with

$$Q_n(\kappa, \varrho) = v_n(\kappa, \varrho) \exp[i\kappa\cdot\varrho].$$

Here z is measured normal to the surface, ϱ is the radius vector parallel with the surface, κ a momentum vector parallel with the surface, and the functions $u(\kappa, \gamma; \mathbf{r})$ and $v_n(\kappa, \varrho)$ are periodic with the lattice period. The energy of the surface state is obtained by choosing the coefficients $c_n(\gamma)$ so that the interior and exterior solutions join at the surface, and then determining γ to make them join smoothly. It is shown that this process leads to a condition similar to (2).

The parameter σ in Shockley's treatment may be associated with Tamm's $[2m(V_s-E)]^{\frac{1}{2}}/\hbar$. Any mechanism which would lower V_s (such as, e.g., an H^+ ion close to the surface) would also lower σ. An inspection of Figs. 4(d) and 4(e) in Shockley's paper makes it clear that this would also improve the chances for an intersection of the σ/μ curve with the others in regions II and III where the surface states originate. This gives rise to a dependence of the minimum energy for surface states on the surface potential V_s which is qualitatively similar to that in (2). The other factor in (2) involving the parameter p would depend on Shockley's γ and μ but the connection between them is not evident.

Application to Adsorption

Consider the approach of an ion of charge Ze to a solid surface. If the solid is a dielectric the region of its surface immediately below the ion becomes polarized; if it is a metal, this region becomes negatively charged in such a way as to reduce the electric field in the interior of the metal to zero. The net effect in either case is an accumulation of electrons on the surface immediately below the visitor. Denote by β the normal distance between the surface and the ion. If for the moment we regard the "induced" surface charge as removed, it is clear that the surface potential V_s is reduced at the point immediately below the ion by an amount Ze/β. This creates a localized potential pocket in the part of the surface below the ion. The way in which this pocket is formed is discussed in detail in Lennard-Jones' paper.[6] One can picture how it arises by thinking of the superposition of the surface potential curve (drawn asymptotic to zero energy and rapidly falling near the surface) and the characteristic horn-shaped potential curve of a proton. The total potential formed by this superposition is reduced near the proton by the ordinate of the surface curve, and in the neighborhood of the surface by the ordinate of the proton curve. The latter reduction forms the pocket. If an electron were now placed on the ion it would distribute itself between the potential hole around the ion and the potential pocket in the surface. The amplitude of its wave function would be large around the ion, small between the ion and the surface, and large again in the neighborhood of the pocket. Since the depth, Ze/β, of the pocket increases with β, the amplitude of the wave function around the ion would decrease with β and that at the surface increase with β.

As measured by the amplitude of the wave function at the surface, it is evident that in this process a type of surface state gradually grows as the ion approaches. At large β this state would be negligible since the electron would remain almost entirely with the ion. The amplitude at the surface would not become appreciable until the depth of the surface hole became comparable with that of the ion. Thus the growth of the surface state would take place in a comparatively narrow range of β.

It is useful to consider the development of this type of state in terms of the surface states of an isolated solid discussed in the previous section. As the visiting core approaches the surface, a position β_0 will eventually be reached at which V_s will be lowered enough to satisfy (2) for a low-lying surface state. β_0 should be regarded as lying in the above narrow range of β. The character of the surface state formed in this way will, however, be quite different from those already con-

[6] Reference 1, p. 344.

sidered because the stability condition (2) will now hold only locally in a small region of the surface below the ion. This will have the effect of altering the character of the functions $Q_n(\kappa, \varrho)$ in Eqs. (3). Instead of being of the type $v_n(\kappa, \varrho) \exp[i\kappa\cdot\varrho]$ corresponding to free transmission over the surface, they must now be large only in a circle directly below the visiting ion with exponentially decreasing character outside. They will form a discrete set $Q_{nl}(\varrho)$ with integral l and have eigen energies

$$E_{il}=\sum_n c_n^2(\gamma_i)(W_n(l)+\epsilon_n)$$

associated with them rather than the $E_i(\kappa)$ of Eq. (29) in the appendix. In order to account for adsorption it is necessary to have one of these energies close to, or lower than, the lowest level of the visiting core. For hydrogen this means a surface state at -13 volts or lower which places it well below the conduction band.

These states are true surface states and would arise whenever the Eqs. (28) of the appendix could be satisfied for functions $Q_{nl}(\varrho)$ of the above type. They cannot, however, be very well interpreted in terms of those obtained by Shockley for an isolated crystal. The reason is that the local broadening of the bands caused by the visiting ion is of equal importance with the broadening arising from the degree of packing of the atoms in the crystal.

In what follows all energies are expressed in units of $Z^2e^2/2a_0$ and all lengths in units of a_0/Z where a_0 is the radius of the first Bohr orbit in hydrogen. Application is made only to the adsorption of H for which $Z=1$ but the results are given in terms of an ion of charge Ze for generality. In the presence of the visiting ion, condition (2) becomes

$$E \geqslant V_s - Ze^2/\beta - \hbar^2p^2/2ma^2.$$

Expressed in the above units with E measured on the basis that the potential energy of an electron far from the solid is zero (instead of the interior of the lattice as in Tamm's model), this condition for all points of the surface within a circle of radius ρ' becomes

$$E \geqslant -2(\beta^2+\rho'^2)^{-\frac{1}{2}} - (p/a)^2$$

or

$$(\beta^2+\rho'^2)^{\frac{1}{2}} \leqslant -2/[E+(p/a)^2]. \qquad (4)$$

The greatest value β_0 of β for which the surface state could exist is

$$\beta_0 = -2/[E+(p/a)^2] \qquad (5)$$

and the radius of the circle on the surface within which the stability condition is satisfied is

$$\rho' = (\beta_0^2-\beta^2)^{\frac{1}{2}}. \qquad (6)$$

The part $Q_{nl}(\varrho)$ of the surface wave function would be large within this circle and exponentially decreasing outside. This circle would have some limiting radius ρ_1 attained for $\beta=\beta_1<\beta_0$ below which no stationary solutions would exist. The surface state would not become possible then until the visiting core came as close as β_1 to the surface.

As the positive core approaches the surface it is attracted to it by a force whose potential at large distances is

$$\Phi_1(\beta) = -Z/2\beta. \qquad (7)$$

There is an accumulation of electrons in the surface immediately below the visiting core with density (number not charge) as given by classical electrostatics,

$$\sigma = Z\beta/[4\pi(\beta^2+\rho^2)^{\frac{1}{2}}]. \qquad (8)$$

This surface charge is in general contributed by the conduction band to reduce the internal electric field to zero. For large β, it has nothing to do with the surface states already discussed. The way in which it arises in quantum mechanics may be seen as follows. In the undisturbed metal the density of charge at any point is given by Fermi statistics as $8\pi[2m(H_0-U)]^{\frac{3}{2}}/3h^3$ where U is the self-consistent periodic potential in the lattice calculated from this charge density.[7] In the neighborhood of the surface this density falls off very rapidly. With a visiting positive charge near the surface, however, the potential U is reduced in the part of the surface nearest the charge. This automatically increases the density through the increase of the term $(H_0-U)^{\frac{3}{2}}$ in it.

When the visiting ion gets sufficiently close to the surface to have $\beta \leqslant \beta_1$, the surface state of low energy whose properties we have been considering becomes stable. If now a transition from the conduction band to this state were possible, it would become populated and the analog of the

[7] J. C. Slater, Rev. Mod. Phys. **6**, 238 (1934).

classical induced charge in the conduction band would become very small. It seems reasonable to identify $\int|\psi|^2dz$ for the surface state with the charge density (8). In the most important case $Z=1$, both integrate to just one electron and both peak at the same point. The local accumulation of charge in the surface state would behave electrically like the image of the visiting core in the metal. The result of a transition to this surface state on the interaction (7) would therefore be very slight.

With this behavior of the ion in mind, consider next the approach of a neutral atom. This is also attracted to the surface but with a force whose potential is[8]

$$\Phi_2(\beta)=-\langle r^2\rangle_{Av}/3Z\beta^3, \tag{9}$$

where $\langle r^2\rangle_{Av}$ is the average value of the square of the radius vector over the whole electron cloud in the visiting atom. The potential arises from interaction with the images in the metal of the dipoles formed by the electrons and nucleus of the visiting atom. In this case, however, a deficiency rather than an excess of electrons exists in the surface immediately below the visitor. When the value β_1 is reached so that the surface state in the field of the core is stable, the whole system can in general materially reduce its energy by transferring its outer electron across the potential barrier between atom and metal into the surface state of the metal. If the surface state has approximately the same energy as the vacated state in the atom, this electron can go into normal exchange between the two states. If the surface state has appreciably lower energy than the atom, the latter will remain ionized. In either case a one electron bond is formed similar to that in H_2^+ or NaCl, respectively.

A question which suggests itself here is whether by approaching closer the ion could not pick up another electron from the conduction band in the metal and so form a two-electron bond as in H_2 with further reduction in total energy. Except in very rare cases this would not happen for the following reasons. The surface state electron is held to the surface by the presence of the ion. In neutralizing the ion, the condition for the stability of the surface state would be destroyed. Even if this condition is ignored, there would be left on the surface a strong local concentration of negative charge in the surface state representing a considerable excess over the local *deficiency* normal for the neutral atom. This highly unstable distribution of charge would doubtless constitute an energy gain for the solid which would more than outweigh the decrease resulting from the neutralization of the ion.

It is important to point out here that these considerations apply only when the binding is dependent on the formation and preservation of the surface state. In cases where no localized surface state is present, such transfers often occur. Neutral atoms or molecules whose ionization potentials are smaller than the energy depth of the top of the conduction band or whose electron affinity is larger than this depth can, respectively, either transfer an electron to the conduction band or receive one from it. The atom or molecule is then converted into either a positive or negative ion and can be bound to its mirror image in the metal. Such processes have been observed experimentally[9] and they have been discussed theoretically by Gurney.[10] The interaction of an H atom with a surface state is similar to the interaction of an atom of small ionization potential with the conduction band. After the H atom has transferred its electron to the surface state, however, the system is similar to an atom of large electron affinity near the surface. The reason that no transfer from the conduction band takes place here lies in the screening of the positive ion by the surface state electron. Insofar as the latter fulfills the function of the classical induced charge, its screening is perfect since it everywhere raises the potential at the surface to the value it had in the absence of the ion.

Calculations with a simplified model

Let ψ_s represent the surface state wave function and ψ_a the wave function of the outer electron in the visiting atom. The wave function of the combined system may be taken to be

$$\psi=C\psi_s+D\psi_a. \tag{10}$$

For $\beta>\beta_1$ the surface state does not exist, the amplitude ψ around the surface pocket is very

[8] Reference 1, p. 334.

[9] See for example, J. A. Becker, Trans. Faraday Soc. **28**, 148 (1932).

[10] R. W. Gurney, Phys. Rev. **47**, 479 (1935).

small, and $C \leqq 0$ and $D \leqq 1$. When $\beta \to \beta_1$ and ψ_s becomes stable, the electron will transfer itself from the atom to the surface state so that after the transfer the coefficients will be $C \leqq 1$ and $D \leqq 0$. As the ion comes closer to the surface, the stability condition (4) becomes less stringent. Provided the two states have nearly the same energy, it will be possible for exchange to take place between them to a limited extent. At still closer distances, the stability of ψ_s is no longer a consideration and the electron will distribute itself between the two states in a manner which leads to the lowest energy. The coefficients C and D will then be determined by minimizing the energy.

As a rough approximation it seems reasonable to regard the limitations imposed by condition (4) as a measure of the degree to which free exchange may take place between the two states, i.e., the degree to which C may differ from unity. This may be accomplished by regarding the positive charge on the ion as $Ze(1-|D|^2)=Ze|C|^2$ instead of Ze as in (4). Inserting this in Eq. (4) and making use of the quantities β_0, and β_1 as introduced in Eqs. (5) and (6) there follows

$$(\beta^2+\rho_1^2)^{\frac{1}{2}} \leqslant \beta_0|C|^2$$

or

$$|C| \geqslant [1-(\beta_1^2-\beta^2)/\beta_0^2]^{\frac{1}{2}}. \qquad (11)$$

There will be some sufficiently small value of β which makes this lower limit on C equal to the value of C for which the energy is a minimum. For all smaller values of β, Eq. (11) will no longer be important and C will be determined by the energy minimum.

If $-V(\mathbf{r}_s)$ is the potential energy of an electron in the self-consistent field of the solid, the Hamiltonian for the electron in the field of solid and ion is

$$H=-\nabla^2+U_c-V(\mathbf{r}_s)-2/r_a,$$

where r_a is measured from the nucleus of the ion, and U_c is the interaction between the atomic core and what remains of the solid after exclusion of the surface state electron. The energy of the distribution (10) with this Hamiltonian becomes

$$E=[|C|^2H_{ss}+C^*DH_{sa}+CD^*H_{as} + |D|^2H_{aa}]/[1+2|C||D|\Delta], \qquad (12)$$

where Δ and the matrix elements of H have their usual meaning. They cannot be evaluated explicitly without introducing some assumptions about the form of the wave functions ψ_s and ψ_a, and the potential $V(\mathbf{r}_s)$. For ψ_a the simplest case to consider is that in which the atomic function is the $1s$ function $e^{-r_a}/\sqrt{\pi}$. For ψ_s we assume no more at present than that the surface state function is a solution of the equation

$$\nabla^2\psi_s+(E_s+V(\mathbf{r}_s))\psi_s=0.$$

The diagonal matrix elements then become

$$H_{ss}=E_s+U_c-\int(2|\psi_s|^2/r_a)d\mathbf{r}_a,$$

$$H_{aa}=E_a+U_c-(1/\pi)\int V(\mathbf{r}_s)\exp[-2r_a]d\mathbf{r}_s.$$

The integral in H_{ss} is the Coulomb interaction J_1 between the surface state electron and the visiting core. Inasmuch as we have identified the surface state charge density with the classical induced charge this is merely the interaction of the core with its image. It does not include the interaction U_c between the core and the metal exclusive of this image. Hence the classical expression (7) should be a fair approximation to it even for small β. Thus

$$H_{ss}=E_s+U_c-J_1, \quad J_1=Z/2\beta. \qquad (13)$$

The interaction J_2 represented by the integral in the expression for H_{aa} is the Coulomb interaction between the distribution $|\psi_a|^2$ and the solid exclusive of the surface state charge. Its evaluation requires an explicit assumption for the form of $V(\mathbf{r}_s)$. This interaction with exchange has been discussed by Bardeen[11] for electrons in the conduction band. Outside the metal it approaches the classical image potential of the electron $-1/2Z\xi$ in the units used here. Inside it is fairly constant but depends on the momentum of the electron. The presence of the ion near the surface does not matter since $V(\mathbf{r}_s)$ is the interaction with the solid after the image of the ion has been removed. The simplest form with the right properties is

$$V(\mathbf{r}_s)=V(\xi)=V_0 \quad \xi \leqslant 0,$$
$$V(\xi)=(1-e^{-\alpha\xi})/2Z\xi \quad \xi \geqslant 0, \qquad (14)$$
$$\alpha=2ZV_0.$$

[11] J. Bardeen, Phys. Rev. **49**, 653 (1936).

The interaction J_2 may then be expressed as

$$J_2=\tfrac{1}{2}\int_{-\infty}^{+\infty} V(\xi)(1+2|\beta-\xi|)e^{-2|\beta-\xi|}d\xi,$$

which may be evaluated without much difficulty. The result is

$$H_{aa}=E_a+U_i-J_2,$$

$$J_2=\frac{1}{4Z}\Big\{\frac{4\alpha}{4-\alpha^2}e^{-\alpha\beta}+\alpha\Big(\frac{1-\alpha}{2-\alpha}+\beta\Big)e^{-2\beta}$$
$$+(1+2\beta)e^{-2\beta}[\overline{Ei}(2\beta)-Ei(-(\alpha-2)\beta)]$$
$$+(1-2\beta)e^{2\beta}$$
$$\times[Ei(-(\alpha+2)\beta)-Ei(-2\beta)]\Big\}.^{*} \quad (15)$$

The exchange terms H_{as} and H_{sa} require for their calculation an explicit knowledge of the form of the surface state function ψ_s. Their evaluation is under any conditions quite difficult. The simplest case mathematically is that in which $\psi_s=\psi_a$. Unfortunately this does not give a very good approximation. The surface state function falls off exponentially both into the surface and out from it. In Shockley's solution the wave function outside the surface is approximately $\exp[-\sigma z]$ which, in our units and in case the surface state has the same energy as the visitor, becomes $\exp[-z]$. This is the same as $\exp[-r_s]$ along the normal to the surface through the visiting core. It is fortunately along this line that the integrand of the exchange integrals is a maximum. In this sense the approximation is good. But the variations parallel to the surface do not seem to be properly given by it. As we have seen ψ_s exhibits exponentially decreasing character outside a circle of radius ρ_1 in the surface. But if we are to judge the rate of this decrease by the classical expression for the induced charge density it is not nearly as large as $e^{-\rho}$. The fraction of an electron to be found in a cylinder of unit radius normal to the surface whose axis passes through the origin is 0.53 for the 1s function $e^{-r}/\sqrt{\pi}$. The corresponding fraction computed from the classical density, Eq. (8), with $Z=1$ is 0.05 when $\beta=2$, 0.15 when $\beta=1$, and 0.55 when $\beta=\frac{1}{2}$. Thus in the range of importance $1<\beta<4$ the approximation gives too strong a local concentration of charge parallel with the surface.

* A definition and tabulation of the functions $\overline{Ei}(x)$ and $Ei(-x)$ may be found in Jahnke and Emde, *Tables of Functions* (Teubner, Second Edition, 1933), pp. 78–86.

TABLE I. *Values of the Coulomb, exchange, and overlap integrals in Rydberg units $e^2/2a_0$ for the case $Z=1$ and $\alpha=4$ tabulated as functions of β in units of the first Bohr orbit radius a_0.*

β	J_1	J_2	K	J	H	Γ	Δ
0.5	1.000	1.078	1.244	1.039	0.039	1.001	0.960
1.0	.500	.750	.970	.625	.125	1.011	.858
1.5	.333	.514	.676	.423	.090	1.014	.725
2.0	.250	.360	.470	.305	.055	1.012	.586
3.0	.167	.202	.210	.185	.018	1.007	.348
4.0	.125	.138	.086	.131	.006	1.005	.189

In the absence of detailed knowledge of the form and properties of ψ_s and the potential $V(\mathbf{r}_s)$, it seems useless to try for anything beyond a rough idea of the magnitude of the results. For this purpose, the fact that $\psi_s=(1/\pi)^{\frac{1}{2}}\exp[-r_s]$ is best in the region which contributes most to the integral is sufficient. The only case of importance in the exchange terms is $E_s \leqq E_a$. When $E_s<E_a$ the important term is H_{ss}. When $E_s>E_a$ the atom is unaffected by the presence of the surface state and no adsorption from this source would result anyway. With these approximations and limitations, the result is

$$H_{sa}=H_{as}=(E_a+U_i)\Delta-K,$$

where

$$K=(1/\pi)\int V(\mathbf{r}_s)\exp[-(r_s+r_a)]d\mathbf{r}_s. \quad (16)$$

The integral for K is best evaluated by transforming to elliptic coordinates. Introducing the expressions (14) for $V(\mathbf{r}_s)$, the integral is written

$$K=(\beta^2/4Z)\int_1^{\infty} e^{-\beta\xi}d\xi\Big\{(\alpha\beta/2)\int_{-1}^{-1/\xi}(\xi^2-\eta^2)d\eta$$
$$+\int_{-1/\xi}^{+1}[1-e^{-\frac{1}{2}\alpha\beta(1+\xi\eta)}]$$
$$\times[(\xi^2-\eta^2)/(1+\xi\eta)]d\eta\Big\}.$$

The second integral in $\{\}$ may be simplified by the substitution $y=\frac{1}{2}\alpha\beta(1+\xi\eta)$. The evaluation from here on is complicated but straightforward. The result is

$$K=\frac{1}{4Z}\Big\{\Big[\Big(1+\alpha+\frac{2}{\alpha^2}\Big)+\Big(\frac{\alpha^2-4}{2\alpha}-\frac{2}{\alpha^2}\Big)\beta$$
$$+\Big(\frac{7}{4}+\frac{12-\alpha^2}{6\alpha}\Big)\beta^2+\frac{\alpha-9}{12}\beta^3-\frac{\alpha}{12}\beta^4\Big]e^{-\beta}$$
$$+\Big[\frac{\alpha^2-4}{2\alpha^2}+\frac{\alpha+2}{\alpha}\beta-\frac{3}{4}\beta^2-\frac{\alpha}{12}\beta^3\Big]\beta^2Ei(-\beta)$$
$$-\beta^2P(\alpha,\beta)+(1+\beta)e^{-\beta}(\ln\gamma\alpha\beta-Ei(-\alpha\beta))$$
$$+e^{\beta}[Ei(-(\alpha+2)\beta)-(1-\beta)Ei(-2\beta)]$$
$$-\frac{\alpha\beta^2(2+\alpha)+4(1-\beta)}{2\alpha^2}e^{-(1+\alpha)\beta}$$
$$-\frac{\alpha\beta(2+\alpha)-2(2-\alpha)}{2\alpha^2}(1+\tfrac{1}{2}\alpha)\beta^2e^{-\frac{1}{2}\alpha\beta}$$
$$\times Ei(-(1+\tfrac{1}{2}\alpha)\beta)\Big\}, \quad (17)$$

where

$$P(\alpha,\beta)=\int_1^{\infty}[\ln\tfrac{1}{2}\gamma\alpha\beta(1+\xi)$$
$$-Ei(-\tfrac{1}{2}\alpha\beta(1+\xi))]e^{-\beta\xi}d\xi/\xi^3.$$

This function was evaluated by numerical integration. γ is Euler's constant.

The electronic part of the energy exclusive of E_a and the interaction U_c of the cores of solid and atom is

$$W_e=E-E_a-U_c.$$

This becomes on substitution of Eqs. (13), (15), and (16) in Eq. (12) for real C and D

$$W_e=-\frac{C^2J_1+D^2J_2+2CDK}{1+2CD\Delta}. \quad (18)$$

In minimizing this expression with respect to C and D it is convenient to introduce the following quantities

$$J=\tfrac{1}{2}(J_1+J_2),$$
$$H=\tfrac{1}{2}(J_2-J_1), \quad (19)$$
$$\Gamma=[1+H^2(1-\Delta^2)/(K-J\Delta)^2]^{\frac{1}{2}}.$$

In terms of these the minimum value of W_e is

$$W_e=\frac{J-K\Delta+(K-J\Delta)\Gamma}{1-\Delta^2}. \quad (20)$$

The percent ionization, χ, of the visiting core is

$$\chi=100(1-D^2)=100C^2.$$

When C is given its limiting value in Eq. (11) and for simplicity β_1 is taken equal to β_0, this is

$$\chi=100\beta/\beta_0. \quad (21)$$

For the case in which C is determined to give W_e its minimum value, however, the percent ionization is given by

$$\chi=\frac{50(K-J\Delta)(1-\Gamma\Delta)^2}{(\Gamma-\Delta)[(K-J\Delta)(\Gamma-\Delta)+H(1-\Delta^2)]}. \quad (22)$$

Computations were made for the special case $Z=1$ and $\alpha=4(V_0=2)$. In this case the visitor is a hydrogen atom, the energy is in the usual Rydberg unit $e^2/2a_0$, and β is in units of a_0. In Table I, the values of the various interactions computed from Eqs. (13), (15), (17), and (19) with these values of the parameters are given as functions of β.

In the upper part of Fig. 2 the percent ionization of the visiting atom is plotted against β. The full curve is a plot of Eq. (22) for the case giving minimum energy. The broken curves are plots of Eq. (21) for $\beta_0=1.5$, 2, 3, and 4. In the figure χ is shown to rise discontinuously from 0 to 100. Actually the rise would take place rapidly in a short interval of β around the value β_0, and would, doubtless not go all the way to $\chi=100$. However, the energy curves are not particularly sensitive to this behavior and the energy minima obtained later would not be appreciably affected by it. In the lower part of Fig. 2 the energy W_e is plotted as a function of β under various conditions. The upper full curve represents the interaction J' of the neutral atom, Eq. (9), before the surface state becomes stable. In this case it is simply $-1/\beta^3$. The lower full curve gives the minimum value of W_e, Eq. (20), in the presence of the surface state, and with $E_s=E_a$. The dotted curve represents the energy $W_e=-J_1$ for the case $E_s<E_a$. The broken curves are plots of Eq. (18) with C given by its minimum value in Eq. (11) (when $\beta_1=\beta_0$) for the same values of β_0 above. Each curve is joined to the minimum energy curve when the corresponding value of C is reached. For comparison the corresponding contribution for H_2^+

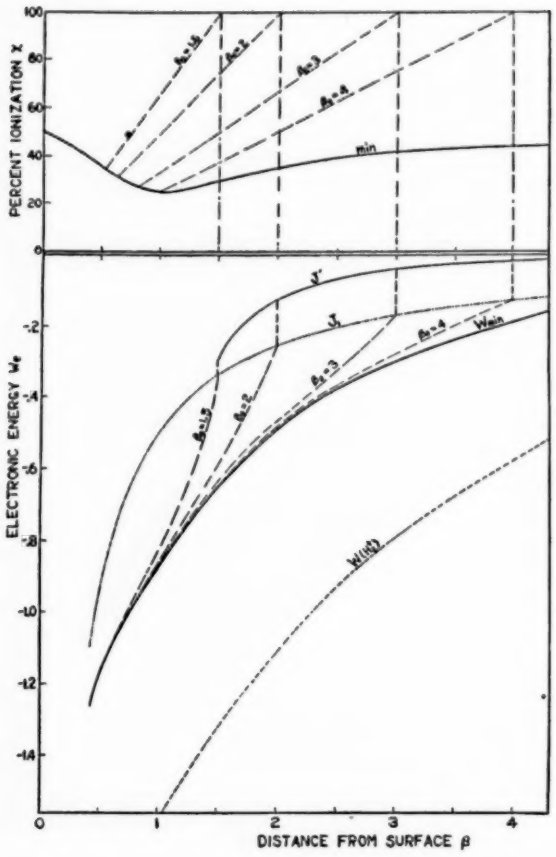

FIG. 2. Upper part: Percent ionization of the hydrogen atom as a function of its distance from the surface. Full curve for minimum energy and broken curves determined by the stability condition. Lower part: Upper full curve J' is classical image interaction of a neutral H atom with the metal and the dotted curve J_1 the corresponding interaction of an H ion. The lower full curve is the minimum electronic energy and the upper broken curves are this energy determined by the stability condition. The lower broken curve is the corresponding term for the hydrogen molecular ion.

$$W(H_2^+) = -2[(1/\beta) - (1+(1/\beta))e^{-2\beta} + (1+\beta)e^{-\beta}]/[1+(1+\beta+(1/3)\beta^2)e^{-\beta}]$$

is shown in the dashed curve.

At first sight it appears that the binding energy is considerably less than in H_2^+. But this may not at all be the case. In H_2^+ there is superposed on the electronic energy W_e a strong repulsion of the two nuclei. In this case no such repulsion exists at large distances. The interaction is given entirely by the electronic energy W_e until the visiting core actually penetrates the electron clouds of the surface atoms. The character of the repulsion due to this penetration depends also on whether the adsorption occurs above a lattice point or on a space intermediate between lattice points. Thus the repulsive term U_e is of much shorter range in this case than in H_2^+ where it is $2/\beta$. From the standpoint of its source in the penetration by the ion of the electron clouds extending from the surface, U_e for this case would presumably be of the approximate form $(2/\beta)\exp[-\beta/b]$. Without attempting to determine a particular value of b, the depths and positions of the minima formed by the superposition of the W_e curves in Fig. 2 and this term were obtained for different β_0. The values so obtained are plotted as functions of b in Fig. 3. For convenience, the equilibrium energy and separation are given in kilogram calories per mol and angstroms, respectively, as well as in the units used here.

Comparison with Experiment

Activated adsorption of H_2 on Cu and Ni has been observed by Benton and White[12] with heat of adsorption from 10,000 to 30,000 calories. Beebe *et al.*[13] give 11,000 to 12,000 calories for the heat of adsorption of H_2 and D_2 on Cu. For H_2 on zinc oxide, Taylor and Sickman[14] give a heat of adsorption of 21,000 calories with activation energies ranging from 7000 calories to 15,000 calories depending on the temperature and the fraction of surface covered. The heat of the low temperature molecular adsorption represented by the minimum in curve (*m*), Fig. 3, is in this case 1100 calories. Taylor and Williamson[15] have examined H_2 on manganous oxide and manganous-chromic oxide. The heat of adsorption on the latter at low temperatures is 1900 calories while at high temperatures the heat of activated adsorption is 20,000 calories per mol. The activation energies are respectively 19,000 and 10,000 calories on the two adsorbates. Kingman[16] obtained 30,000 calories activation energy for H_2 on charcoal.

The theory in the form presented here cannot hope to account for the specific properties of activated adsorption of H_2 on particular

[12] A. F. Benton and T. A. White, J. Am. Chem. Soc. **52**, 2325 (1930).
[13] R. A. Beebe *et al.*, J. Am. Chem. Soc. **57**, 2531 (1935).
[14] H. S. Taylor and D. V. Sickman, J. Am. Chem. Soc. **54**, 611 (1932).
[15] H. S. Taylor and A. T. Williamson, J. Am. Chem. Soc. **53**, 2177 (1931).
[16] F. E. T. Kingman, Trans. Faraday Soc. **28**, 269 (1932).

adsorbates. It should, however, be capable of accounting for heats of adsorption between 10,000 and 30,000 calories per mol and for activation energies between 5000 and 30,000 calories. The latter are easily accounted for by Lennard-Jones' proposed mechanism since the intersection G of curves (a) and (m), Fig. 3, is subject to considerable variation. It could easily occur for values of the activation energy A between, say, 0 and $\frac{1}{2}D$ which for H_2 gives it a range of 50,000 calories. To account for the former, use is made of the result obtained at the outset that the required binding per mol of atomic hydrogen adsorbed in the activated state is $\frac{1}{2}(D+E-A)$. The above ranges of E and A mean a maximum range in $E-A$ of $-20{,}000$ to $+25{,}000$ calories. Since D is 103,000 for H_2, this means that a binding between 40,000 and 65,000 calories per mol of H is needed to account for the observed activated adsorptions of H_2. An inspection of Fig. 3 shows that for $\beta_0 \gtrsim 3$ this range of binding energy is obtained for values of b between 1.5 and 2.0. This is a highly probable range for the parameter b.

The model employed here is of course a rather crude representation of the actual conditions and the form assumed for the repulsive term U_c is only a very rough approximation to the truth. It would be unwise, therefore, to draw any conclusions from the curves of Fig. 3 as to the actual values or ranges of values of the parameters β_0 and b to be associated with observed adsorptions.

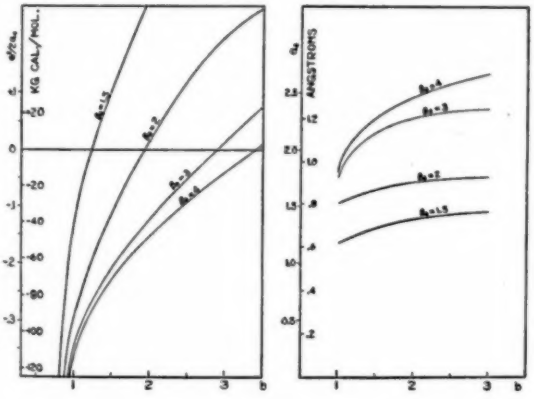

FIG. 3. Left: Value of the energy minimum in Rydberg units $e^2/2a_0$ and kilogram calories per mol as a function of the parameter b in the assumed repulsive potential $U_c=(2/\beta)\exp[-\beta/b]$. Right: Position of the energy minimum in atomic units a_0 and in angstroms as a function of b.

But it does seem possible to conclude that the proposed scheme of binding to surface states leads to the right order of magnitude of binding energy and gives enough flexibility to account for the wide range in the observed values of E and A.

In conclusion the author wishes to express his gratitude to Dr. William Shockley for the priviledge of seeing and using his paper on surface states before publication and for his several helpful criticisms of this paper.

APPENDIX

In the interior of a crystal lattice the potential may be expressed in the usual Fourier series and the solution has the general form (1). If the surface of the solid is regarded as lying in the x, y plane with the origin in the surface, then the wave function analogous to Shockley's one-dimensional case may be written for the interior

$$\psi_i(\mathbf{r})=u(\mathbf{r})\exp[\gamma z+ik_x x+ik_y y];\quad z\leqslant 0. \tag{23}$$

Outside the solid, the potential may be expanded as

$$V(\mathbf{r})=V_{00}(z)+\sum_{\mathbf{g}} V_{\mathbf{g}}(z)\exp[2\pi i\mathbf{g}\cdot\boldsymbol{\rho}], \tag{24}$$

where $\boldsymbol{\rho}$ is the vector (x, y) and $\mathbf{g}$ is a two-component vector drawn to points of the reciprocal lattice of the surface. The Schroedinger equation for this potential function is not separable and hence its solutions are rather difficult to discuss even approximately.

We denote by $\boldsymbol{\kappa}$ the vector (k_x, k_y) and by $\psi_e(\mathbf{r})$ the solution of Schroedinger's equation in the region exterior to the surface. The fitting at the surface where $z=0$ is performed by making

$$\psi_e(\boldsymbol{\rho}, 0)=u(\boldsymbol{\kappa}, \gamma; \boldsymbol{\rho}, 0)\exp[i\boldsymbol{\kappa}\cdot\boldsymbol{\rho}]$$

and

$$\gamma=[(\partial/\partial z)\ln(\psi/u)]_{z=0}. \tag{25}$$

The second of these conditions means that in the neighborhood of $z=0$, $\psi_e(\mathbf{r})$ must have the form

$$\psi_e(\mathbf{r})=f(z)h(\boldsymbol{\rho})u(\mathbf{r})$$

in order to make the fitting possible for all $\boldsymbol{\rho}$. By comparison with the first of the conditions (25), this means that

$$\lim_{z\to 0}\psi_e(\mathbf{r})=f(z)u(\boldsymbol{\kappa}, \gamma; \mathbf{r})\exp[i\boldsymbol{\kappa}\cdot\boldsymbol{\rho}]$$

with

$$f(0)=1.$$

It is possible to introduce an alteration of the potential (24) which makes the Schroedinger equation separable. The basis for the alteration is the observation that the periodic variations with ϱ of the potential of an electron in the surface field must be fairly rapidly damped out with increasing distance from the surface. As a first approximation it is therefore quite proper to neglect all terms in (24) except the first $V_{00}(z)$. The electron wave function in this field is then quite simple being given by

$$\psi_e(\mathbf{r}) = f_n(z) \exp [i\boldsymbol{\kappa}\cdot\boldsymbol{\varrho}]$$

with

$$\frac{d^2 f_n}{dz^2} + \frac{2m}{\hbar^2}(E_n^0 - \hbar^2|\boldsymbol{\kappa}|^2/2m - V_{00}(z))f_n = 0. \quad (26)$$

It is convenient to denote the eigenvalues of this equation by $\epsilon_n = E_n^0 - \hbar^2|\boldsymbol{\kappa}|^2/2m$. The subscript n enumerates a set of solutions of Eq. (26) which are regular at infinity and appropriate for the fitting involved in Eqs. (28).

As a second approximation we regard the neglected terms in the potential (24) as a perturbation. The first-order correction to the energy is then $\sum_{\mathbf{g}} V_n(\mathbf{g})$ where

$$V_n(\mathbf{g}) = \int f_n^*(z)\, V_{\mathbf{g}}(z) f_n(z) dz.$$

In view of this the substitute potential

$$U_n(\mathbf{r}) = V_{00}(z) + \sum_{\mathbf{g}} V_n(\mathbf{g}) \exp [2\pi i \mathbf{g}\cdot\boldsymbol{\varrho}]$$

will give the same energies for an electron in the exterior field of the solid as the true potential (24) to the extent of first-order perturbation theory. This potential makes the Schroedinger equation separable and leads to the solution

$$\psi_e(\mathbf{r}) = f_n(z) Q_n(\boldsymbol{\kappa}, \boldsymbol{\varrho}), \quad (27)$$

where

$$\frac{\partial^2 Q}{\partial x^2} + \frac{\partial^2 Q}{\partial y^2} + \frac{2m}{\hbar^2}\{W - \sum_{\mathbf{g}} V_n(\mathbf{g}) \exp [2\pi i \mathbf{g}\cdot\boldsymbol{\varrho}]\} Q = 0$$

and

$$\frac{d^2 f}{dz^2} + \frac{2m}{\hbar^2}(E - W - V_{00}(z))f = 0.$$

The solutions of the equation for Q with the proper physical behavior are of the well-known form

$$Q_n(\boldsymbol{\kappa}, \boldsymbol{\varrho}) = v_n(\boldsymbol{\kappa}, \boldsymbol{\varrho}) \exp [i\boldsymbol{\kappa}\cdot\boldsymbol{\varrho}]$$

while the equation for $f(z)$ has the same solutions as before with the same eigenvalues ϵ_n. The energies E_n are therefore given by $\epsilon_n = E_n - W_n(\boldsymbol{\kappa})$ or by

$$E_n = W_n(\boldsymbol{\kappa}) + \epsilon_n = E_n^0 + W_n(\boldsymbol{\kappa}) - \hbar^2|\boldsymbol{\kappa}|^2/2m.$$

The eigenvalues $W_n(\boldsymbol{\kappa})$ of the equation for Q are functions of both n and $\boldsymbol{\kappa}$ since the coefficients of the substitute potential depend on n. W_n plotted against k_x, k_y would give the usual discontinuous bands around a paraboloid-like surface.

In order to perform the fitting of the interior and exterior wave functions, generalize the exterior solution by taking a linear combination of the solutions (27) with respect to n,

$$\psi_e(\mathbf{r}) = \sum_n c_n f_n(z) Q_n(\boldsymbol{\kappa}, \boldsymbol{\varrho}).$$

Smooth fitting of this at the boundary $z=0$ with the interior wave function (23) is performed by taking

$$u(\boldsymbol{\kappa}, \boldsymbol{\gamma}; \boldsymbol{\varrho}, 0) = \sum_n c_n f_n(0) v_n(\boldsymbol{\kappa}, \boldsymbol{\varrho})$$

and

$$[(\partial/\partial z) u(\boldsymbol{\kappa}, \boldsymbol{\gamma}; \boldsymbol{\varrho}, z)]_{z=0} = \sum_n c_n (f_n'(0) - \gamma f_n(0)) v_n(\boldsymbol{\kappa}, \boldsymbol{\varrho}). \quad (28)$$

The solution of these equations implies the determination of the c_n's as functions of γ, $c_n(\gamma)$, to satisfy the first equation in whatever range or ranges of γ it is possible to do so. Then a particular value or values of γ must be found if possible for which the second of the equations is satisfied. This would in general be possible only for discrete values γ_i. For these values, stable surface states would exist and their energy would be given by

$$E_i(\boldsymbol{\kappa}) = \sum_n c_n^2(\gamma_i)(\epsilon_n + W_n(\boldsymbol{\kappa})). \quad (29)$$

As a practical attack on the problem of surface states, this particular method is probably out of the question. The functions $v_n(\boldsymbol{\kappa}, \boldsymbol{\varrho})$ are not orthogonal for different n so that the determination of the coefficients c_n would be most difficult. To make matters worse, γ appears implicitly in the functions $u(\mathbf{r})$ as indicated in

Eqs. (28) so that the determination of the particular values which satisfy the equations would be extremely difficult.

Certain general conclusions can, however, be drawn from this treatment. If the energies E_i are plotted against k_x and k_y, the resulting surface would show the usual characteristics of continuous bands with forbidden regions between. This must be the case since the behavior of the solution in any plane parallel with the surface is identical with that of the interior solutions. In the corresponding plot of energy (but not now of E_i) against k_z (not γ) at constant k_x and k_y, the bands obtained represent possible energies for the interior electrons and form the spectrum of the totality of solutions for which μ_z is pure imaginary. If there is no degeneracy between surface states and interior states, this spectrum will not overlap the spectrum of E_i as a function of γ. This places the surface states in the energy gaps between allowed bands of the interior states.

Now introduce the energies

$$E_i' = E_i - \sum_n c_n^2(\gamma_i) W_n(\kappa) = \sum_n c_n^2(\gamma_i)\epsilon_n,$$

which may be regarded as the contribution to the total energy E_i by the z dependent part of the wave function. They are therefore directly comparable to the energy in the one-dimensional solutions of Tamm and of Shockley. None of the energies E_i' can be smaller than the lowest eigenvalue ϵ_1 of Eq. (26). This in turn together with all the other eigenvalues ϵ_n is determined by the form and magnitude of the potential $V_{00}(z)$. A decrease in the surface potential would decrease all the ϵ_n's and so the surface state energies E_i'. It would seem, however, that as a result of the complicated dependence of the ϵ_n's on the form as well as magnitude of $V_{00}(z)$, the relation (2) for actual solids might involve V_s in a much more complicated manner. The other factor which limits the energies E_i' is the set of coefficients $c_n(\gamma)$. As the coefficients for large n become larger at the expense of those for small n, the lower limit to the energies E_i' increases. Since these coefficients arise from the fitting of the functions $v_n(\kappa, \varrho)$ and $u(\kappa, \gamma; \varrho, 0)$, this dependence may be associated with the term involving p in (2). The actual dependence is, however, very complex. It is on the whole far better to interpret the energy above which surface states appear in terms of the intersection of the bands as described in Shockley's paper. The other alternative of expressing it in terms of parameters associated with the surface and interior potentials as in (2) would seem to lead to considerable complexity. At the same time the use of (2) which is made in this paper is probably justifiable as a simplification of the same order as the others employed.

As a particular example, we may chose $V_{00}(z)$ equal to the image potential, $-e^2/4z$, for $z \geqslant z_0$ and equal to the mean potential energy, $-e^2/4z_0$, in the interior for $0 \leqslant z \leqslant z_0$. Eq. 26 then possesses solutions which are regular at infinity and also at $z=0$ even for $z_0=0$ as follows

$$\begin{aligned} f_n(z) &= [2n!(na_0)^{\frac{1}{2}}]^{-1} \exp[-z/4na_0] \\ &\quad \times [L_n(z/2na_0) - nL_{n-1}(z/2na_0)]; \quad z \geqslant z_0 \\ &= [4n!(na_0)^{\frac{1}{2}}]^{-1} \exp[-z_0/4na_0] \\ &\quad \times \{A_n \exp[ip_n(z_0-z)] \\ &\quad + A_n^* \exp[-ip_n(z_0-z)]\}; \quad z \leqslant z_0 \end{aligned}$$

with

$$\begin{aligned} A_n &= (1 - i/4np_n a_0) L_n(z_0/2na_0) \\ &\quad - n(1+i/4np_n a_0) L_{n-1}(z_0/2na_0), \\ p_n &= 1/2z_0 - 1/16n^2 a_0. \end{aligned}$$

These functions are normalized for $z_0 \to 0$. The functions $L_n(x)$ are Laguerre polynomials of degree n. The eigen energies associated with these functions are $\epsilon_n = -e^2/32a_0n^2$, so that the lowest state ϵ_1 corresponds to only about 0.85 volt.

In addition solutions regular at infinity exist for all $\epsilon < 0$ which are highly singular at $z=0$ if $z_0=0$. These solutions are

$$\begin{aligned} f(z) &= e^{-\alpha z/a_0}\left[\frac{a_0}{z} - \frac{4}{(8\alpha+1)}\left(\frac{a_0}{z}\right)^2\right. \\ &\quad \left. + \frac{48}{(12\alpha+1)(8\alpha+1)}\left(\frac{a_0}{z}\right)^3 - \cdots\right]; \quad z \geqslant z_0 \end{aligned}$$

with $\epsilon = -e^2\alpha^2/2a_0$. When $z_0 > 0$ these solutions can be made everywhere finite by setting

$$\begin{aligned} f(z) &= B \exp[ip_0(z_0-z)] \\ &\quad + B^* \exp[-ip_0(z_0-z)]; \quad z \leqslant z_0 \end{aligned}$$

and fitting continuously to the above at $z=z_0$. If now this solution is denoted by $f_0(z)$ and the

associated energy by $\epsilon_0 = -e^2\alpha^2/2a_0$, a sufficiently general linear combination of solutions for use in Eqs. (28) is probably obtained by taking

$$\psi_e(\mathbf{r}) = \sum_{n=0}^{\infty} c_n f_n(z) v_n(\kappa, \varrho).$$

The coefficient c_0, the energy ϵ_0, and the function $v_0(\kappa, \varrho)$ will all be functions of the adjustable parameter α. The corresponding quantities for all other values of n will be independent of α. The energy E_i' is

$$E_i' = -(e^2/2a_0)[c_0^2\alpha^2 + \sum_{n=1}^{\infty} c_n^2/16n^2].$$

The fitting is performed by choosing the c_n's including c_0 and the parameters α and γ to satisfy both Eqs. (28) and the condition that α and γ shall lead to the same total energy.

AUGUST 15, 1939 PHYSICAL REVIEW VOLUME 56

The Structure of Liquid Potassium

NEWELL S. GINGRICH, *University of Missouri, Columbia, Missouri,*

AND

C. N. WALL, *North Central College, Naperville, Illinois*

(Received June 13, 1939)

The method of Wall for calculating the free volume per atom in a liquid has been applied to liquid potassium, using the atomic distribution curves for potassium at 70°C and at 395°C given by Thomas and Gingrich. From the free volumes at these temperatures, the entropies of the liquid at its melting point and at its boiling point are obtained. These values, together with the entropy of solid potassium at its melting point and the entropy of potassium vapor at its boiling point, supply the entropies of fusion and of vaporization. Hence the latent heat of fusion is calculated as 2.06 *kj*/mol, and the latent heat of vaporization is calculated as 87.5 *kj*/mol. These values are to be compared with the observed values 2.38 *kj*/mol and 84.0 *kj*/mol, respectively.

THE atomic distribution curves, as obtained from x-ray diffraction patterns of liquid elements, have been used in the determination of certain characteristics of the liquid state. Wall[1] has made use of the atomic distribution curves for liquid sodium at two temperatures to obtain the free volume of the liquid, and the dependence of this free volume upon temperature. These quantities were used to calculate numerical values of the latent heats of fusion and vaporization, which values compared favorably with the corresponding experimental values. Hildebrand[2] used a somewhat different method to calculate the ratio of the energies of vaporization of liquid potassium at two temperatures from the results of Thomas and Gingrich.[3] The experimental value of this ratio was nearly identical with the calculated value. De Boer and Michels[4] use the liquid potassium results[3] in a qualitative comparison with their theoretical calculation of atomic distribution functions at various temperatures. In the present work, the method of Wall is used to calculate the free volume and its temperature dependence in the case of liquid potassium. These quantities are then used to calculate the latent heat of fusion and the latent heat of vaporization for comparison with the corresponding experimental values.

In developing an analytical expression for the atomic distribution function, Wall has adopted a quasi-solid model for the liquid. This model is essentially equivalent to that proposed by Lennard-Jones and Devonshire,[5] i.e., each atom in the liquid is assumed to be trapped (at least

[1] C. N. Wall, Phys. Rev. **54**, 1062 (1938).
[2] J. H. Hildebrand, J. Chem. Phys. **7**, 1 (1939).
[3] C. D. Thomas and N. S. Gingrich, J. Chem. Phys. **6**, 411 (1938).
[4] J. de Boer and A. Michels, Physica **6**, 97 (1939).
[5] J. E. Lennard-Jones and A. F. Devonshire, Proc. Roy. Soc. **A163**, 53 (1937).

temporarily) in a small spherical cell by its immediate neighbors. The potential energy function within the cell is assumed to be a discontinuous box type in which the potential is practically constant throughout the cell except at the cell boundary where it becomes infinite. On the basis of this assumption, it is shown that*

$$4\pi R^2\rho_1(R)=\frac{3N_1R}{5\sigma R_1}\left\{1-\frac{5(R_1-R)^2}{4\sigma^2}\times\left[1-\frac{|R_1-R|}{2\sigma}+\frac{|R_1-R|^3}{40\sigma^3}\right]\right\} \quad (1)$$

$$\text{for} \quad R_1-2\sigma\leqq R\leqq R_1+2\sigma,$$

$$4\pi R^2\rho_1(R)=0 \quad \text{for all other values of } R.$$

In this expression, $\rho_1(R)$ is the density of nearest neighbors surrounding an atom in the liquid, i.e., the density of those atoms whose cell centers lie on the first coordination sphere of radius R_1, $4\pi R^2\rho_1(R)dR$ is the number of nearest neighbors between distances R and $R+dR$ from a given atom, N_1 is the average number of nearest neighbors of a given atom, σ is the radius of the sphere whose volume represents the free volume for the trapped atom (i.e., its center) within it. It is assumed that the density of nearest neighbors, $\rho_1(R)$, is practically the total density of atoms for the interval $0\leqq R\leqq R_1$, and hence, in this interval, Eq. (1) gives the atomic distribution function of the liquid. In order to extend the range of the distribution curve, it is necessary to consider density contributions from atoms whose cell centers lie on coordination spheres of order higher than the first. If ρ_i is the density contribution of the N_i atoms lying on the coordination sphere i of radius R_i, then the total distribution curve is given by the equation

$$4\pi R^2\rho(R)=4\pi R^2\sum_{i=1}\rho_i(R), \quad (2)$$

where $\rho_i(R)$ is given by an equation of the same form as Eq. (1) with N_1 and R_1 replaced by N_i and R_i. On the assumption of molecular homogeneity in a liquid, N_i and R_i are functions of N_1 and R_1, and eventually it may be possible to construct a complete distribution curve from determinations of σ, N_1 and R_1. For the present, however, we restrict our calculations to the interval $0\leqq R\leqq R_1$ which, in the case of potassium near the melting point, is probably free from any contribution due to coordination spheres higher than the first.

The parameters σ, N_1 and R_1 are evaluated by fitting the distribution function given in Eq. (1) to the experimental values for liquid potassium. For this purpose it is convenient to use $4\pi R\rho_1(R)$ rather than $4\pi R^2\rho_1(R)$, and Eq. (1) may be rewritten in the form

$$\sigma^2=\frac{y_1}{y_1-y}\frac{5(R_1-R)^2}{4}\times\left[1-\frac{|R_1-R|}{2\sigma}+\frac{|R_1-R|^3}{40\sigma^3}\right], \quad (3)$$

where $y=4\pi R\rho_1(R)$ and $y_1=3N_1/5\sigma R_1$. It is clear that y_1 is the maximum value of y. From the experimental results, a curve of y *vs.* R may be constructed, and both y_1 and R_1 are immediately determined from this curve. Hence σ may be calculated from Eq. (3) for various values of R. Table I shows the experimental values of $4\pi R^2\rho(R)$ and the calculated values of σ for several values of $R<R_1$ for liquid potassium at 70°C and at 395°C. There is some variation in the values of σ at 70°C and there is considerable variation in the values of σ at 395°C. However, the ratio $\sigma_{70}/T^{\frac{1}{3}}$ is very nearly equal to the ratio $\sigma_{395}/T^{\frac{1}{3}}$, where T is the appropriate absolute temperature, and σ is the average value given in Table I. This indicates that σ depends upon T in the same manner for potassium as for sodium. Hence the free volume $v=4\pi\sigma^3/3=bT^{\frac{1}{3}}$ and $b=191\times10^{-30}$ c.g.s. unit. In order to compare

TABLE I. *Calculated and observed constants for potassium.*

70°C			395°C		
R	$4\pi R^2\rho(R)$ (obs.)	σ (calc.)	R	$4\pi R^2\rho(R)$ (obs.)	σ (calc.)
3.8	1.01	0.60	3.8	0.95	0.74
4.0	2.87	0.64	4.0	2.46	0.84
4.1	3.98	0.67	4.1	3.18	0.92
4.2	5.01	0.70	4.2	3.90	1.00
4.3	5.87	0.70	4.3	4.46	1.15
$R_1=4.55$A		Ave.—0.66A	$R_1=4.67$A		Ave.—0.93A
$y_1=1.55$			$y_1=1.18$		
$\sigma_{70}/T^{\frac{1}{3}}=0.0356$			$\sigma_{395}/T^{\frac{1}{3}}=0.0359$		
$v=4\pi\sigma^3/3=bT^{\frac{1}{3}}$			$b=191\times10^{-30}$ c.g.s. units		

* It is suggested that the subscript 1 be used in place of the subscript 0, as in the paper of Wall, in order that the more usual notation of ρ_0 for the average density of the liquid may be preserved.

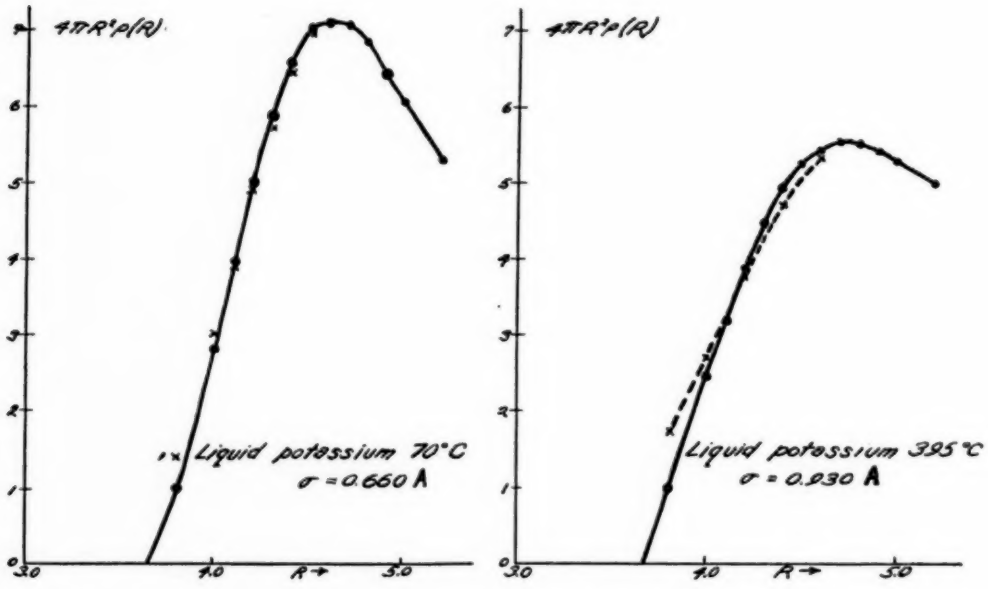

FIG. 1. Comparison of observed and calculated curves. The experimental values of $4\pi R^2\rho(R)$ are shown by solid dots. The values calculated from Eq. (1) with $\sigma_{70}=0.66$ for the 70°C case and $\sigma_{395}=0.93$ for the 395°C case are shown by crosses.

the distribution function given in Eq. (1) with the experimental curve, the average value of σ is used and $4\pi R^2\rho_1(R)$ is calculated for several values of $R<R_1$. These values are plotted, together with the experimental curve, in Fig. 1. The agreement in the case of 70°C is good, but in the case of 395°C, the experimental curve has a slope somewhat different than the calculated curve. Whether this difference is due to the nature of the assumptions made in developing Eq. (1), or to the difficulties in obtaining a good experimental curve in this region it is hard to say. For the two distribution curves shown in Fig. 1, the same small glass correction to the intensity curve has been made in each case. The curve for 395°C is slightly different here than that reported by Thomas and Gingrich.[3] Applying slightly different glass corrections to a given intensity curve does not alter the position of the first peak in the distribution curve, nor does it alter the area under this peak appreciably, but it does alter the slope of the fore part of the curve. Since this correction is somewhat arbitrary, it appears essential that the same correction be applied for the two temperatures. And it also appears that for reliable results from an analysis of this sort, the utmost care must be exercised to obtain as good and as complete an intensity pattern as possible.

Since we have determined the free volume of liquid potassium per atom and its dependence upon temperature, it is possible to calculate certain properties of liquid potassium. Guggenheim[6] has shown that the free energy of a simple liquid is given approximately by the equation

$$F=-NkT[\ln J(T)+\ln v]+\Phi, \qquad (4)$$

where Φ is the minimum potential energy of the molecular assembly, $J(T)$ is the ordinary partition function for the molecules and is assumed to take its classical value $(2\pi mkT/h^2)^{\frac{3}{2}}$, and v is the free volume per atom. The other symbols have their usual significance. Since $v=bT^{\frac{3}{2}}$, we may write,

$$F=-NkT\left[\ln\left(\frac{2\pi mkT}{h^2}\right)^{\frac{3}{2}}+\ln(bT^{\frac{3}{2}})\right]+\Phi. \qquad (5)$$

From this the entropy of liquid potassium may be obtained from the relation $S=-(\partial F/\partial T)v$. Hence

$$S=Nk\left[\ln\left(\frac{2\pi mkT}{h^2}\right)^{\frac{3}{2}}+\ln(bT^{\frac{3}{2}})+3\right]. \qquad (6)$$

The value of the entropy of liquid potassium at its melting point (335°K) as calculated by Eq.

[6] E. A. Guggenheim, Proc. Roy. Soc. **A135**, 181 (1932).

(6), with conversion from ergs to calories, is 17.5 cal./deg./mol. The corresponding entropy of solid potassium at this temperature according to Simon and Zeidler[7] and Kelly[8] is 16.03 cal./deg./mol. The difference of these two values, 1.47 cal./deg./mol, is the entropy of fusion of potassium. The latent heat of fusion corresponding to this entropy change is 2.06 *kj*/mol whereas the experimental value for the latent heat of fusion is given in the *International Critical Tables*[9] as 2.38 *kj*/mol.

In like manner, the entropy of liquid potassium at its boiling point (1033°K) may be calculated from Eq. (6). This leads to a value of 24.2 cal./deg./mol. The approximate entropy of the vapor at this temperature may be calculated from the equation[10]

$$S_{\text{vapor}} = Nk\left[\ln\left(\frac{2\pi mkT}{h^2}\right)^{\frac{3}{2}} + \ln\left(\frac{V}{N}\right) + \frac{5}{2} + \ln 2\right], \quad (7)$$

where V is the volume of a mol of the vapor at the boiling point. The calculation gives $S_{\text{vapor}} = 44.4$ cal./deg./mol. The entropy of vaporization is thus 20.2 cal./deg./mol which corresponds to a heat of vaporization of 87.5 *kj*/mol. The observed value of the latent heat of vaporization is given as 84.0 *kj*/mol in the *International Critical Tables*.[11]

The comparison of calculated and observed latent heats of fusion and vaporization is probably as good as can be expected from this somewhat simplified theory, and from experiments in which extremely low intensities of diffracted x-rays must be measured. It is possible that improvements will be made in both phases of this problem. However, the approximate agreement between calculated and observed latent heats and the close similarity between calculated and observed distribution curves tend to give one some confidence that the correct approach to the interpretation of the experimental results has been made in the method used in the present work.

[7] F. Simon and W. Zeidler, Zeits. f. physik. Chemie **A123**, 383 (1926).
[8] K. K. Kelly, Bureau of Mines Bulletin, No. 350 (1932).
[9] *International Critical Tables*, Vol. I, p. 104.
[10] R. H. Fowler, *Statistical Mechanics* (second edition), pp. 192, Theorem 6.31; pp. 213; 218–220.
[11] *International Critical Tables*, Vol. I, p. 102.

Forces in Molecules

R. P. FEYNMAN
Massachusetts Institute of Technology, Cambridge, Massachusetts
(Received June 22, 1939)

Formulas have been developed to calculate the forces in a molecular system directly, rather than indirectly through the agency of energy. This permits an independent calculation of the slope of the curves of energy *vs.* position of the nuclei, and may thus increase the accuracy, or decrease the labor involved in the calculation of these curves. The force on a nucleus in an atomic system is shown to be just the classical electrostatic force that would be exerted on this nucleus by other nuclei and by the electrons' charge distribution. Qualitative implications of this are discussed.

MANY of the problems of molecular structure are concerned essentially with forces. The stiffness of valence bonds, the distortions in geometry due to the various repulsions and attractions between atoms, the tendency of valence bonds to occur at certain definite angles with each other, are some examples of the kind of problem in which the idea of force is paramount.

Usually these problems have been considered through the agency of energy, and its changes with changing configuration of the molecule. The reason for this indirect attack through energy, rather than the more qualitatively illuminating one, by considerations of force, is perhaps twofold. First it is probably thought that force is a quantity that is not easily described or calculated by wave mechanics, while energy is, and second, the first molecular problem to be solved is the analysis of band spectra, strictly a problem of energy as such. It is the purpose of this paper to show that forces are almost as easy to calculate as energies are, and that the equations are quite as easy to interpret. In fact, all forces on atomic nuclei in a molecule can be considered as purely classical attractions involving Coulomb's law. The electron cloud distribution is prevented from collapsing by obeying Schrödinger's equation. In these considerations the nuclei are considered as mass points held fixed in position.

A usual method of calculating interatomic forces runs somewhat as follows.

For a given, fixed configuration of the nuclei, the energy of the entire system (electrons and nuclei) is calculated. This is done by the variation method or other perturbation schemes. This entire process is repeated for a new nuclear position, and the new value of energy calculated. Proceeding in this way, a plot of energy *vs.* position is obtained. The force on a nucleus is of course the slope of this curve.

The following method is one designed to obtain the forces at a given configuration, when only the configuration is known. It does not require the calculations at neighboring configurations. That is, it permits a calculation of the slope of the energy curve as well as its value, for any particular configuration. It is to be emphasized that this allows a considerable saving of labor of calculations. To obtain force under the usual scheme the energy needs to be calculated for two or more different and neighboring configurations. Each point requires the calculation of the wave functions for the entire system. In this new method, only one configuration, the one in question, need have its wave functions computed in detail. Thus the labor is considerably reduced. Because it permits one to get an independent value of the slope of the energy curve, the method might increase the accuracy in the calculation of these curves, being especially helpful in locating the normal separation, or position of zero force.

In the following it is to be understood that the nuclei of the atoms in the molecule, or other atomic system, are to be held fixed in position, as point charges, and the force required to be applied to the nuclei to hold them is to be calculated. This will lead to two possible definitions of force in the nonsteady state, for then the energy is not a definite quantity, and the slope of the energy curve shares this indefinite-

ness. It will be shown that these two possible definitions are exactly equivalent in the steady-state case, and, of course, no ambiguity should arise there.

Let λ be one of any number of parameters which specify nuclear positions. For example, λ might be the x component of the position of one of the nuclei. A force f_λ is to be associated with λ in such a way that $f_\lambda d\lambda$ measures the virtual work done in displacing the nuclei through $d\lambda$. This will define the force only when the molecule is in a steady state, of energy U, for then we can say $f_\lambda = -\partial U/\partial\lambda$. In the non-steady-state case we have no sure guide to a definition of force. For example, if $\bar{U} = \int \psi^* H \psi dv$ be the average energy of the system of wave function ψ and Hamiltonian H, we might define

$$f_\lambda' = -\partial(\bar{U})/\partial\lambda'. \tag{1}$$

Or again, we might take f_λ to be the average of $-\partial H/\partial\lambda$ or

$$f_\lambda = -\left\langle \frac{\partial H}{\partial\lambda} \right\rangle_{Av} = -\int \psi^* \frac{\partial H}{\partial\lambda} \psi dv. \tag{2}$$

We shall prove that under steady-state conditions, both these definitions of force become exactly equivalent, and equal to $-\partial U/\partial\lambda$, the slope of the energy curve. Since (2) is simpler than (1) we can define force by (2) in general. In particular, it gives a simple expression for the slope of the energy curve.

Thus we shall prove, when $H\psi = U\psi$ and $\int \psi\psi^* dv = 1$ that,

$$\frac{\partial U}{\partial\lambda} = \int \psi^* \frac{\partial H}{\partial\lambda} \psi dv.$$

Now

$$U = \int \psi^* H \psi dv,$$

whence,

$$\frac{\partial U}{\partial\lambda} = \int \psi^* \frac{\partial H}{\partial\lambda} \psi dv + \int \frac{\partial\psi^*}{\partial\lambda} H\psi dv + \int \psi^* H \frac{\partial\psi}{\partial\lambda} dv.$$

Since H is a self-adjoint operator,

$$\int \psi^* H \frac{\partial\psi}{\partial\lambda} dv = \int \frac{\partial\psi}{\partial\lambda} H\psi^* dv.$$

But $H\psi = U\psi$ and $H\psi^* = U\psi^*$ so that we can write,

$$\frac{\partial U}{\partial\lambda} = \int \psi^* \frac{\partial H}{\partial\lambda} \psi dv + U\int \frac{\partial\psi^*}{\partial\lambda} \psi dv + U\int \frac{\partial\psi}{\partial\lambda} \psi^* dv.$$

These last two terms cancel each other since their sum is,

$$U\frac{\partial}{\partial\lambda}\int \psi^*\psi dv = U\frac{\partial}{\partial\lambda}(1) = 0.$$

Whence

$$\frac{\partial U}{\partial\lambda} = \int \psi^* \frac{\partial H}{\partial\lambda} \psi dv$$

in the steady state. This much is true, regardless of the nature of H, (whether for spin, or nuclear forces, etc.). In the special case of atomic systems when $H = T + V$ where T is the kinetic energy operator, and V the potential, since $\partial H/\partial\lambda = \partial V/\partial\lambda$ we can write

$$f_\lambda' = f_\lambda = -\frac{\partial U}{\partial\lambda} = -\int \psi^*\psi \frac{\partial V}{\partial\lambda} dv. \tag{3}$$

The actual calculation of forces in a real molecule by means of this theorem is not impractical. The $\int \psi^*\psi(\partial V/\partial\lambda)dv$ is not too different from $\int \psi^*\psi V dv$, which must be calculated if the energy is to be found at all in the variational method. Although the theorem (3) is the most practical for actual calculations, it can be modified to get a clearer qualitative picture of what it means. Suppose, for example, the system for which ψ is the wave function contains several nuclei, and let the coordinates of one of these nuclei, α, be X^α, Y^α, Z^α or $X_\mu{}^\alpha$ where $\mu = 1, 2, 3$, mean X, Y, Z. If we take our λ parameter to be one of these coordinates, the resultant force on the nucleus α in the μ direction will be given directly by

$$f_\mu{}^\alpha = -\int \psi\psi^*(\partial V/\partial X_\mu{}^\alpha)dv$$

from (3).

Now V is made up of three parts, the interaction of all nuclei with each other ($V_{\alpha\beta}$), of each nucleus with an electron ($V_{\beta i}$), and of each

electron with every other (V_{ij}); or

$$V=\sum_{\alpha,\beta} V_{\alpha\beta}+\sum_{\beta,i} V_{\beta i}+\sum_{i,j} V_{ij}.$$

Suppose $x_\mu{}^i$ are the coordinates of electron i, and as before $X_\mu{}^\alpha$ those of nucleus α of charge q_α. Then $V_{\beta i}=q_\beta e/R_{\beta i}$, where

$$R_{\beta i}{}^2=\sum_{\mu=1}^{3}(X_\mu{}^\beta-x_\mu{}^i)^2.$$

So we see that

$$\frac{\partial V_{\beta i}}{\partial X_\mu{}^\alpha}=-\delta_\beta{}^\alpha\frac{\partial V_{\beta i}}{\partial x_\mu{}^i} \quad \text{and that} \quad \frac{\partial V_{ij}}{\partial X_\mu{}^\alpha}=0.$$

Then (3) leads to

$$f_\mu{}^\alpha=+\int\psi\psi^*\sum_i\frac{\partial V_{\alpha i}}{\partial x_\mu{}^i}dv-\sum_\beta\int\frac{\partial V_{\alpha\beta}}{\partial X_\mu{}^\alpha}\psi\psi^*dv$$

$$=\int\sum_i\frac{\partial V_{\alpha i}}{\partial x_\mu{}^i}\left[\int i\int\psi\psi^*dv\right]dv-\sum_\beta\frac{\partial V_{\alpha\beta}}{\partial X_\mu{}^\alpha} \quad (4)$$

since $\partial V_{\alpha i}/\partial x_\mu{}^i$ does not involve any electron coordinate except those of electron i. $\int i\int\cdots dv$ means the integral over the coordinates of all electrons except those of electron i. The last term has been reduced since $\partial V_{\alpha\beta}/\partial x_\mu{}^\alpha$ does not involve the electron coordinates, and is constant as far as integration over these coordinates goes. This term gives ordinary Coulomb electrostatic repulsion between the nuclei and need not be considered further. Now $e\int i\int\psi\psi^*dv$ is just the charge density distribution $\rho_i(x)$ due to electron i, where e is the charge on one electron. The electric field $E_\mu{}^\alpha(x^i)$ at any point x^i due to the nucleus α is $(1/e)\partial V_{\alpha i}/\partial x_\mu{}^i$, so that (4) may be written

$$f_\mu{}^\alpha=\int[\sum_i\rho_i(x)]E_\mu{}^\alpha(x)dv-\sum_\beta\frac{\partial V_{\alpha\beta}}{\partial X_\mu{}^\alpha}.$$

The $3N$ space for N electrons has been reduced to a 3 space. This can be done since $E_\mu{}^\alpha(x^i)$ depends only on x^i and is the same function of x^i no matter which i we pick. This implies the following conclusion:

The force on any nucleus (considered fixed) in any system of nuclei and electrons is just the classical electrostatic attraction exerted on the nucleus in question by the other nuclei and by the electron charge density distribution for all electrons,

$$\rho(x)=\sum_i\rho_i(x).$$

It is possible to simplify this still further. Suppose we construct an electric field vector F such that

$$\nabla\cdot F=-4\pi\rho(x); \quad \nabla\times F=0.$$

Now from the derivation of $E_\mu{}^\alpha$ we know that it arises from the charge q_α on nucleus α, so that $\nabla\cdot E^\alpha=0$ except at the charge α where its integral equals q_α. Further,

$$-\sum_\beta\frac{\partial V_{\alpha\beta}}{\partial X_\mu{}^\alpha}=q_\alpha[\sum_\beta E_\mu{}^\beta]_{\text{at } x^\alpha}.$$

Then

$$f_\mu{}^\alpha=-\frac{1}{4\pi}\int(\nabla\cdot F)E_\mu{}^\alpha dv-\sum_\beta\frac{\partial V_{\alpha\beta}}{\partial x_\mu{}^\alpha}$$

$$=+\frac{1}{4\pi}\int F_\mu(\nabla\cdot E_\mu{}^\alpha)dv-\sum_\beta\frac{\partial V_{\alpha\beta}}{\partial x_\mu{}^\alpha}$$

$$=q_\alpha[F_\mu]_{\text{at } x^\alpha}+q_\alpha[\sum_\beta E_\mu{}^\beta]_{\text{at } x^\alpha} \quad (5)$$

the transformation of the integral being accomplished by integrating by parts. Or finally, the force on a nucleus is the charge on that nucleus times the electric field there due to all the electrons, plus the fields from the other nuclei. This field is calculated classically from the charge distribution of each electron and from the nuclei.

It now becomes quite clear why the strongest and most important attractive forces arise when there is a concentration of charge between two nuclei. The nuclei on each side of the concentrated charge are each strongly attracted to it. Thus they are, in effect, attracted toward each other. In a H_2 molecule, for example, the antisymmetrical wave function, because it must be zero exactly between the two H atoms, cannot concentrate charge between them. The symmetrical solution, however, can easily permit charge concentration between the nuclei, and hence it is only the solution which is symmetrical that leads to strong attraction, and the formation of a molecule, as is well known. It is

clearly seen that concentrations of charge between atoms lead to strong attractive forces, and hence, are properly called valence bonds.

Van der Waals' forces can also be interpreted as arising from charge distributions with higher concentration between the nuclei. The Schrödinger perturbation theory for two interacting atoms at a separation R, large compared to the radii of the atoms, leads to the result that the charge distribution of each is distorted from central symmetry, a dipole moment of order $1/R^7$ being induced in each atom. The negative charge distribution of each atom has its center of gravity moved slightly toward the other. It is not the interaction of these dipoles which leads to van der Waals' force, but rather the attraction of each nucleus for the distorted charge distribution of its *own* electrons that gives the attractive $1/R^7$ force.

The author wishes to express his gratitude to Professor J. C. Slater who, by his advice and helpful suggestions, aided greatly in this work. He would also like to thank Dr. W. C. Herring for the latter's excellent criticisms.

AUGUST 15, 1939 PHYSICAL REVIEW VOLUME 56

Intercrystalline Thermal Currents as a Source of Internal Friction*

R. H. RANDALL, F. C. ROSE AND C. ZENER
College of the City of New York, New York

(Received June 12, 1939)

An experiment has been designed to detect the contribution of intercrystalline thermal currents to the internal friction of polycrystalline metals. In accordance with a theory developed by one of the writers (C.Z.), the internal friction is a maximum when the vibration is partly isothermal and partly adiabatic with respect to adjacent grains. By passing in small steps from the nearly isothermal case of very small grain size through maximum internal friction to the nearly adiabatic case of large grain size, one can detect the relative importance of the intercrystalline thermal currents. Such an experiment has been performed on single phase 69–31 brass, with mean grain size ranging in small steps from 0.0006 cm to 0.4 cm, and with frequencies of 6000, 12,000 and 36,000 cycles per second. Not only was a maximum obtained with the anticipated grain size, but the maximum is of a larger order of magnitude than the background upon which it is superimposed. The internal friction in the extreme isothermal case ($Q > 300{,}000$) was lower than has ever been observed for metals; in the extreme adiabatic case it approached the low values obtained for single crystals. This experiment indicates that in annealed nonferromagnetic metals at room temperature, intercrystalline thermal currents are the dominant cause of internal friction measured at small strains, aside from possible macroscopic thermal currents.

§1. INTRODUCTION

THE term internal friction refers to the capacity of a solid to transform its ordered energy of vibration into disordered internal energy. One of the authors (C. Z.) has recently made a start at understanding the mechanism of this transformation.[1, 2, 3] His basic idea was that the direct coupling between the macroscopic and the internal coordinates may be treated by examining the thermoelastic effects which accompany vibration. Thus the increase in internal energy per cycle is equated to the temperature times the increase in entropy per cycle. The increase in entropy per cycle is obtained by studying the thermal currents which flow back and forth during vibration between stress inhomogeneities.

If these thermal currents are able nearly to maintain temperature equilibrium between the stress inhomogeneities, the vibration proceeds isothermally with little internal dissipation of energy. In the other extreme case of adiabatic vibration, the internal dissipation of energy is

* This research was supported by a grant from the Penrose Fund of the American Philosophical Society, and by a grant from the Rumford Fund of the American Academy of Arts and Sciences.

[1] C. Zener, Phys. Rev. **52**, 230 (1937).
[2] C. Zener, Phys. Rev. **53**, 90 (1938).
[3] C. Zener, Proc. Phys. Soc. (in print).

also very small. It reaches a maximum when the vibration is partly isothermal and partly adiabatic.

The condition for isothermal and for adiabatic vibration may be obtained from dimensional considerations. The degree of adiabaticity of the vibration can be a function only of some measure L of the linear dimension of the stress inhomogeneity, of the frequency of vibration ν, and finally of the thermal diffusion coefficient D. Since D has dimensions of (length)^2/time, the degree of adiabaticity can depend upon these factors only in the dimensionless combination $\nu L^2/D$. As this combination changes from a number much less than unity to a number much greater than unity, the vibration passes from the nearly isothermal to the nearly adiabatic case. The thermoelastic internal friction may thus be detected experimentally by varying this parameter $\nu L^2/D$ over a wide range. The internal friction will be at a maximum when this parameter has a value comparable to unity, and will fall to low values when this parameter becomes either very small or very large.

The thermoelastic internal friction accompanying transverse vibrations has been studied in this manner.[4, 5] In such vibrations the stress varies across the specimen. Hence the dimension of the stress inhomogeneities may be taken as the transverse width a of the specimen. The parameter $\nu a^2/D$ was varied by taking measurements at various frequencies. The frequency range from where the internal friction is at half its maximum value on the isothermal side, to where it is at half its maximum on the adiabatic side covers nearly four octaves. Over this wide frequency range the internal friction due to the transverse thermal currents has been found to be of a larger order of magnitude than that due to all other causes.

All types of elastic vibrations in polycrystalline specimens are accompanied by stress inhomogeneities between adjacent crystallites. These microscopic stress inhomogeneities are caused by the elastic anisotropy and at least partial random orientation of the individual crystallites.[2] They give rise to microscopic thermal currents. The present paper describes an experiment which investigates the internal friction arising from these intercrystalline thermal currents.

The diameter d of the average grain may here be taken as the linear dimension of the stress inhomogeneity. In order to obtain a wide variation of the parameter $\nu d^2/D$, measurements were made not only at various frequencies, but also on specimens with a wide range of average grain diameter. These specimens were prepared by C. S. Smith and E. W. Palmer of the American Brass Company. The material, 69-31 brass, was chosen in preference to a pure metal in order to avoid possible energy dissipation by slipping. With this variation of both ν and d, measurements were made at values of $\nu d^2/D$ ranging from 0.005 to 16,000.

In the present investigation it was desirable to avoid damping arising from macroscopic thermal currents. For this reason longitudinal vibrations were used in preference to transverse vibrations. Here the only macroscopic stress inhomogeneity has dimensions of the wave-length of the vibration. The corresponding parameter $\nu\lambda^2/D$ is very large for ordinary frequencies. Longitudinal vibrations are thus macroscopically adiabatic.

§2. Preparation of Material*

The alpha-brass obtained for this investigation was normal high grade commercial material of the following analysis:

Copper	68.74 percent.
Zinc (diff.)	31.23 "
Lead	0.02 "
Iron	0.008 "

It had been cold rolled to 0.315 inch following standard practice, annealed at about 600°C to produce a grain size of 0.06 mm, then cold rolled to 0.125 inch thickness (60 percent reduction), slit to ½ inch width and straightened. Slight curvature at the edges resulted from the slitting rolls, but had no noticeable effect upon the internal friction measurements. The cold-rolled

[4] C. Zener, W. Otis and R. Nuckolls, Phys. Rev. **53**, 100 (1938).

[5] K. Bennewitz and H. Rötger, Zeits. f. tech. Physik **19**, 521 (1938).

* This material and the following description of the method of preparing it was furnished through the generosity of C. S. Smith and E. W. Palmer of the American Brass Company, whose assistance the authors gratefully acknowledge. Without their assistance this research would have been impossible.

TABLE I. *Grain size data.*

ANNEALING TEMP. (IN °C)	DIAMETER AVE. GRAIN BY COMPARISON	TWINS PER GRAIN CROSSED BY LINE
350	0.006 mm	
400	0.009	0.6
450	0.015	0.7
500	0.025	1.0
550	0.037	1.0
600	0.055	1.1
650	0.080	1.4
700	0.11	1.1
750	0.15	1.6
800	(0.25)	1.7
850	(0.5)	1.7
900	(1.0)	1.4

strips, cut to 12-inch lengths and numbered, were annealed in the laboratory at temperatures between 50 and 900°C in 50° steps. Anneals were for 30 minutes, followed by air cooling. Separate samples were given identical treatment alongside the 12-inch test pieces to provide material for grain size measurement. The specimens were supported on edge in a jig during annealing and great care was taken at all times to avoid distortion. The largest grain size obtainable by straight annealing this material was about 1 millimeter. A still larger grain size, 0.04 mm, was obtained by stretching a piece briefly annealed at 900°C to about one percent elongation, and then reheating it at 900°C for 30 minutes.

Table I shows the annealing temperatures and the average grain diameters obtained. The grain size (diameter of average grain) of each specimen was obtained by comparison of the projected image of a polished and etched section parallel to the rolled surface, at a magnification of 75, with the standard micrographs of the A. S. T. M. (A. S. T. M. Standard E2-36). These standards were established by counting the total number of individual grains visible in a large typical field of known area, and express the grain size as the square root of the average area of grain. A constant factor would convert this "grain size" to the true average diameter of the grains.

Figure 1, A, B, C, D shows the appearance of typical samples at a magnification of 75 diameters, and Fig. 1, E, F the appearance of a large and a small grain size, respectively, at magnifications at which they compare with a medium grain size, thereby showing the differences in grain characteristics. All samples were etched with ammonium and hydrogen peroxide.

For the present measurements it is possible that the significant structural unit should be based on twin dimensions as well as grain size. The average number of twins in a grain is greater in large than in small grains, but the increase appears to be a gradual one. This is shown in Table I, where the third column gives the ratio of the number of twins to the number of grains crossed by a line normal to the rolling direction. It should also be noted that the grain size distribution varies somewhat with the grain size, at least at the lower annealing temperatures where recrystallization is barely complete.

§3. EXPERIMENTAL PROCEDURE

Several measures of internal friction have been used in the literature. One is to measure, under forced oscillations, the frequency width $\Delta\nu$ of a resonance curve for an amplitude half that at resonance. The ratio of $\Delta\nu$ to the resonance frequency ν is a measure of the internal dissipation. Another measure is the logarithmic decrement δ. Then from the electrical analogy there is the ratio of the effective electrical resistance to the effective electrical reactance, $R/2\pi L=1/Q$. The relation between these measures is

$$1/Q=3^{-\frac{1}{2}}\Delta\nu/\nu=\delta/\pi.$$

The general method of measurement was similar to that used by Wegel and Walther.[6] Fig. 2 shows the arrangement. It was found possible to use an electromagnetic drive without attaching pole pieces. The driver and detector were air core solenoids whose impedances were matched to the oscillator and amplifier, respectively. An alternating current of variable frequency was supplied to the driving coil from a General Radio type 377 oscillator. The eddy currents induced in the reed reacted with the nonaxial components of a steady external magnetic field (furnished by permanent magnets) to produce longitudinal vibrations. At the pick-up end a small alternating potential was induced in a reciprocal manner, which was fed into the input circuit of a linear amplifier. The latter consisted of four pentode stages, giving a maximum voltage gain of over 10^6, the last two plate circuits containing tuned coupling elements. The "Q" of the reed was at least 100 times that of the over-all amplifier

[6] R. L. Wegel and H. Walther, Physics **6**, 141 (1935).

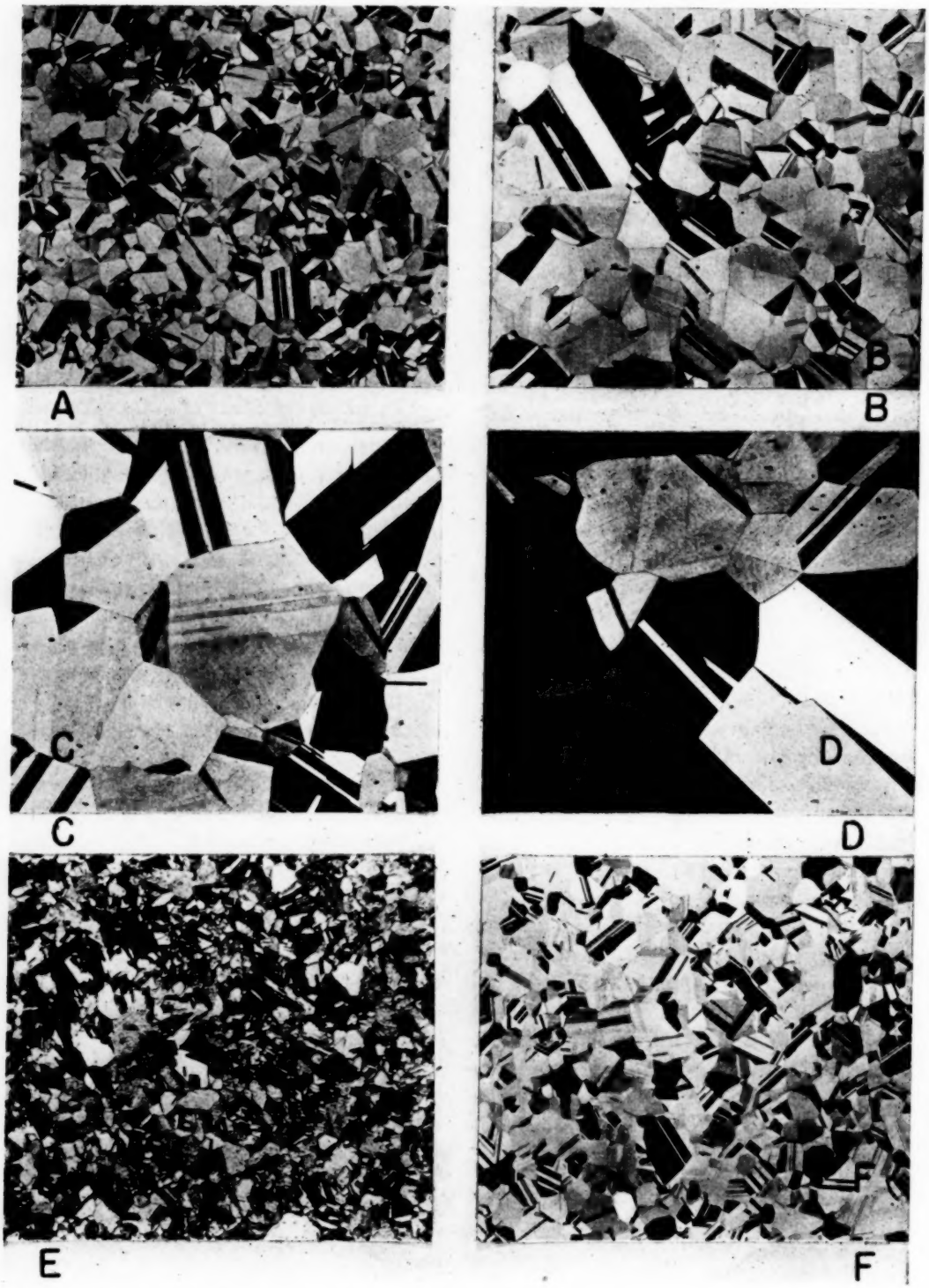

FIG. 1. Micrographs of brass specimens with different grain size. The horizontal axis is parallel to the rolling direction. Micrographs A, B, C, D have the same magnification of 75. The corresponding diameters of average grains are 0.037, 0.080, 0.15, 0.5 mm, respectively. Micrographs E and F compare a small and a large grain size specimen (d=0.009, 0.15 mm). Their magnifications (×300, ×17) are such as to give the same apparent grain size. Annealing temperatures are, respectively, 550°C, 650°C, 750°C, 850°C, 400°C and 750°C.

characteristic, making the response linear to frequency over the resonance curve of the reed. Tuning the amplifier very greatly increased the useful amplification by cutting down background noise. Final voltage amplitudes were read on a d.c. microammeter in a diode rectifier circuit.

In order to eliminate direct inductive feed over between driver and pick-up, which occurred despite the use of shielding, a counter magnetic field was supplied with a coil similar to the driver connected to the oscillator.

Both the method of forced oscillations and the method of free oscillation decay were used. In cases of very low internal friction the method of forced oscillations was found to involve too critical an oscillator adjustment. It was sometimes then possible to observe the time of decay of the free oscillations. Whenever the two methods could both be used, the agreement was within the precision of measurement. The time t to decay to the fraction $1/n$ of the original amplitude is related to δ by the equation: $t = \log_e n/\delta\nu$.

Minimum support dissipation occurred with suspension on silk threads at a pair of displacement nodes. For the fundamental frequency, placing the two supports within about 1/50 of a wave-length of the central nodal point gave negligible dissipation.

The radiation and viscous losses due to the surrounding air were only important in the cases of low damping. Reduction of the surrounding air pressure to several mm of mercury made these losses negligible.

Varying the strength of the steady fields by moving the permanent magnets back and forth produced no noticeable change in the measured internal friction, showing that eddy current losses were a negligible factor.

It was the intention in this experiment to keep well below vibration amplitudes at which plastic flow might occur. No attempt was made to control amplitude and no amplitude effect on the internal friction was observed at any time, indicating that small amplitude conditions prevailed throughout.

§4. Results and Discussion

In Fig. 3 we give the variation of internal friction with grain size and with annealing temperature measured at each of the three frequencies 6000, 12,000 and 36,000 cycles per second. These frequencies were the first, second and sixth harmonics of our specimens. Four specimens of

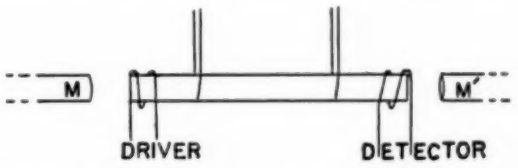

FIG. 2. Method of forcing and of detecting longitudinal vibrations. The specimen is supported by silk threads at nodes of vibration. The driving force is obtained by the reaction upon a permanent magnet M of the eddy currents induced by an alternating current in the driving coil. An alternating electromotive force is induced in a detector coil at the other end by the eddy currents arising from the motion of the specimen in the field of a second permanent magnet M'.

intermediate grain size appeared to have abnormally high internal friction at the highest frequency. In one of these specimens the resonance curve showed a distinct double peak, indicating a near coincidence of two natural frequencies. All four observations were discarded. Accurate measurements at all three frequencies could not be obtained on the specimens of smallest grain size. In these cases the resonance curve was too sharp to follow with our oscillator, while the half-decay time was too short to measure.

Figure 3 is in marked disagreement with the only previously published variation of internal friction with grain size. Förster and Köster[7] have reported the internal friction of 72-28 brass to increase with grain size up to at least a mean diameter of 3.7 mm. Since internal strains raise the internal friction of metals, and since such strains are more readily introduced in large than in small grain size specimens, the explanation of this discrepancy may lie in the presence of strains introduced in handling their specimens of largest grain size.

The initial rise of internal friction, shown in Fig. 3, as the annealing temperature is raised above the recrystallization temperature, has frequently been observed.[6-8] The most extensive measurements on brass, by Förster and Köster,[7]

[7] F. Förster and W. Köster, Zeits. f. Metallkunde **29**, 116 (1937).
[8] W. Köster and K. Rosenthal, Zeits. f. Metallkunde **30**, 345 (1938).

were made up to an annealing temperature of only 800°C. No indication of a maximum was observed. Since they did not report their frequency of measurement, direct comparison with our measurements is impossible. A slight maximum has been observed by Wegel and Walther[6] for copper at the annealing temperature of 300°C.

All the measurements shown in Fig. 3 have been replotted in Fig. 4 against the parameter $\nu d^2/D$. All measurements at the three frequencies lie upon a single curve. This is evidence that the microscopic thermal currents were the dominant cause of internal friction in our specimens. To the left of the maximum the vibration approaches the isothermal case, to the right the adiabatic case.

To the extreme right the internal friction should approach that of a single crystal. The only published values of single crystals are those of Read[9] for Cu, Pb, Sn. Copper, the metal most like brass, gave $Q^{-1}=1.1\times10^{-5}$. The internal friction shown in Fig. 4 seems to approach an asymptote of this order of magnitude at large grain sizes.

The internal friction on the extreme isothermal

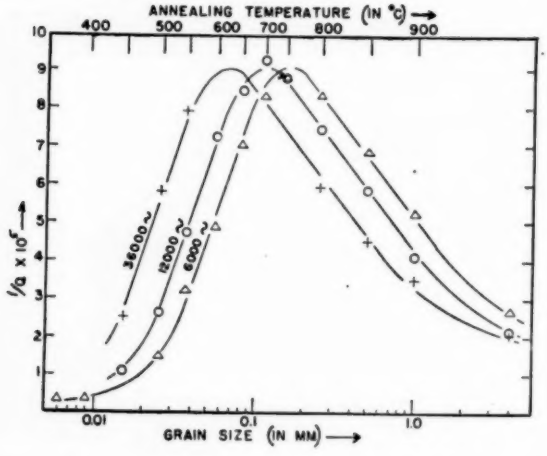

FIG. 3. Internal friction as a function of grain size and of annealing temperature. The triangles, circles, and crosses represent measurements at the frequencies 6000, 12,000 and 36,000 cycles/second. The three curves have been drawn identical save for a horizontal shift.

[9] T. A. Read, Phys. Rev. **54**, 389 (1938).

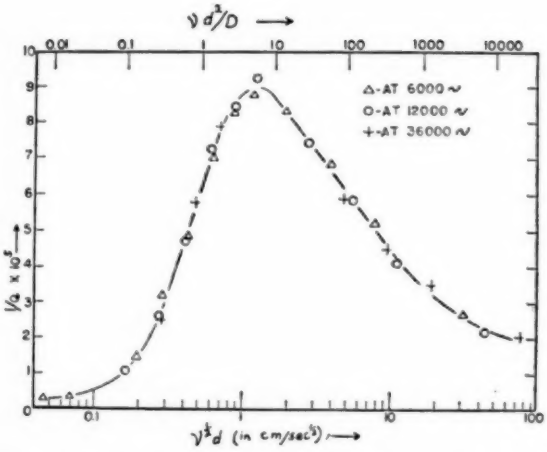

FIG. 4. Internal friction as a function of parameter $\nu d^2/D$. In this figure the three curves of Fig. 3 coincide.

side of the curve is surprisingly small. The lowest value, 0.3×10^{-5}, is three times as low as has ever been reported for a metal. The failure of Köster and Rosenthal[8] to obtain values lower than 2×10^{-5} in their recent extensive work on brass can probably be attributed to excessive external dissipation of energy, either through their supports or to the surrounding air.

In the dimensional argument leading to the prediction that the internal friction be a function only of the parameter $\nu d^2/D$, it was implicitly assumed that all the microscopic dimensions varied linearly with d. The detailed information concerning the specimens given in §2 shows this assumption to be slightly in error. A comparison of the two specimens in Fig. 1, E and F, shows that the specimens with smallest grain size have the greatest distribution in grain size. Further, Table I shows that the average number of twins per grain increases with grain size. Although these factors may have affected the shape of the curve in Fig. 4, they varied sufficiently slowly with d so that the measurements were, within our experimental error, determined solely by the parameter $\nu d^2/D$. The dimensional argument will also be slightly in error at the largest grain sizes where d is comparable to the width of the specimens.

Dielectric Breakdown in Ionic Crystals

H. FRÖHLICH
H. H. Wills Physical Laboratory, University of Bristol, England
(Received April 6, 1939)

A critical consideration of the theories of dielectric breakdown in ionic crystals proposed by Seeger and Teller and by Fröhlich is given. It is shown that the main difference in the formulae for the breakdown field is due to the fact that Seeger and Teller make the unjustified assumption that an electron transfers energy to the lattice vibration without changing its direction of motion. A mistake in the interaction between an electron and an ion, used by Seeger and Teller, is corrected. The author's condition for breakdown is discussed in greater detail than has been done hitherto.

§1.

A THEORY of dielectric breakdown in polar crystals has recently been given by the author.[1] More recently, Seeger and Teller[2] have presented a theory which differs in important respects from that of Fröhlich. The purpose of this paper is to show where, in the author's opinion, the theory of Seeger and Teller is incorrect, and to discuss the fundamentals of Fröhlich's theory in rather greater detail than has been done hitherto.

In both theories it is necessary to consider the interaction of free electrons in a polar lattice with the lattice vibrations. This leads to expressions for the mobility of electrons which, in the case of slow electrons, can be compared with experiments on photoconductivity. This will be done in another paper[3] in which it will be shown that Fröhlich's theory, modified for slow electrons, leads to a fair agreement with experiment.

Both authors follow von Hippel's original ideas in considering an electron with an arbitrary energy E in the conduction band of the crystal (i.e., the first empty band of allowed energy levels). The energy E is measured from the lowest state in the conductive band. There is evidence, as we shall see, that for high fields a certain number of electrons find their way into the conduction band.

In an external field F such an electron will lose energy to the lattice vibrations of the solid and gain energy from the field. If the field is strong enough, the energy of the electron will increase indefinitely until it is great enough to produce a secondary. For small fields, on the other hand, the electron will be slowed down until it reaches thermal energies. Both authors agree that breakdown will take place when the field is strong enough to accelerate electrons having energy greater than a critical value E_c. They disagree however as to (1) the value to be taken for E_c, and (2) the method of calculating the rate of loss of energy to the lattice.

§2. The Rate of Loss of Energy of an Electron in a Polar Lattice

The rate of loss of energy may be calculated either per unit time $-dE/dt$ or per unit path *in the direction of the field* F. We denote this by $-dE/dx$. They are connected by

$$dE/dx=(dE/dt)(1/\omega F), \tag{1}$$

where ω is the mobility of the electron. Instead of ω, the conception of the time of relaxation τ may be introduced, defined by $\omega=(e/m)\tau$ as, for instance, by Fröhlich.[1] The magnitude

$$\bar{v}=\omega F=e\tau F/m \tag{2}$$

is the average velocity over several collisions. Seeger and Teller, on the other hand, consider an electron moving always in a straight line. They obtain, therefore

$$dE/dx=dE/vdt \tag{3}$$

where $\frac{1}{2}mv^2=E$, forgetting that an electron will continually change its direction of motion.* This seems to be entirely unjustified.

It is the neglect by Seeger and Teller of the variation in direction which is responsible for the

[1] H. Fröhlich, Proc. Roy. Soc. **160**, 230 (1937).
[2] R. J. Seeger and E. Teller, Phys. Rev. **54**, 515 (1938).
[3] H. Fröhlich and N. F. Mott, Proc. Roy. Soc. (in press).

* The motion of an α-particle in a gas, to which Seeger and Teller refer, is entirely different, because of the much greater mass of an α-particle.

main differences in their and the author's final formulae for the breakdown field. Moreover, there seems to be also a mistake in the interaction which they take between an electron and an ion. The field at the distance r from the electron is $e/\kappa r^2$, and we may take the force, acting on an ion to be

$$e^2/\kappa r^2.$$

This neglects the Lorentz-Lorenz terms, which seems correct.[4] κ is the effective dielectric constant and will be defined more carefully below.

Now the following approximation is made in the calculation of Seeger and Teller. It is assumed that all ions at distances greater than $v/2\pi\nu$ (ν = lattice frequency) can follow the force acting on them adiabatically. At smaller distances, however, the interaction between electron and an ion is treated as an impulse of infinitely short duration. This then may lead to a loss of energy. According to this assumption only ions at distances greater than $v/2\pi\nu$ from the electron give a contribution to the polarization of the lattice by moving from their equilibrium positions, whereas inside this range, only the deformation of the ions may contribute. For the interaction of the electron with ions inside this range, therefore, κ must have values within the limits

$$1 \leqslant \kappa \leqslant \epsilon_0. \tag{4}$$

Here $(\epsilon_0 - 1)/4\pi$ is the polarizability of the ions.

Seeger and Teller's expression for κ, however, may be written in the form

$$\kappa = (\epsilon\epsilon_0)^{\frac{1}{2}},$$

making use of Born's lattice theory,[5] according to which

$$\epsilon - \epsilon_0 = e^2/2\pi a^3 M\nu^2. \tag{5}$$

Here, ϵ is the static dielectric constant, M is the resultant mass of the ions and a is the lattice distance. Since $\epsilon > \epsilon_0$, Seeger and Teller find $\kappa > \epsilon_0$ which is in contradiction with Eq. (4).

In the author's treatment any polarization would appear only in the second order of approximation. The first-order processes include only scattering and correspond to a value of κ equal to unity. It should be noted, however, that in contrast to a remark by Seeger and Teller, the interaction energy W between an electron and a dielectric medium is entirely correct in Fröhlich's treatment since W was given as

$$W = e\varphi$$

$$\nabla^2\varphi = 4\pi \operatorname{div} \mathbf{P}(r)$$

($\mathbf{P}$ = polarization of the dielectric). This is equivalent with

$$W = -e\int \frac{\operatorname{div} \mathbf{P}}{r} d\tau,$$

an expression which follows immediately from Maxwell's equations.

It is easy to see that in the case of fast electrons it is correct to assume that any possible screening of the electronic charge (i.e., a value of $\kappa > 1$) is an effect of a higher order. According to Fröhlich's treatment, the contribution of polarization waves of a wave number w to the time of relaxation τ is given by

$$\frac{1}{\tau} \sim \int_0^{w_0} w dw, \quad w_0 = 2^{\frac{1}{2}}\pi/a,$$

if the energy of the electron $E > \hbar^2 w_0^2/8m$. This means that the main contribution to the scattering is due to the ions in the immediate surrounding of the electron, where there can hardly be any screening. The effect on the energy loss dE/dt is greater since $dE/dt \sim \int dw/w$ which means that ions at greater distances contribute too. But even so the effect on the breakdown field is not greater that one would expect from an effect of a higher order (<30 percent).

For slower electrons one might expect a more important influence of a screening. For very slow (thermal) electrons, however, this effect should again be unimportant (as for fast electrons), as will be shown by Fröhlich and Mott.[3]

§3. The Condition for Breakdown

As we have seen, both authors assume that breakdown takes place when the field is so strong that all electrons with energy greater than a critical value E_c gain energy from the field more quickly than they lose it to lattice vibrations.

[4] Cf. N. F. Mott and M. J. Littleton, Trans. Faraday Soc. **34**, 485 (1938).

[5] Cf. M. Born and M. Göppert-Mayer, *Handbuch der Physik*, 2nd ed. 24/2, 623 (1933).

The condition for breakdown is thus

$$eF=(dE/dx)_{E=E_c}.$$

It may easily be seen that, as E is decreased, dE/dx rises to a maximum at a value of E in the neighborhood of several $h\nu$. Seeger and Teller assume with von Hippel[6] that E_c is equal to this value of E; thus *all* electrons in the conduction band will be accelerated by the field. Thus any electron in the conduction band will produce a secondary; the two electrons will be accelerated again so that finally an electron avalanche is built up.

In contrast to this it was considered by Fröhlich to be sufficient that electrons with an energy only a little below the ionization energy I should gain more energy from the field than they lose to the lattice. Thus the field would cause, it was argued, irreversible ionization processes so that no stationary state could exist. In the following we hope to go more deeply into the details of this question.

We shall discuss first the difficulties connected with the behavior of an electron gas in a constant external electric field. Assume a gas of N electrons which are in interaction with lattice vibrations. We shall assume that the interaction of the electrons with each other may be neglected and that N is so small that in the absence of a field the electrons are distributed over the energies according to the Maxwell distribution law. Now apply an external electrical field F. The electrons take up energy from the field in an irreversible way. To obtain a stationary state for the electrons in which a steady current flows, it must be possible for them to transfer this energy to the lattice. It has been shown previously (Fröhlich[1]) that in the case of an ionic lattice this is only possible for electrons with an energy $E<E'$, where the energy E' still depends on the field: $E'\sim 1/F$. For $E>E'$, the electrons will gain more energy from the field than they can transfer to the lattice. Thus, a stationary state is impossible unless a new kind of collision process is considered.

Now, for energies $E>I$ the distribution function is certainly determined rather by the collisions leading to ionization than by collisions with the lattice vibration, for the probability of ionization should be nearly 100 times bigger than the probability for scattering by the lattice vibrations. To obtain an equilibrium, we have, of course, to consider the inverse processes too, which means that as many electrons as leave the energy region $E>I$ by ionization, will come back by the reverse process. Now, as long as the field strength F is so small that $E'>I$ it seems to be possible to obtain a stationary state by means of the ionization processes. The energy which the electrons for which $E>E'$ obtain from the field must, of course, still finally go to the lattice. Such electrons spend, however, only a very short time in the energy region $E>E'$. As long as $E'>I$ they will, after the ionization, have an energy $E>E'-I>0$ and, therefore, there will be an opportunity to lose energy to the lattice.

Although an equilibrium is possible, it should be noted that the distribution function may be very different from a Maxwell distribution.

Now, if the field F is so strong that $E'<I$ an equilibrium should no longer be possible. For in this case, an electron with the energy E' will, on the average, gain the energy $I-E'$ from the field and then carry out an ionization process after which it will have an energy $E\sim 0$; thus it cannot transfer the energy $I-E'$ to the lattice.

It might be possible, of course, that the probability of finding an electron with an energy $E>E'$ is extremely small so that the deviation from a stationary state would not be serious. For $E'\sim I$ this would, in fact, be the case if an electron with the energy E' could be obtained only by thermal fluctuations, as Seeger and Teller suppose. Under the influence of an electrical field of about 10^6 volts/cm, however, there is a rather large chance for an electron to attain a high energy. Let $\phi(E)$ be the probability that an electron makes a collision per second. Then

$$W=\exp\left[-\int_0^t \phi(E)dt\right]$$

will be the probability that after t seconds it has *not* yet made a collision. During the whole time it is under the influence of the external field. It takes about $t=10^{-13}$ second to accelerate an electron from $E=0$ to $E=I$, i.e., to a velocity $v\sim 10^8$ cm/sec. The mean free path l of such electrons is $\sim 10^{-6}$ cm, for slow electrons ($v\sim 10^7$ cm/sec.) it is $\sim 10^{-7}$ cm. Thus $\phi=v/l\sim 10^{14}$ sec.$^{-1}$

[6] A. v. Hippel, Ergebn. exakt. Naturwiss. **14**, 79 (1935).

for all energies and $W \cong e^{10} \sim 10^4$. It thus follows that it will take only about $W \cdot t \sim 10^{-9}$ second to bring an electron up to energies $E' \sim I$. This shows that in strong fields (but below the breakdown strength where a stationary state is still possible) the equilibrium distribution of electrons is such that a considerable fraction of electrons have energies of the order $E \sim I$.

It should be emphasized that by a direct acceleration of an electron, which moves in the direction of the field, an ionization process may be caused even at field strengths below breakdown. Since, however, the reverse process exists (i.e., as electrons may as well be retarded by the field) the field will, in a first approximation, not change the number of ionization processes since it accelerates as many electrons as it retards. Thus it has to be decided by the second approximation, i.e., by the energy transfer A, whether or not a net increase of ionization processes is caused by the field.

There is still a possibility of obtaining a stationary state if we consider the recombination of an electron. Very little is known about recombination in solids, but it seems to be rather certain that such a process will take much longer* than 10^{-9} sec. Therefore, even if in principal a stationary state may eventually be reached, this state would be entirely different from the state where $E' > I$.

* The cross section for recombination with emission of light is $< 10^{-20}$ cm.

We shall now connect the above model with the actual case with which we have to deal in the breakdown problem. We note the experimental fact that for field strengths near the critical field of breakdown, but below it, there exists a stationary current in the dielectric medium. This means that in fact we deal with an electron gas in a stationary state. We shall not, at present, investigate theoretically how these electrons come into the conductive levels of the dielectric but accept it as an experimental fact. Then, it seems that the above considerations about the possibilities of reaching a stationary state may be applied.

The experimental evidence too seems to justify this condition. Hippel's condition (used by Seeger and Teller) would yield theoretical values for the breakdown field which are too high by a factor ~ 5 in the case of the alkali halides. The fact that Seeger and Teller obtained better values is due to a compensation by the different mistakes, discussed in §§2 and 3.

Finally I should like to mention in this connection that experiments by S. Whitehead, A. E. W. Austen and W. Hackett carried out at the laboratory of the British Electrical and Allied Industries Research Association (kindly communicated to the author before publication) have now confirmed most of the conclusions of the author's theory.*

* Cf. Austen and Hackett, Nature **143**. 637 (1939).

AUGUST 15, 1939 PHYSICAL REVIEW VOLUME 56

Remarks on the Dielectric Breakdown

R. J. SEEGER AND E. TELLER
The George Washington University, Washington, D. C.

(Received June 7, 1939)

IN the foregoing paper Fröhlich touches upon a number of questions that are of importance in the theory of breakdown of insulators. Since we do not find ourselves in agreement with his conclusions, we should like to clarify our point of view.

In the first place Fröhlich correctly remarks that in our treatment[1] of the interaction between an electron and a lattice the variation of direction in the motion of the electron has been neglected. Such variation of direction may, in fact, become very important either for electrons of high speed

[1] R. J. Seeger and E. Teller, Phys. Rev. **54**, 515 (1938).

or for crystals at high temperatures. In these two cases an electron after being scattered by a lattice vibration may still have a considerable velocity, and hence the direction of its motion is of importance. For electrons of low speed, however, and for crystals of sufficiently low temperature (i.e., the actual cases of interest in our paper) an electron will be practically at rest after a collision with a lattice vibration so that its direction of motion does not matter very much.

From a systematic point of view, of course, it would be desirable to have a treatment which includes the changes of electronic momentum and does not have to restrict itself to the calculation of energy loss. Such a treatment seems to exist, at present, only for those cases where Born's approximation applies. In the present problem this approximation is not valid owing to the strong interaction of an electron with the vibrations of the ions. It may be hoped that an approximation similar to the one used for molecules can be developed. In such an approximation the electronic wave function would depend on the displacements of the ions, while the force acting on the ions would be obtained by averaging over the electronic wave function. Such an approximation would probably also permit a more detailed discussion as to what extent Bohr's theory of deceleration of α-particles can be used to describe the interaction of a free electron with the lattice vibrations of an insulator.

A second point raised by Fröhlich is the form of the interaction between a free electron and the ions of the lattice. Fröhlich states that in the expression for the force acting on the ions $e^2/\kappa r^2$ the quantity κ must have a value between unity and ϵ_0 (e=charge of the electron, r=distance between electron and ion, ϵ_0=dielectric constant for a crystal in which the ions may be polarized but may not be moved). This is correct, however, only so long as one assumes that the electric effect of the displacement of an ion can be represented by moving a charge of the magnitude e. The treatment given in our paper avoids such an assumption of a charge rigidly bound to an ion.

Nevertheless Fröhlich is correct in objecting to our final formula since that formula gives $\kappa=(\epsilon_0\epsilon)^{\frac{1}{2}}$ (ϵ=actual dielectric constant of the crystal) rather than ϵ_0 for the limiting case of a charge of magnitude e rigidly bound to the ions. In this connection Professor Mott has kindly pointed out to us that since the longitudinal rather than the transversal lattice vibrations should appear in our derivation, the frequency of the former should appear in our final formula. Now this longitudinal frequency is considerably higher for a finite wave-length than that of a transversal vibration since electric charges accumulating in the nodes of the wave contribute to the restoring forces. This difference of frequencies has often escaped notice. Actually as soon as the wave-length becomes long as compared to the dimensions of the crystal the difference between longitudinal and transversal vibrations vanishes and a dependence of the frequency on the shape of the crystal appears instead. If the frequency of the longitudinal vibration is used in our formula then the correct value of ϵ_0 is obtained for the case of rigid ions. Thus it was apparently not correct for us to use the "*reststrahl*" frequency which—as one would assume—corresponds to a transversal vibration.

The difficulty of finding valid values for longitudinal and transversal vibrations becomes, however, apparent from measurements of Fermi and Rasetti[2] on the Raman effect of rocksalt. They find a continuous range of Raman shifts which, in accordance with selection rules, they interpret as first overtones of the lattice vibrations. The maximum shift agrees closely with twice the value of the "*reststrahl*" frequency. Now the latter frequency is supposed to be transversal. The maximum shift in the Raman effect on the other hand should be at least equal to twice the longitudinal frequency. Thus the question which values should be used for the longitudinal and transversal vibrations in crystals remains to be settled. In cases where the frequencies of the relevant vibrations are known it seems to us best to use the formula derived in our paper.

We agree, of course, with Fröhlich that for very fast electrons the screening by the bound electrons of the lattice would not be complete and that in this case κ should be smaller than

[2] E. Fermi and F. Rasetti, Zeits. f. Physik **71**, 689 (1931).

given by our formula. However, if the time of passage of an electron near an ion is longer than the reciprocal values of the electron-frequencies within the ion, simple arguments would lead us to expect that the electronic polarizability has its full effect as has been assumed in our paper.

The factors discussed so far are of importance only for the details of the theory. The main point of difference, however, remains, namely, whether the condition for the breakdown proposed by von Hippel and adopted by us is the correct one, or whether the condition set forth by Fröhlich is preferable. Our above discussion, however, is closely related to the answer to that very question since for electrons of very high speed Fröhlich's approximations are justified whereas for electrons of low speed (which are the important ones if von Hippel's criterion holds) our treatment seems more adequate.

Fröhlich has shown that, if the capture of free electrons can be neglected, then no stationary state exists for $E' < I$ (E' = electronic energy above which there is a net acceleration of electrons, I = ionization energy of the lattice). However, it is not quite clear that under such conditions even a value of $E' > I$ will make a stationary state possible. In fact, even if $E' > I$ is assumed, some electrons may gain sufficient energy from the field to produce ionization in the lattice. Inasmuch as no corresponding reverse process is considered, no stationary state can exist.

We believe, on the contrary, that the capture of free electrons may be a highly probable process. In particular, the possibility of "trapping"[3] of free electrons may be of importance. Although such removal of free electrons is not strictly the reverse process of ionization, a subsequent diffusion of the trapped electrons in the lattice may reunite the electrons with the halogen atoms. In our paper we have emphasized that in order for an electron avalanche to be built up it is not necessary that the field should be able to accelerate electrons of all energies. In order to find out how much smaller fields suffice it would be necessary to discuss in detail the trapping and the capture of free electrons. Such discussion would also give some information on the temperature dependence of the breakdown.

Unfortunately a direct experimental decision between the two proposed criteria for breakdown is difficult because of the appearance of the effective mass of the electron as an unknown constant in both theories. It would be interesting in this connection to investigate the breakdown of a crystal in which all relevant vibrations are hydrogen-vibrations. By comparing the breakdown of such a crystal with the breakdown of a similar crystal in which hydrogen is replaced by deuterium we could eliminate the effective mass of the electron and get a better insight into the breakdown mechanism. According to our theory the breakdown fields at low temperature should be inversely proportional to the square root of the reduced masses. If for the moment the logarithmic factor in Fröhlich's expression be neglected, the ratio of the breakdown fields at low temperatures should, according to his theory, be the ratio of the reduced masses to the $(-\frac{3}{4})$th power. The logarithmic factor brings the ratios predicted by the two theories more closely together. But even so the ratios should differ by approximately 10 percent so that an experimental decision is possible. The most clear cut example of this kind would be a comparison of lithium hydride and lithium deuteride. It is, however, very difficult to obtain these substances in a form which permits one to measure the breakdown strength.

[3] L. Landau, Physik. Zeits. Sowjetunion **3**, 664 (1933); A. von Hippel, Zeits. f. Physik **93**, 86 (1934).

The Normal Modes of Vibration of a Body-Centered Cubic Lattice

PAUL CHARLES FINE*
California Institute of Technology, Pasadena, California
(Received June 26, 1939)

An atomic model is set up for the purpose of finding the normal modes of vibration of a body-centered cubic lattice. A method is presented for selecting suitable atomic force constants from the macroscopic elastic properties of tungsten, which satisfy the isotropy condition but not the Cauchy relation. Actual solutions of the secular equation are then carried out under the assumption that each atom is affected by only its fourteen nearest neighbors. Numerical computations yield a frequency distribution characterized by two steep maxima. This is used in evaluating the specific heat and the intensity of reflection of x-rays as functions of temperature, and the results are compared with the Debye theory.

VARIOUS models have been proposed for the description of solid bodies and the consequences worked out in more or less detail. One of the most productive theories was formulated by Debye,[1] who considered a solid as an isotropic continuum, found that the number of vibrations in a given frequency range was proportional to the square of the frequency, and investigated the thermal variation of specific heats and the intensity of reflection of x-rays. At first the results were thought to be in very good agreement with experiment but discrepancies soon appeared. Several attempts have been made to explain these deviations by regarding a crystal as an atomic lattice rather than a continuum. Born and v. Kármán[2] derived an approximate expression for the specific heat by considering a simple cubic lattice. The general theory of atomic vibrations has been discussed by Born[3] and applied to two-dimensional lattices and polar crystals by Blackman.[4] In the present work an actual numerical calculation of the frequency distribution has been carried out for a model related to tungsten, a body-centered cubic crystal with elastic constants which happen to satisfy the isotropy condition.

The potential energy of the lattice is to a first approximation a quadratic function of the displacements of the atoms from their equilibrium positions. Let $u_r{}^j$ denote the component in the jth coordinate direction of the displacement of the atom whose lattice position is specified by the vector $\mathbf{r}$. Suppose that the potential energy V is expanded in a power series in terms of the displacements. Then,

$$V=V_0+\sum_j\sum_{\mathbf{r}}(\partial V/\partial u_r{}^j)_0 u_r{}^j$$
$$+(\tfrac{1}{2})\sum_j\sum_k\sum_{\mathbf{r}}\sum_{\mathbf{r}'}(\partial^2 V/\partial u_r{}^j\partial u_{r'}{}^k)_0 u_r{}^j u_{r'}{}^k+\cdots. \quad (1)$$

The summations with respect to $\mathbf{r}$ and $\mathbf{r}'$ are taken over all the atoms in the crystal and the superscripts j and k are summed over the three coordinate directions. The derivatives are to be evaluated when the displacements are all zero. The force in the j direction on the atom with a lattice position specified by $\mathbf{r}$ is $(\partial V/\partial u_r{}^j)_0$ when all other atoms are also in their lattice positions, and this force must vanish since the solid is then in equilibrium. If V_0 is taken as the zero reference value for the potential energy, then

$$V=(\tfrac{1}{2})\sum_j\sum_k\sum_{\mathbf{r}}\sum_{\mathbf{r}'}C_{jk}{}^{\mathbf{r}\mathbf{r}'}u_r{}^j u_{r'}{}^k, \quad (2)$$

where

$$C_{jk}{}^{\mathbf{r}\mathbf{r}'}=(\partial^2 V/\partial u_r{}^j\partial u_{r'}{}^k)_0.$$

Higher order terms are neglected for displacements small compared with the distances between atoms. By definition,

$$C_{jk}{}^{\mathbf{r}\mathbf{r}'}=C_{kj}{}^{\mathbf{r}'\mathbf{r}},$$

because both constants are factors of the same displacement product, $u_r{}^j u_{r'}{}^k$. For a monatomic cubic lattice, where every atom is situated in exactly the same way with respect to its

* Now at the University of Oregon.
[1] P. Debye, Ann. d. Physik **39**, 789 (1912); **43**, 49 (1914).
[2] M. Born and Th. v. Kármán, Physik. Zeits. **13**, 297 (1912); 14, 15 (1913).
[3] M. Born, *Atomtheorie des festen Zustandes* (Berlin, 1923).
[4] M. Blackman, Proc. Roy. Soc. **A148**, 365 (1935); Phil. Trans. Roy. Soc. **A236**, 103 (1936).

neighbors, there is an additional relation,

$$C_{kj}^{\mathfrak{r}\mathfrak{r}'}=C_{jk}^{\mathfrak{r}\mathfrak{r}'}=C_{jk}^{\mathfrak{r}'-\mathfrak{r}}, \tag{3}$$

so that the atomic force constants are symmetrical in their subscripts and depend only on the difference in the lattice positions of the atoms involved.

The kinetic energy of the atoms in the crystal can be written as

$$T=(\tfrac{1}{2})m\sum_j\sum_{\mathfrak{r}}(\dot{u}_{\mathfrak{r}}{}^j)^2, \tag{4}$$

where m is the mass of the atom and $\dot{u}_{\mathfrak{r}}{}^j$ is the time derivative of the displacement. The problem is to reduce the potential energy to a simpler form by introducing normal coordinates without thereby complicating the kinetic energy expression. This can be done for a general translation lattice but only the special case of a body-centered cubic crystal will be considered here. The basic cell then consists of two atoms, one situated at the point (0, 0, 0) and the other at $(a/2, a/2, a/2)$, where a is the length of one edge of the basic cube. The lattice position of any atom in the crystal is given either by $r_j=q_ja$ or by $r_j=(q_j+\frac{1}{2})a$, the integer q_j having values which range from zero to N_j, the total number of cells along the jth axis of the crystal.

The displacement of each atom is regarded as resulting from the superposition of plane waves in the solid, so that

$$u_{\mathfrak{r}}{}^j=\sum_n\{w^j{}_{0,\,n}\exp[2\pi i\sum_j(n_jq_j/N_j)]+w^j{}_{\frac{1}{2},\,n}\exp[2\pi i\sum_j n_j(q_j+\tfrac{1}{2})/N_j]\}, \tag{5}$$

where n_j is an integer related to the direction of the wave and having values from $-(\frac{1}{2})(N_j-1)$ to $(\frac{1}{2})(N_j-1)$. For the right side of this equation to be real, it is necessary that the normal coordinates $w^j{}_{0,\,n}$ and $w^j{}_{\frac{1}{2},\,n}$ be complex and that $w^j{}_{0,\,-n}=w^j{}_{0,\,n}{}^*$ and $w^j{}_{\frac{1}{2},\,-n}=w^j{}_{\frac{1}{2},\,n}{}^*$. The number of independent coordinates is therefore equal to the number of degrees of freedom of the atoms in the crystal.

When this change of variables is made in the potential energy, the result is

$$V=(\tfrac{1}{2})N_1N_2N_3\sum_j\sum_k\sum_n[C_{jk}{}^n(w^j{}_{0,\,n}w^k{}_{0,\,-n}+w^j{}_{\frac{1}{2},\,n}w^k{}_{\frac{1}{2},\,-n})+2C_{jk}{}^{n'}w_{0,\,n}w_{\frac{1}{2},\,-n}], \tag{6}$$

where

$$C_{jk}{}^n=\sum_g C_{jk}{}^g\exp[-2\pi i\sum_j(n_jg_j/N_j)]$$

and

$$C_{jk}{}^{n'}=\sum_g C_{jk}{}^{g+\frac{1}{2}}\exp[-2\pi i\sum_j n_j(g_j+\tfrac{1}{2})/N_j].$$

The quantity g_j is equal to $q_j'-q_j$ and the summation is from $g_j=-(N_j-1)$ to $g_j=(N_j-1)$. The kinetic energy has the following form after reduction:

$$T=(\tfrac{1}{2})N_1N_2N_3m\sum_j\sum_n\left[\left(\frac{\partial w^j{}_{0,\,n}}{\partial t}\right)\left(\frac{\partial w^j{}_{0,\,-n}}{\partial t}\right)+\left(\frac{\partial w^j{}_{\frac{1}{2},\,n}}{\partial t}\right)\left(\frac{\partial w^j{}_{\frac{1}{2},\,-n}}{\partial t}\right)\right], \tag{7}$$

The equations of motion found by Lagrange's method are then

$$\begin{aligned}\sum_j(C_{jk}{}^nw^j{}_{0,\,n}+C_{jk}{}^{n'}w^j{}_{\frac{1}{2},\,n})&=m\frac{\partial^2w^k{}_{0,\,n}}{\partial t^2},\\ \sum_j(C_{jk}{}^{n'}w^j{}_{0,\,n}+C_{jk}{}^nw^j{}_{\frac{1}{2},\,n})&=m\frac{\partial^2w^k{}_{\frac{1}{2},\,n}}{\partial t^2}.\end{aligned} \tag{8}$$

If now it is assumed that

$$w_{0,\,n}{}^j=A_{0,\,n}{}^j\exp[i\omega_nt]$$

and

$$w_{\frac{1}{2},\,n}{}^j=A_{\frac{1}{2},\,n}{}^j\exp[i\omega_nt]$$

where ω_n is proportional to the frequency of vibration, homogeneous linear equations are obtained for the unknown amplitudes. The condition for a nontrivial solution is a sixth-order determinant set equal to zero. However, two third-order factors can be found and the two determinantal equations written together in the form,

$$\begin{vmatrix}(C_{11}{}^n\pm C_{11}{}^{n'}-m\omega_n{}^2) & (C_{12}{}^n\pm C_{12}{}^{n'}) & (C_{13}{}^n\pm C_{13}{}^{n'})\\ (C_{12}{}^n\pm C_{12}{}^{n'}) & (C_{22}{}^n\pm C_{22}{}^{n'}-m\omega_n{}^2) & (C_{23}{}^n\pm C_{23}{}^{n'})\\ (C_{13}{}^n\pm C_{13}{}^{n'}) & (C_{23}{}^n\pm C_{23}{}^{n'}) & (C_{33}{}^n\pm C_{33}{}^{n'}-m\omega_n{}^2)\end{vmatrix}=0. \tag{9}$$

The positive sign gives one equation and the negative sign another.

There is a frequency for every value of n so that a whole spectrum is obtained. For certain special directions in the crystal the determinant can be reduced to linear or quadratic factors and explicit solutions obtained immediately, but in general numerical methods must be used in solving the cubic equations. This necessitates information about the values of the atomic constants involved. By equating the potential energy arising from a large scale distortion of the solid to that resulting from the corresponding atomic displacements it is possible to secure relations between the atomic force constants and the macroscopic elastic properties of the crystal. However, these are not sufficient to determine the atomic constants uniquely unless simplifying assumptions are made. Thus, for the body-centered cubic lattice, only the interactions between a given atom and its fourteen nearest neighbors will be considered. After the symmetry properties of the crystal are utilized, only five atomic force constants remain and these are related to the macroscopic elastic constants, c_{11}, c_{12} and c_{44}, by the following equations:

$$\begin{aligned} C_{11}^{0,0,0}+2C_{11}^{1,0,0}+4C_{11}^{0,1,0}+8C_{11}^{\frac{1}{2},\frac{1}{2},\frac{1}{2}}&=0,\\ C_{11}^{1,0,0}+C_{11}^{\frac{1}{2},\frac{1}{2},\frac{1}{2}}&=-(\tfrac{1}{2})ac_{11},\\ C_{11}^{0,1,0}+C_{11}^{\frac{1}{2},\frac{1}{2},\frac{1}{2}}&=-(\tfrac{1}{2})ac_{44},\\ C_{12}^{\frac{1}{2},\frac{1}{2},\frac{1}{2}}&=-(\tfrac{1}{2})ac_{12}. \end{aligned} \tag{10}$$

The superscripts refer to the difference in lattice positions for the atoms concerned.

If central forces are postulated, $C_{11}^{0,1,0}$ may be neglected, since a displacement at right angles to the line connecting two atoms gives rise to a second-order effect in the potential energy. Moreover, the model used leads to the Cauchy relations, which state that $c_{12}=c_{44}$ for a cubic crystal. This relation is not experimentally verified for metals, so that some modification is necessary in order to obtain suitable atomic constants from empirical data. A way of doing this is suggested by the work of Fuchs,[5] who showed by means of the Wigner-Seitz quantum-mechanical methods that the failure of the Cauchy relation for a monovalent metal is due to the effect of the valence electrons on the compressibility of the crystal. The constants c_{44} and $c_{11}-c_{12}$ are not affected because they are involved in strains where the volume is not changed. Since, in the present work, the atom is represented as a point mass and no provision is made for the electrons, it seems reasonable in securing appropriate force constants to make use of the Cauchy relation as the third condition instead of the observed compressibility.

The experimental values[6] for the elastic constants of a tungsten single crystal at room temperature are as follows:

$$\begin{aligned} c_{11}&=5.13\times10^{12}\ \text{dynes/cm}^2,\\ c_{12}&=2.06\times10^{12},\\ c_{44}&=1.53\times10^{12}. \end{aligned} \tag{11}$$

The isotropy condition, $c_{44}=(\frac{1}{2})(c_{11}-c_{12})$, is therefore satisfied[7] and the equations for the atomic force constants can be solved.

$$\begin{aligned} C_{11}^{0,0,0}&=6ac_{44},\\ C_{11}^{1,0,0}&=-ac_{44},\\ C_{11}^{\frac{1}{2},\frac{1}{2},\frac{1}{2}}&=C_{12}^{\frac{1}{2},\frac{1}{2},\frac{1}{2}}=-(\tfrac{1}{2})ac_{44}. \end{aligned} \tag{12}$$

Without isotropy the atomic constants would be expressed in terms of two parameters instead of the single one appearing here. The sums which enter the secular equation (9) may now be evaluated and the determinant written out as follows:

$$\begin{vmatrix} (1+\sin^2 x\mp\cos x\cos y\cos z-f_n^2) & (\pm\sin x\sin y\cos z) & (\pm\sin x\cos y\sin z)\\ (\pm\sin x\sin y\cos z) & (1+\sin^2 y\mp\cos x\cos y\cos z-f_n^2) & (\pm\cos x\sin y\sin z)\\ (\pm\sin x\cos y\sin z) & (\pm\cos x\sin y\sin z) & (1+\sin^2 z\mp\cos x\cos y\cos z-f_n^2) \end{vmatrix}=0. \tag{13}$$

Here, $x=\pi n_1/N_1$, $y=\pi n_2/N_2$, $z=\pi n_3/N_3$, and $f_n=(m\omega_n^2/4ac_{44})^{\frac{1}{2}}$, a quantity directly proportional to the frequency.

In order to find the values of f_n^2 at various points in ten planes perpendicular to the z axis, 140 cubic equations were solved. Then, by interpolation, curves of constant frequency in these

[5] K. Fuchs, Proc. Roy. Soc. **A153**, 622 (1936); **157**, 444 (1936).
[6] P. W. Bridgman, Proc. Nat. Acad. **10**, 411 (1924).
[7] S. J. Wright, Proc. Roy. Soc. **A126**, 613 (1930).

planes were determined, their areas found numerically, and the volumes bounded by surfaces of constant frequency built up out of these

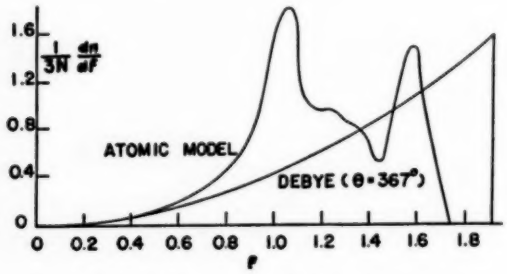

FIG. 1. Frequency distribution.

slices. This gives the number of modes of vibration having a frequency less than a certain value and may be designated by n. To obtain the frequency distribution an approximate differentiation was performed and the curve in Fig. 1 secured for $(1/3N)(dn/df)$, a quantity equal to the fraction of the total number of vibrations in a given frequency range. N is equal to $2N_1N_2N_3$, the total number of atoms in the lattice.

It is found that at very low frequencies the Debye type of distribution is valid, a result to be expected when the wave-length is long in comparison with interatomic dimensions. A parabolic extension of this part of the curve gives a Debye function with a characteristic temperature $\theta=367°$, agreeing closely with the value of 373° calculated from the elastic constants by means of the Debye theoretical formula. However, it is clear that there is agreement between the two curves only over an insignificant portion of the complete spectrum. The most distinctive feature of the distribution for the atomic model is the presence of two steep maxima. This is to some extent a justification of the Nernst-Lindemann specific heat formula where two frequencies are utilized instead of the single frequency of the Einstein theory. Another difference between the distributions for the atomic model and the Debye theory is in the determination of the upper limit of the frequency. According to Debye, the distribution derived for a continuum is abruptly terminated at a point where the number of vibrations equals the number of degrees of freedom of the atoms in the solid. This sudden use of the atomicity of the crystal as a last resort is artificial and contradictory. In the present work where the atomic nature of the solid is considered from the beginning, the existence of a maximum frequency is a natural and necessary consequence.

One of the applications of the frequency distribution is in computing the specific heat at constant volume, which can be written in the form,

$$C_v=\int_0^{\nu_m}\frac{(h^2\nu^2/kT^2)(e^{h\nu/kT})}{(e^{h\nu/kT}-1)^2}(dn/d\nu)d\nu. \quad (14)$$

A numerical integration has been carried out for the atomic model, and the comparison between theory and experiment is shown in Table I. The Debye values for $\theta=310°$ are the result of fitting the empirical data for tungsten. The fact that the Debye characteristic temperature is often selected to give the best fit with the observed specific heats instead of being calculated from the theoretical formula involving the elastic constants is perhaps a cause of undue confidence in the theory. Although the present work also gives a specific heat which depends on a single constant, it was not thought advisable to evaluate it from observations which include the effect of electrons as well as atomic vibrations and probably interactions between the two.

It is seen that the Debye values for $\theta=367°$ are too low at all temperatures, while those for $\theta=310°$ are in very good agreement with experiment. The atomic model and the Debye theory

TABLE I. *Specific heats (cal. per mole per °K).*

T	C_v (ATOMIC MODEL)	C_v (OBS.)*	C_v (DEBYE, $\theta=367°$)	C_v (DEBYE, $\theta=310°$)
26.01° K	0.242	0.213	0.165	0.272
32.3	0.495	0.434	0.310	0.506
38.8	0.842	0.750	0.528	0.826
46.7	1.34	1.21	0.861	1.28
54.7	1.84	1.80	1.25	1.77
74.4	2.94	2.87	2.25	2.85
78.3	3.12	3.07	2.42	3.03
84.2	3.37	3.33	2.69	3.29
91.1	3.63	3.60	2.97	3.55
100	3.92	3.77	3.30	3.85
150	4.90		4.50	4.86
200	5.32	5.30	5.06	5.30
250	5.52		5.36	5.52
300	5.66	5.87	5.54	5.65

* F. Lange, Zeits. f. physik. Chemie **110**, 343 (1924). (For temperatures from 26.01 to 91.1.) C. Zwikker, Zeits. f. Physik **52**, 668 (1928). (For temperatures from 100 to 300.)

TABLE II. *Root mean square displacements.*

T	$\mu^{\frac{1}{2}}$ (ATOMIC MODEL)	$\mu^{\frac{1}{2}}$ (DEBYE, $\theta=367°$)	$\mu^{\frac{1}{2}}$ (DEBYE, $\theta=310°$)
0°K	0.0251A	0.0231A	0.0251A
100	0.0307	0.0279	0.0319
200	0.0401	0.0356	0.0417
300	0.0480	0.0426	0.0502
400	0.0550	0.0488	0.0576
500	0.0613	0.0544	0.0642

have in common the variation of the specific heat as the third power of the temperature near absolute zero and the asymptotic approach to the equipartition value at high temperatures. The specific heat for the atomic model checks very well with the empirical data at intermediate temperatures, but the results are too high at low temperatures. This is probably due in part to the fact that it was necessary to use elastic constants which had been measured at room temperature. An increase in the elastic constants as the temperature is lowered would lead to a smaller specific heat. Although no information is available for tungsten, metals with similar crystal structures do have elastic properties which behave in such a way. On the other hand, the rise of the observed specific heat above the equipartition value at high temperatures may be caused in part by anharmonic vibrations which are responsible for the thermal expansion of the solid and in part by the excitation of electronic motions.

Another application deals with the variation of the intensity of reflection of x-rays with temperature. The theory was first developed by Debye and has been put in more concise form by Zener and Jauncey.[8] Because of their thermal motion the atoms do not remain in the lattice planes but undergo displacements which increase with the temperature and result in destructive interference and lower intensity for the reflected x-rays. The temperature factor may be written as e^{-M}, where

$$M=(8\pi^2\mu \sin^2 \varphi)/\lambda^2, \tag{15}$$

φ being the grazing angle of incidence, λ the wave-length, and μ the mean square displacement of an atom from a given plane. For a cubic crystal μ has the same value for all planes and is given by the following expression:

$$\mu=(h/12\pi^2Nm)\int_0^{\nu_m}(1/\nu)\times\{[1/(e^{h\nu/kT}-1)]+\tfrac{1}{2}\}(dn/d\nu)d\nu, \tag{16}$$

where ν_m is the maximum frequency. This integral has also been evaluated numerically for the atomic model and the results are compared with the Debye theory in Table II, where the root mean square displacements are given in angstroms.

At high temperatures the theoretical formula for μ is particularly simple and significant, showing a linear temperature variation with a slope equal to the average value of the reciprocal of the square of the frequency with respect to the frequency distribution.

Atomic model:
$$\mu=(6.28+0.0742T)\times10^{-20}\ \text{cm}^2$$
Debye ($\theta=367°$):
$$\mu=(5.34+0.0583T)\times10^{-20} \tag{17}$$
Debye ($\theta=310°$):
$$\mu=(6.32+0.0815T)\times10^{-20}.$$

Thus, the various theories give different values for the intensity of x-ray reflections at high temperatures, although the specific heats all agree in approaching the equipartition value. However, it is not possible at present to compare these results with experiment since there are no data available for tungsten.

It is hoped that this work may be continued by applications to other body-centered cubic lattices and also to face-centered cubic crystals. The numerical difficulties increase with the complexity of the crystal structure and a less complicated method of obtaining the frequency distribution from the secular equation would be desirable.

The author is greatly indebted to Dr. W. V. Houston for many valuable suggestions without which this work would not have been possible.

[8] C. Zener and G. E. M. Jauncey, Phys. Rev. **49**, 17 (1936); C. Zener, Phys. Rev. **49**, 122 (1936).

Theory of Magnetic Effects in the Plasma of an Arc

L. TONKS
Research Laboratory, General Electric Company, Schenectady, New York

(Received May 29, 1939)

The equations governing electron drift in the presence of a magnetic field are applied to the low pressure uniform positive column plasma. (1) An exponential variation of electron concentration with distance across an arc in a transverse magnetic field, found experimentally, is accounted for quantitatively. (2) A longitudinal magnetic field leaves the point-to-point concentration of electrons unchanged and does not alter the relative potentials in the cross section although transverse potential differences in the plasma decrease everywhere in proportion as the magnetic field increases. The transverse plasma fields vanish or even reverse slightly for large enough fields. (3) The plasma exhibits a diamagnetic susceptibility for longitudinal fields, which is proportional to the electron current density to the tube walls. With nonconducting walls electron wall current is automatically adjusted to the ion wall current. The magnetic polarization then increases oppositely to the magnetic field at first, reaches a maximum and then decreases hyperbolically to zero, so that beyond the maximum the plasma is paramagnetic for small variations in the field. Qualitatively this is the same behavior predicted by a previous erroneous theory which was itself checked only qualitatively by experiment. The present theory predicts that the diamagnetic polarization shall be directly proportional to the electron current to the tube wall and the magnetic field. (4) The magnetic field of the arc itself has a concentrating pinch effect which would cause the axial concentration of electrons to become infinite at a finite arc current if other limitations did not intervene. This may be the cause of rapidly increasing arc gradients in the neighborhood of certain critical currents in large mercury arc rectifiers. Larger diameter arc columns and higher pressures favor the magnetic pinch effect as a cause of current limitation over a blowout effect due to the outward-moving positive ions driving the gas before them.

I. INTRODUCTION

THE fundamental equations describing the motion of electrons in a gas under the simultaneous action of electric and magnetic fields and concentration gradients have been known for some time[1–3] but they have not been systematically applied to phenomena occurring in the plasma of an arc. In the present article this application will be made in two cases which have already been investigated experimentally, and also to two cases in which the direct experimental evidence is more meager but on which the theory can shed light. These cases are, in order of treatment:

(1) Killian's measurements[4] on the effect of a transverse field on a positive column in low pressure mercury vapor.

(2) The effect of a longitudinal magnetic field on a uniform positive column.

(3) Steenbeck's determination[5] of the diamagnetic susceptibility of a positive column.

(4) The constrictive effect of the arc's own magnetic field.[6]

For a magnetic field H_z in the positive z direction, the components of electron drift velocity ξ and η in the x and y directions, respectively, are, according to the paper by Tonks and Allis[3]

$$\xi=\tfrac{1}{3}l_e\bar{c}(\alpha b_x+\beta b_y), \quad (1)$$

$$\eta=\tfrac{1}{3}l_e\bar{c}(\alpha b_y-\beta b_x), \quad (2)$$

where l_e is the electron mean free path; $\bar{c}$ the mean electron speed; α and β are constants which depend on l_e, the electron temperature T_e, and H_z. The quantities b_x and b_y are space derivatives of what may be called the "Boltzmann velocity potential function"[3]

$$B=-(eV/kT_e+\ln n_e). \quad (3)$$

It will often be convenient later to use the diffusion coefficient of electrons, D_e, to eliminate the electron mean free path by

$$D_e=l_e\bar{c}/3. \quad (4)$$

It will also be convenient to introduce

$$\omega_H=eH_z/(m_ec)=-1.778\times10^7H_z, \quad (5)$$

[1] F. B. Pidduck, Proc. London Math. Soc. **15**, 89 (1915) and Phys. Rev. **53**, 197 (1938).
[2] R. Gans, Ann. d. Physik **20**, 293 (1906).
[3] L. Tonks and W. P. Allis, Phys. Rev. **52**, 710 (1937).
[4] Unpublished work done in this laboratory.
[5] M. Steenbeck, Wissen. Veröff. Siemens **15** (2) 1 (1936).
[6] A brief statement of the result of this analysis has been given: L. Tonks, Trans. Electrochem. Soc. **72**, 167 (1937).

the angular momentum corresponding to the magnetic field. The negative sign is a consequence of the negative charge on the electron. Another useful quantity will be h', which is related to the h of reference 3 and is defined by

$$h' = \omega_H l_e/\bar{c} = (eH/m_e c)(3D_e/\bar{c}^2) = 0.886h. \quad (6)$$

The exact equations for α and β are inconveniently complicated. But we can circumvent this difficulty by putting

$$\alpha = \gamma_\alpha \alpha_a, \quad \alpha_a = (1/(1+h'^2), \quad (7)$$

$$\beta = \gamma_\beta \beta_a, \quad \beta_a = h'/(1+h'^2), \quad (8)$$

where γ_α and γ_β are correction factors which do not differ greatly from unity in the whole range of h' (or h) from zero to infinity, as can be seen from Fig. 1.

It has been noted that the actual drift velocity is only slightly less than the product of the b for the drift direction and the normal nonmagnetic mobility.[3] In effect the magnetic field determines simply that the electrons shall drift at an angle (whose tangent is $\gamma_\beta h'/\gamma_\alpha$) to the direction which they would take under the influence of the existing potential and concentration gradients alone. Since the electrons are constrained to move at this angle (almost as if by an inclined plane) only the components of the gradients in this direction are effective, but these components have almost the full effectiveness (between 88.3 and 100 percent) which they would have were the magnetic field absent. Thus

$$u_d = \gamma_r D_e b_d, \quad (8.5)$$

where b_d is the b in the drift direction, u_d is the drift velocity, and γ_r is the correction factor given by

$$\gamma_r = \alpha + \beta^2/\alpha. \quad (9)$$

This also is plotted in Fig. 1. It varies between unity at zero h and 0.883 at infinite h. Fig. 1 contains, besides, a plot of

$$\gamma = (\beta/\alpha)/(\beta_a/\alpha_a) = \beta/(\alpha h') = \gamma_\beta/\gamma_\alpha. \quad (10)$$

These curves furnish an idea of the numerical magnitude of any error which arises from treating the γ's as if they were constants.

II. Effect of a Transverse Magnetic Field on a Positive Column

In 1928 in these laboratories T. J. Killian made some measurements on a low pressure mercury arc subjected to a uniform transverse magnetic field (in the z direction). The arc tube was the same one that served for experiments already described.[7] It suffices here to note that the vapor pressure in his 6.2-cm diameter tube was under control and that a fine wire probe parallel to the tube axis (y direction, positive toward anode) could be moved along a tube diameter which was perpendicular to the magnetic field (x direction). By analyzing probe characteristics, the electron temperatures and concentrations were determined from one wall to the other. Fig. 2 shows the results of such measurements at the saturated mercury vapor temperature 38.6°C, corresponding to 7.1 bars. This temperature has been chosen because at lower vapor pressures the electron mean free paths become so long relative to arc tube diameter that diffusion and mobility relations do not strictly apply.

The question of interpreting probe characteristics in the presence of a magnetic field naturally arises. In the z direction electrons could reach the probe unhampered by H_z. But the

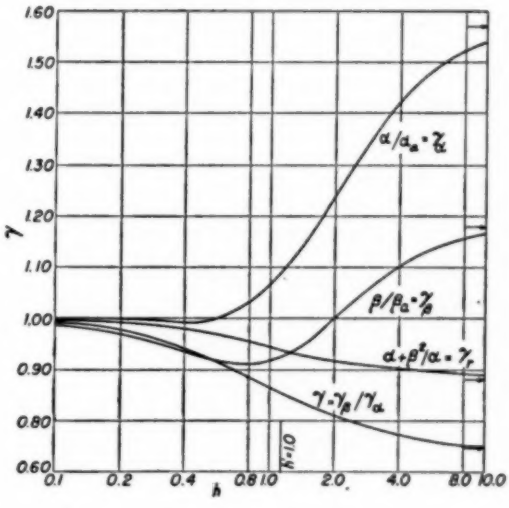

FIG. 1. Correction factors for approximate electron drift formulas. The h' scale is slightly displaced from the h scale, but this is only of minor importance in evaluating the γ's.

[7] T. J. Killian, Phys. Rev. **35**, 1238 (1930).

decrease of mobility in the x direction leads to the expectation of smaller maximum probe currents with the magnetic field than without.

This affects the possibility of calculating absolute values of electron concentration from the characteristics but in no way changes the proportionality of the probe currents to the electron concentrations. Thus the probe current where the characteristic ceases to be exponential is still a measure of relative electron concentration and the potential at this current is the space potential.

Finally, it must be certain that the probe characteristics give the electron temperature. In general a perfectly reflecting negative probe would establish electron concentrations and current densities in its vicinity in accord with the Boltzmann equation irrespective of the presence of a magnetic field. The electrons very close to the surface of the probe which are moving toward it and would, therefore, strike it can be thought of as consisting of two classes, C and F. Class C consists of electrons whose last atom collision lay close to the probe. Class F consists of those which last collided at some distance from the probe. Of the class C electrons, an appreciable fraction (class C_r) will have just previously been reflected from the probe. For Class F geometrical considerations make this fraction negligible. Hence, if the probe becomes nonreflecting and actually collects the electrons striking it, the concentration of C electrons is depleted by the loss of the C_r electrons while the F electrons are unaffected. If the concentration of C_r electrons is negligible relative to that of the F electrons or the C electrons, or their sum, the actual flow of current to the probe causes no departure from the ideal characteristic. Unless the magnetic field sufficiently increases the number of Class C_r electrons relative to Class F or Class C, it will not distort the probe characteristic.

Such distortion was certainly not present in Killian's work. The electron mean free path was about 1 cm, the probe radius 0.013 cm so that in the absence of magnetic field few electrons leaving the vicinity of the probe would have made their first collision near the probe and the number of C_r electrons would have been negligible.

The presence of the field would, by spiraling the electron paths around the z direction, confine them to helical paths having the average radius

$$r_\lambda = 3.35 V_e^{\frac{1}{2}}/H_z, \quad V_e = T_e/11{,}600.$$

For $V_e \sim 1.5$ v and $H_z = 12$ oersteds

$$r \leq 0.34 \text{ cm}$$

and this represents the average progress of an electron in the x direction before its next impact. Since the z component of electron motion is unaffected by H_z, the average progress of an electron in the z direction can be found by averaging the z components of mean free paths of random directions. This leads to half the normal mean free path, or 0.5 cm.

We now define as C electrons those whose last collision prior to striking the probe lay within the xz section extending 0.5 cm in the z direction and 0.34 cm in the x direction. Of these, half came from the direction away from the probe. Of the other half only the fraction represented by the ratio of probe thickness, 0.025 cm, to section width, 0.68 cm would have collided with the probe. Thus the ratio of C_r to C electrons is $\frac{1}{2} \times 0.025/0.68 = 0.018$. This rough estimate therefore indicates a correction of less than 2 percent arising from a field of 12 oersteds, which will be neglected.

Since the experimental results can be interpreted to give relative electron concentration, space potential, and electron temperature, the

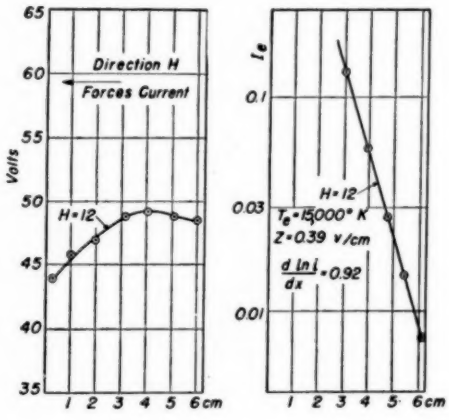

FIG. 2. Space potential and electron current density distributions across a Hg arc positive column in a transverse magnetic field. Tube diameter 6.2 cm. Condensed Hg temperature 38.6°C. Arc current 5 amp. Longitudinal gradient without magnetic field 0.31 v/cm, with field 0.39 v/cm. Data by T. J. Killian, 1928.

theoretical equations can be applied. The ratio of transverse ion current density, and hence transverse electron current density, to arc current is of the order of 1 : 400. Accordingly, in Eqs. (1) and (2)

$$\xi/\eta \sim 1/400$$

so that

$$b_x/b_y = -\frac{\beta/\alpha - 1/400}{1+\beta/(400\alpha)} = -\beta/\alpha = -\gamma h' \quad (10.5)$$

as long as

$$400 \gg \gamma h' \gg 1/400.$$

Since n_e is constant along the plasma axis, Eq. (3) yields eY/kT_e for b_y where $-Y$ is the arc gradient. In the x direction Fig. 2 shows that V is approximately constant from 3 to 6 cm so that for b_x in this region we have $-d \ln n_e/dx$. Making use of Eqs. (10.5) and (6) we can write

$$d \ln n_e/dx = \omega_H l_e e Y \gamma / \bar{c} k T_e.$$

Now

$$l_e/\bar{c} = 1.605 \times 10^{-6} l_e T_e^{-\frac{1}{2}} \quad (11)$$

and

$$eY/kT_e = -1.16 \times 10^4 Y/T_e \text{ (practical)}.$$

Combining and using Eq. (5) we have:

$$d \ln n_e/dx = 3.31 \times 10^5 l_e H_z Y T_e^{-\frac{1}{2}} \gamma. \quad (12)$$

Killian's own data[7] on Hg arcs without a magnetic field yield a mean free path of 1.5 cm for the electrons at 38.6° condensed Hg temperature. From the experimental data and curves: $H_z = 12$, $Y = -0.39$ v/cm, $T_e = 15{,}000°$K. Accordingly, from Eq. (12)

$$d \ln n_e/dx = -1.23\gamma.$$

Now from Eqs. (6), (4) and (11)

$$h = 32.2 H l_e T_e^{-\frac{1}{2}},$$

whence

$$h = 4.74,$$

thus justifying the approximation in Eq. (10.5). From Fig. 1,

$$\gamma = 0.77,$$

so that

$$d \ln n_e/dx = -0.95.$$

This is to be compared with the direct experimental determination of the variation of random electron current with x, shown in Fig. 2. That gives

$$d \ln n_e/dx = -0.92.$$

This is a very satisfactory check.

Unfortunately, probe characteristics taken at 30 oersteds field strength show deviations from the classical shape which make it impossible to compare the theoretical and observed gradient of electron concentration at this field strength.

III. Theory of a Positive Column Plasma in a Longitudinal Magnetic Field

The pressure range for which this theory will be developed is that in which the quasi-neutral diffusion relations apply in the absence of magnetic field.

The essential difference of the magnetic from the nonmagnetic[8, 9] case is that we cannot ignore the resistance of the gas to the radial flow of electrons. In a tube with nonconducting walls the radial drift velocities of electrons u_e and ions u_p are everywhere equal, but the ratio of the two can be controlled by the potential of conducting walls so that in general

$$u_e = \mu u_p \quad (13)$$

with any value from zero to several hundred possible for μ.

Choosing cylindrical coordinates with the z axis along the tube axis, we have the following relations left unaffected by the magnetic field:

$$n_e = n_p, \quad (14)$$

$$u_p = -D_p[\partial \ln n_p/\partial r - (e/kT_p)\partial V/\partial r], \quad (15)$$

$$\partial(n_p u_p r)/\partial r = r\lambda n_e, \quad (15.5)$$

where D_p is the positive ion diffusion coefficient, T_p is the positive ion temperature, and λ is the number of ions formed per electron per second. Eqs. (1) and (2) applied to the cylindrical case give

$$u_e = D_e(\alpha b_r + \beta b_\varphi), \quad (16)$$

$$v_e = D_e(\alpha b_\varphi - \beta b_r), \quad (17)$$

---

[8] W. Schottky, Zeits. f. Physik **31**, 163 (1925) and Physik. Zeits. **25**, 342 (1924).

[9] L. Tonks and I. Langmuir, Phys. Rev. **34**, 876 (1929). In referring to this paper it will be called "General Theory."

where v_e is the tangential drift velocity, and

$$b_r=-\frac{e}{kT_e}\frac{\partial V}{\partial r}-\frac{\partial \ln n_e}{\partial r},$$
$$b_\varphi=-\frac{e}{kT_e}\frac{\partial V}{r\partial \varphi}-\frac{\partial \ln n_e}{r\partial \varphi}. \tag{18}$$

Obviously, there is axial symmetry so that $b_\varphi=0$.

Relating (15) and (16) in accordance with (13) we have

$$\alpha D_e\left(-\frac{e}{kT_e}\frac{\partial V}{\partial r}-\frac{\partial \ln n_e}{\partial r}\right)=-\mu D_p\left(\frac{\partial \ln n_e}{\partial r}-\frac{e}{kT_p}\frac{\partial V}{\partial r}\right),$$

whence $$n_e=n_0 \exp(-eV/kT_e\tau) \tag{19}$$

with $$\tau=\frac{\alpha D_e-\mu D_p}{\alpha D_e+\mu D_p T_e/T_p}. \tag{20}$$

Eq. (19) replaces the Boltzmann equation among those whose solution gives the plasma relations. Since, mathematically Eq. (19) is simply the Boltzmann equation with $T_e\tau$ in place of T_e, and since T_e appears nowhere else among the original equations which are to be solved simultaneously, we can immediately write the equations for the radial distribution of electrons in a column of radius a as modifications of the usual equations:[10]

$$n_e=n_0 J_0(2.40r/a) \tag{21}$$

with $$a=2.40\left(\frac{D_p(\tau T_e+T_p)}{\lambda T_p}\right)^{\frac{1}{2}} \tag{22}$$

or, by Eq. (20)

$$a=2.40\left[\frac{(T_e+T_p)D_eD_p\alpha}{\alpha D_eT_p+\mu D_pT_e}\lambda^{-1}\right]^{\frac{1}{2}}. \tag{23}$$

(It must be noted that only in Eq. (22) does the modification of T_e to τT_e appear. In relating D_e to the electron mean free path or in relating λ to the ionization probabilities, the unchanged value of T_e still applies.) Also by Eq. (19)

$$V=(kT_e\tau/e)\ln[J_0(2.40r/a)]. \tag{24}$$

[10] The elimination of u_p between Eqs. (15) and (15.5) and then V by Eq. (19) and n_p by Eq. (14) gives Bessel's equation with the boundary condition $n_e=0$ at $r=a$.

Several conclusions are now possible. First, Eq. (21) shows that the radial distribution of ions and electrons remains unchanged from the nonmagnetic case. Second, Eq. (20) shows that τ decreases with magnetic field due to the decrease of the numerator, with the consequence that λ in Eq. (22) decreases. Since λ increases rapidly[11] with T_e, this means that T_e decreases with increase of magnetic field. Looked at qualitatively, the decrease in outward flow of electrons and hence ions balances with a lower rate of ionization per electron and hence a lower electron temperature. It is easily observed that an axial magnetic field reduces the longitudinal gradient in an arc. Third, by Eq. (24) the potential distribution remains the same, but the scale of potential variation is reduced. As the transverse mobility of the electrons decreases toward that of the ions, the electric field whose function it is to equalize the ion and electron drifts becomes less.

It would even appear that τ could become zero and reverse in sign, accompanied by a complete flattening of the potential distribution across the arc with a subsequent reversal so that the axis of the arc is negative.

How negative the axis can become depends upon μ. Even if an electron wall current many times the magnitude of the ion current (large μ) is drawn the reversal is relatively small and unimportant. The fact that the fields in the plasma become small is probably of importance, however. For the purpose of discussion we fix our attention on the case where μ is unity, that is ion and electron currents are equal. Zero plasma field occurs when α has decreased to

$$\alpha=D_p/D_e,$$

but even when α is T_e/T_p times this, τ has already reached the value $\frac{1}{2}$ and the plasma fields are halved. In this range

$$\alpha \propto H_e^{-2},$$

so that when H is only $(T_p/T_e)^{\frac{1}{2}}$, roughly 15 percent, of its critical (zero plasma field) value, this marked effect has already appeared.

It seems fairly likely that the approach to the zero field condition may be a contributing

[11] Equation (16) of reference 7 or Eq. (92) of General Theory (reference 9).

factor among those which cause an arc to pull away from the tube walls with sufficiently strong magnetic fields, but it is probable that the action is indirect—that the effect of other factors such as those which control higher pressure arcs are enhanced by the strong field. However, another factor, which has not been sufficiently investigated experimentally, is that the initial concentration of the arc in the converging lines of force where the longitudinal field is increasing is, at least partially, a transition state so that a long enough column in the field might eventually fill the whole tube cross section.

The positive ion current density to the wall follows directly from General Theory

$$I_p = 0.216 a n_0 e \lambda.$$

With the substitution for λ from Eq. (23) this becomes

$$I_p = 1.248 \frac{\alpha D_e D_p (T_e + T_p)}{\alpha D_e T_p + \mu D_p T_e} e n_0 / a. \quad (24.5)$$

At first I_p to a nonconducting tube wall ($\mu = 1$) will not be affected by the decrease of α attendant upon increasing H because $D_e T_p$ is so much greater than $D_p T_e$. Only when α becomes comparable with $D_p T_e / D_e T_p$ will I_p begin to decrease. Under the conditions of measuring positive ion current, however, $\mu \ll 1$, so that the effect would set in at somewhat larger fields. Experimentally this would appear as more difficult positive ion current saturation the stronger the field.

The quasi-neutral diffusion theory of the positive column exhibits two important weaknesses. One is that the λ calculated from the observed ion currents to the wall is two to ten times larger than the λ calculated from the electron temperature and the known probability of ionization by single impact of electrons. Although the discrepancy increases with arc current, an explanation based on two-stage ionization is not without difficulties. The other discrepancy appears when the value of λ from the ion current is substituted in the plasma balance equation, (22), to find D_p. The ionic mean free path corresponding to the diffusion coefficient found is only a fraction of the expected value and varies too slowly with gas pressure.

This is not the place to discuss this question at length, but these difficulties in the theory of the nonmagnetic arc mean that for the present it is not wise to pursue the theory of the magnetic arc beyond the point of showing the modifications required in "accepted" equations and drawing simple conclusions from them. An application of the theory which is justified, however, particularly in view of theoretical and experimental work already done, is the calculation of the magnetic susceptibility of the positive column.

IV. The Diamagnetic Susceptibility of a Plasma

M. Steenbeck[5] has determined the diamagnetic susceptibility of a cylindrical plasma for axial magnetic fields with various gas pressures and magnetic field strengths. The positive column which he used was confined within the walls of a glass tube.

To account for his experimental results he developed a theory which, like a theory of diamagnetism in electrical conductors proposed by H. A. Wilson,[12] traces the path of a single electron and seeks to calculate the areas embraced by its path in the course of time. The moving electron thus constitutes a current flowing about the peripheries of such areas and contributes a magnetic moment to the plasma. Thus the magnetic moment of the plasma would seem to depend on the details of each electron path, and hence on what happens to the electrons in the course of time. Actually, of course, the moment depends only on the instantaneous motions of the electrons, and we should not sum areas but rather sum the instantaneous angular velocities of the electrons about an axis.

Now, in a plasma which is in equilibrium there can be no net drift of electrons through any volume element. Therefore, in such an element all directions of motion are equally probable and the total angular velocity of all the electrons passing through it is zero. It follows that the diamagnetic susceptibility of a plasma in equilibrium is zero.

In this respect the plasma electrons resemble the classical conduction electrons in a metal. Steenbeck himself points out that N. Bohr and

[12] H. A. Wilson, Proc. Roy. Soc. **97**, 321 (1920).

H. A. Lorentz have shown (in references not easily accessible) that free electrons in a conductor would as a whole have zero diamagnetic susceptibility by virtue of a surface current whose moment would exactly cancel the moment of the amperian currents in the body of the metal. The metal is bounded by a sharp potential barrier which concentrates this current in a single layer. The plasma potential on the other hand decreases continuously from the axis outward to a point near the tube walls, and the compensating current is, consequently, distributed through this region. The sharpness of the concept of the reversed surface current is lost, but an examination of the details of the electron paths as in Steenbeck's Fig. 6 shows how contributions of both positive (paramagnetic) and negative (diamagnetic) magnetic moment are made by many electrons in the plasma. While Steenbeck recognized this factor he was unable to calculate the relative contributions and erroneously judged that the paramagnetic moments were negligible compared to the diamagnetic, instead of being exactly equal to them.

It follows that the experimentally observed susceptibility must be accounted for by the disequilibrium in the plasma, which consists chiefly of the outward radial drift of electrons toward the walls. This possible origin of the magnetic response was suggested by Steenbeck but not examined more closely than to observe that it would give a result of the proper sign. The theory of Section III furnishes the means of calculating the plasma susceptibility on this basis.

The tangential component v_e of the electron drift velocity is the significant one for calculating magnetic moment M, per axial cm of the plasma, because

$$M=(\pi e/c)\int_0^a n_e v_e r^2 dr. \tag{25}$$

From Eqs. (17), (18) and (19)

$$v_e=(1-\tau)\beta D_e(\partial n_e/n_e\partial r).$$

From Eq. (21)

$$v_e=-\frac{2.4n_0}{an_e}(1-\tau)\beta D_e J_1(2.4r/a).$$

Substitution in Eq. (25) and integration gives

$$M=-\frac{1.04\pi a^2 e}{2.40c}n_0(1-\tau)\beta D_e.$$

With Eq. (20) this gives

$$M=-(0.432\pi a^2 n_0 e/c)\frac{(T_e+T_p)D_pD_e\mu\beta}{\alpha D_eT_p+\mu D_pT_e}. \tag{26}$$

Comparison with Eq. (23) shows that

$$M=-(0.0746\pi a^4 n_0 e/c)\mu\lambda\beta/\alpha.$$

Now the ion current density I_p (intrinsically negative to conform to experimental convention) at the tube wall is related[13] to λ:

$$2\pi a I_p=0.432\pi a^2 e n_e\lambda, \tag{27}$$

so that, by eliminating λ and using Eq. (10)

$$\begin{aligned} M&=-(0.346\pi a^3 I_p/c)\gamma h'\mu \\ &=-0.1086a^3 I_p\gamma h'\mu \text{ (practical)}, \end{aligned} \tag{28}$$

a form convenient for experimental test when the electron current density to the wall, which is $-\mu I_p$, is under direct control. Under this condition M is seen to be directly proportional to electron wall current and magnetic field. A change in field will, of course, profoundly affect the wall current at any fixed wall potential.

When, however, the wall is nonconducting so that $\mu=1$ we shall have to determine in effect the behavior of $I_p h'$ with increasing H. It is this problem which concerns us from now on.

We note that the right-hand member of Eq. (26) divides naturally into two factors, the first, included within the parentheses giving the total electronic charge Q per axial centimeter in e.m.u. and the second giving its average areal velocity, A. Thus,

$$\left.\begin{aligned} Q&=0.432\pi a^2 n_0 e/c \\ &=-2.17\times10^{-20}a^2 n_0 \quad \text{(e.m.u.)}, \end{aligned}\right\} \tag{29}$$

$$A=-\frac{(T_e+T_p)D_pD_e\mu\beta}{\alpha D_eT_p+\mu D_pT_e}, \tag{30}$$

$$M=QA \tag{31}$$

and, per electron,

$$M_1=Ae/c=-1.6\times10^{-20}A. \tag{32}$$

[13] See, for instance, Eq. (51) of General Theory (reference 9).

Let us neglect T_p in comparison with T_e in the numerator in Eq. (30), set μ equal to unity, then

$$A=\frac{-T_eD_pD_eh'\gamma_\beta}{\gamma_\alpha D_eT_p+(1+h'^2)D_pT_e}. \tag{33}$$

As h' increases negatively from zero with the impressed magnetic field, γ_α and γ_β vary in accordance with Fig. 1 and D_e and T_e change as well. The changes in the γ's will be taken into account later, those in D_e and T_e will be entirely neglected. Watching the change in A from h' alone then, we see that initially it increases linearly with h' and that finally it decreases as $1/h'$, with a maximum between. This is the behavior found by Steenbeck in his experiment, where μ was unity.

In Eq. (33) we can neglect unity in comparison with h'^2 without error, because D_pT_e is small in any case relative to $\gamma_\alpha D_eT_p$. Then A can be written

$$A=\frac{-\gamma h'D_pT_e/T_p}{1+h'^2D_pT_e/(\gamma_\alpha D_eT_p)}. \tag{34}$$

For variation of h' (or H) the maximum value of A is then found to be

$$A_{\max}=(\gamma\gamma_\alpha^{\frac{1}{2}}/2)(D_eD_pT_e/T_p)^{\frac{1}{2}}, \tag{35}$$

occurring at

$$h'_{\max}=-[\gamma_\alpha D_eT_p/(D_pT_e)]^{\frac{1}{2}}. \tag{36}$$

The various quantities appearing in the above equations have now to be related to measurable quantities in the arc.

For h', Eq. (6) and

$$\bar{c}=[8kT/(\pi m_e)]^{\frac{1}{2}} \tag{37}$$

give

$$h'=(3\pi/8)(e/kc)H_zD_e/T_e$$
$$=-1.375\times10^{-4}H_zD_e/T_e. \tag{38}$$

Comparison with Eq. (36) gives

$$H_{\max}=7.27\times10^3[\gamma_\alpha T_eT_p/(D_pD_e)]^{\frac{1}{2}}. \tag{39}$$

It is to be noted that the behavior of A with increasing H_z is qualitatively the same as that found both theoretically and experimentally by Steenbeck. The occurrence of a maximum magnetic moment has just been pointed out. For small values of H_z Eqs. (34) and (38) show that[14]

$$A=1.375\times10^{-4}(\gamma D_eD_p/T_p)H_z,$$
$$\chi=1.375\times10^{-4}Q\gamma D_eD_p/T_p \tag{40}$$

so that the magnetic moment is proportional to the field and the susceptibility is constant. Considerably beyond the maximum in M (or A)

$$A=7.27\times10^3\gamma\gamma_\alpha T_e/H_z,$$
$$=8.57\times10^3T_e/H_z, \qquad \text{(e.m.u.)} \tag{41}$$
$$\chi=QdA/dH_z=-8.57\times10^3QT_e/H_z^2.$$

It is interesting that in this range Steenbeck's Eq. (10) leads to the identical expression. Otherwise, however, the occurrence of ion temperature and diffusion coefficient in the present equations emphasize the essential difference of the present treatment from the other, even though the qualitative behavior of M is the same.

Unfortunately Steenbeck has given sufficient arc data to permit a comparison of these formulas with his experimental results. Accordingly it seems best to apply the present theory to a case in which more complete data are available in order to obtain some idea as to the magnetic magnitudes to be expected.

Excellent measurements on a Hg arc in a 3.2-cm diameter tube have recently been published by Klarfeld.[15] He has analyzed his data even up to 7.5×10^{-3} mm of pressure in terms of the ion-free-fall case. There is some reason to expect the quasi-neutral diffusion theory to apply here and at his higher pressure of 20×10^{-3} mm. For the present purpose we shall analyze the data for the 0.3-amp. arc at these pressures in this way. The small correction for wall sheath thickness has not been made.

Equation (28) requires that the ion wall current be measured in the presence of a magnetic field, so that it cannot be applied now. We must rather determine the necessary quantities in Eqs. (33), (35), (36) and (39).

---

[14] The γ has been included in this formula because, even though γ approaches unity as h' approaches zero, it will appear later that Eq. (40) may still be a good approximation for values of h' so large that γ is appreciably less than unity.

[15] B. Klarfeld, Zeits. f. Tech. Physik U. S. S. R. **5**, 913 (1938).

Eliminating λ between Eqs. (27) and (22) (with $\mu=1$ and T_p neglected relative to T_e) gives

$$D_p/T_p=5.02\times10^{18}aI_p/(T_e n_0) \qquad (42)$$

in practical units.

We obtain D_e from the arc current and longitudinal gradient Z,

$$i_z=0.432\pi a^2 n_0 e^2 D_e Z/(kT_e),$$

whence

$$D_e=3.96\times10^{14} i_z T_e/(Za^2 n_0) \qquad (43)$$

in practical units.

Table I contains in its first six rows Klarfeld's data on a 0.3-amp. arc in a 3.2-cm diameter arc tube. The following rows contain the magnetic quantities already defined, each accompanied by the number of the equation by which it was calculated. First $h'_{max}/\gamma_a^{\frac{1}{2}}$ was found from Eq. (36). Since this can differ from h'_{max} by 20 percent at the most, sufficiently accurate values of the corresponding α and γ can be found from Fig. 1. These have been used in Eq. (36) itself to determine h' and also in all other equations. In the present example h'_{max} is so great that γ_a and γ take on their extreme values of $\pi/2$ and $\frac{3}{4}$, respectively. The calculation of the remaining quantities, maximum magnetic moment per axial cm M_{max} and the magnetic field H_{max} at which this occurs, also the low and high field susceptibilities follow in straightforward fashion.

The values of H_{max} calculated here are higher than the 50 oersteds shown by Steenbeck in his Fig. 12. The present values of M_{max} have to be divided by $\pi a^2=8.05$ cm^2 to yield the average moment per cm^3 which is, presumably the ordinate in that same figure. Since Steenbeck shows 1.3×10^{-3} as the value of that quantity, the present values would seem to be some ten times smaller.

If the γ's were not present in the formulas relating M and H_z, this relationship could be represented by a single universal curve. This is still true if we are content to relate $M\gamma^{-1}$ to $H_z\gamma_a^{-\frac{1}{2}}$. By plotting $\log(-M\gamma^{-1})$ against $\log(H_z\gamma_a^{-\frac{1}{2}})$ we obtain the curve of Fig. 3. The two asymptotes are then 45° straight lines, the curve lies symmetrically with respect to them, and it resembles a hyperbola. The value of $-M_{max}\gamma^{-1}$ lies log 2 below the intersection of the asymptotes. Any plot of $\log(-M\gamma^{-1})$ against $\log(H\gamma_a^{-\frac{1}{2}})$ is simply the fundamental curve and its asymptotes translated with respect to the coordinate system. Roughly speaking, pressure change translates with respect to H_z and arc current change with respect to M.

TABLE I. *Calculation of magnetic properties of a positive column. Arc current = 0.3 amp., tube radius = 1.6 cm*[14].

QUANTITY	UNITS	EQUATION	NUMERICAL VALUES		
P	mm		7.5	20	$\times10^{-3}$
T_{gas}	°K		315	329	$\times1$
T_{em}	°K		1.86	1.31	$\times10^{4}$
I_p	amp. cm^{-2}		0.105	0.155	$\times10^{-3}$
I_{em}	amp. cm^{-2}		82.5	175	$\times10^{-3}$
Z	v cm^{-1}		0.478	0.538	$\times1$
n_0	cm^{-3}		2.44	6.16	$\times10^{10}$
D_p/T_p		42	1.86	1.54	$\times1$
D_e		43	7.4	1.83	$\times10^{7}$
$-Q$		29	1.36	3.42	$\times10^{-9}$
$\gamma_a^{-\frac{1}{2}}h'_{max}$		36	46.2	30.1	$\times1$
$\gamma_a^{\frac{1}{2}}$ (at max.)		Fig. 1	1.253	1.253	$\times1$
γ (at max.)		Fig. 1	0.75	0.75	$\times1$
$\gamma\gamma_a^{\frac{1}{2}}$ (at max.)			0.94	0.94	$\times1$
h'_{max}		36	57.9	37.7	$\times1$
A_{max}		35	7.52	2.86	$\times10^{5}$
$-M_{max}$	oersted cm^2	31	1.026	0.978	$\times10^{-3}$
H_{max}	oersted	39	106	196	$\times1$
$-\chi/\gamma$ (small H)		40	2.57	1.33	$\times10^{-5}$
χH^2 (large H)		41	0.217	0.384	$\times1$
H_0	oersted	45	800	1240	$\times1$

Before leaving this question it should be pointed out that the attempt has been made to apply the electron drift theory over a distance, the positive column radius, which is comparable with, if greater than, the electron mean free path. For magnetic fields so great that the electron orbit diameter is small compared to that of the column, the application is justifiable, but for lower fields some question can be raised and some modification of the theory may be necessary.

Two other points should be recalled. The first is that the quasi-neutral diffusion theory on which the present treatment is based is itself unsatisfactory. Secondly, the relatively small changes in T_e and D_e, and possibly D_p/T_p with H_z have been omitted from consideration. Any complete experimental test of the theory would have to include the measurement of T_e, I_{em}, I_p and Z in the presence of the magnetic field from which to calculate all the necessary quantities for each field condition.

While a numerical example is before us it is interesting to calculate the magnetic field H_0 at

which the plasma field vanishes, according to Eqs. (20) and (24) for μ equal to unity. We have, to a sufficient degree of approximation:

$$0 = D_e - D_p/\alpha = D_e - h'^2 D_p \gamma_\alpha^{-1},$$

whence

$$h' = (\gamma_\alpha D_e/D_p)^{\frac{1}{2}}. \quad (44)$$

Combining with Eqs. (38) and (39) gives for H_0,

$$H_0 = H_{\max}(T_e/T_p)^{\frac{1}{2}}. \quad (45)$$

The values of H_0 from this formula are included in Table I.

V. Constriction of Arc Under Its Own Magnetic Field—Pinch Effect

The electron drift equations can be applied in quite another direction. In arcs of large cross section and carrying large currents the magnetic field of the arc itself has an influence on the plasma relations. This factor, as well as others which become important, has been discussed in the *Transactions of the Electrochemical Society* article,[6] under the heading Pinch Effect, but only in general outline. Here the theory will be developed more completely. In doing this, the other factors, such as multiple stage ionization, transverse pressure differences in the column and the longitudinal pressure gradient will be neglected, partly because of theoretical complications and partly because they probably do not change the essential mechanism and effect of the self-magnetic fields although they undoubtedly modify such effects.

The magnetic field which arises from the arc current itself is circular and has no radial component. Let us adopt a cylindrical coordinate system in which x lies along the tube axis and is directed toward the anode, r is radial, and the angular coordinate is φ so that x, r, φ form a right-handed system. Thus r takes the place of y and φ of z in the usual formulation (see Eqs. (1) and (2)) of the drift equations.

The field influences the radial and longitudinal drift of electrons in accordance with the equations

$$u_x = D_e(\alpha b_x + \beta b_r),$$

$$u_r = D_e(\alpha b_r - \beta b_x).$$

Using Eq. (3) and noting that $\partial n_e/\partial x$ is zero, these become

$$u_x = -D_e[\alpha\xi + \beta(\partial\eta/\partial r + \partial \ln n_e/\partial r)], \quad (46)$$

$$u_r = -D_e[\alpha(\partial\eta/\partial r + \partial \ln n_e/\partial r) - \beta\xi], \quad (47)$$

where

$$\eta = eV/kT_e \quad (47.5)$$

and

$$\xi = \partial\eta/\partial x.$$

(In terms of the longitudinal gradient X of the arc

$$\xi = -(e/kT_e)X. \quad (48)$$

Both X and ξ are intrinsically negative.)

The continuity equation for the ions, Eq. (15.5) and the ion drift equation Eq. (15) remain unchanged. If, in addition, we retain Eq. (13) corresponding to a nonconducting tube wall, the resulting equations become unmanageable. Great simplification results if the wall is supposed to be conducting and held so negative that there is no radial flow of electrons. It appears highly unlikely that changes in the small radial flow would make appreciable differences in the main arc

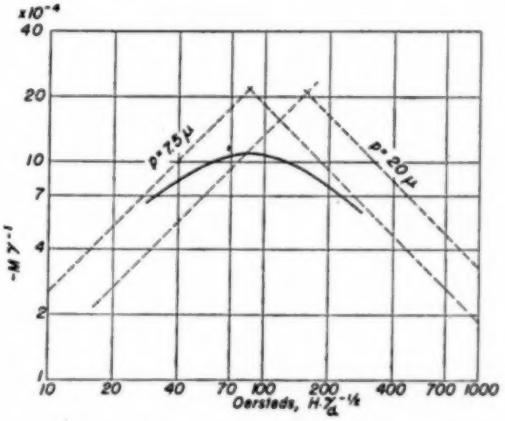

Fig. 3. Calculated diamagnetic moment of positive column, per cm length, *vs.* longitudinal magnetic field strength, uncorrected for γ's. Arc data from Klarfeld (reference 15).

flow. Accordingly we abandon Eq. (13) and set $u_r = 0$ in Eq. (47) so that

$$\partial\eta/\partial r + \partial \ln n_e/\partial r - \gamma\xi h' = 0. \quad (49)$$

Elimination of u_p and η between this and Eqs. (15) and (15.5) (remembering Eqs. (14)

and (47.5)) leads to

$$\frac{1}{r}\frac{d}{dr}\left(r\frac{dn_e}{dr}\right)+\frac{\lambda T_p}{(T_e+T_p)D_p}n_e - \frac{T_e}{T_e+T_p}\frac{d(\gamma h' n_e r)}{rdr}=0. \quad (50)$$

This equation contains not only n_e but also h' (with γ) as dependent variables. The second equation which is required for a solution is furnished by the relation of the magnetic field H_φ to the current density i_z in the arc:

$$r^{-1}d(rH_\varphi)/dr=4\pi i_z/c.$$

Since the cross drift u_r is zero the effective longitudinal mobility (see Eq. (8.5)) is $\gamma_r D_e e/kT_e$ so that

$$i_z=-e\xi\gamma_r D_e n_e. \quad (51)$$

Combining the two we have

$$r^{-1}d(rH_\varphi)/dr=-4\pi e\xi\gamma_r D_e n_e/c, \quad (52)$$

which is the second of the two necessary equations.

From this point it will be necessary to treat γ and γ_r as constants, and since the interest lies in large fields, their values for infinite h' will be used. Also, a set of substitutions simplifies Eqs. (50) and (52) greatly and finally permits the elimination of H_φ (h') between them. The substitutions with an explanation of each are:

(1)
$$s=\frac{T_p\lambda r^2}{4(T_e+T_p)D_p}, \quad (53)$$

so that

$$s_0/a^2=\frac{T_p\lambda}{4(T_e+T_p)D_p}, \quad (54)$$

where a is as usual the tube radius and s_0 is the value of s at which n_e falls to zero. We can also write

(2)
$$r^2=(a^2/s_0)s, \quad (55)$$
$$\theta=n_e/n_0, \quad (56)$$

where n_0 is the axial electron concentration so that θ ranges from unity at the tube axis to zero at the wall.

(3)
$$J=\int_0^s \theta ds, \quad (57)$$

so that J is a measure of the current within a certain radial distance. This allows Eq. (52) to be simplified to

$$H_\varphi=-s^{-\frac{1}{2}}J[\pi e\xi\gamma_r D_e n_0 a/(s_0^{\frac{1}{2}}c)], \quad (58)$$

(4)
$$L=\frac{3\pi^2 D_e^2 e^2\xi^2 a^2\gamma_r\gamma n_0}{8c^2k(T_e+T_p)s_0}, \quad (59)$$

which assembles all of the quantities appearing in the coefficient of the third term of Eq. (50) after the previous substitutions have been made and H_φ has been eliminated with h' by Eq. (6). L is the quantity denoted by A in reference 6.

As a result of these substitutions Eq. 50 assumes the form

$$\frac{d}{ds}\left(s\frac{d^2J}{ds^2}\right)+\frac{dJ}{ds}+L\frac{d}{ds}\left(J\frac{dJ}{ds}\right)=0,$$

which is directly integrable to

$$sd^2J/ds^2+J(1+LdJ/ds)=0. \quad (60)$$

That the constant of integration is zero follows from Eqs. (56) and (57).

Near the origin

$$J=s-\frac{1+L}{2}s^2\left[1-\frac{1+3L}{6}s+\frac{1+13L+18L^2}{72}+\cdots\right]. \quad (61)$$

Equation (60) has been integrated by numerical quadrature for a succession of values of L. In each case the process was carried to the value s_0 of s at which dJ/ds passed through zero because the relation

$$\theta=dJ/ds \quad (62)$$

shows that there is where the tube wall lies. The value J_0 of J at this point is directly related to the average electron concentration $\bar{n}_e$ in the cross section:

$$\bar{n}_e=a^{-2}\int_0^a 2n_e r dr=(n_0/s_0)\int_0^{s_0}\theta ds=n_0 J_0/s_0. \quad (63)$$

Referring back to Eq. (51) the total arc current is now seen to be

$$i_z=\pi a^2 e\xi\gamma_r D_e n_0 J_0/s_0. \tag{64}$$

By eliminating n_0 with Eq. (59) we find

$$\left.\begin{aligned} i_z&=\frac{8c^2k(T_e+T_p)}{3\pi e\gamma\xi D_e}J_0L,\\ i_z&=3.32\frac{(T_e+T_p)T_e}{XD_e}J_0L \text{ (practical)}\end{aligned}\right\} \tag{65}$$

and rearranging Eq. (59)

$$\left.\begin{aligned} n_0&=\frac{8c^2k(T_e+T_p)}{3\pi^2e^2\gamma\gamma_r D_e^2\xi^2a^2}Ls_0,\\ n_0&=9.2\times10^{15}\frac{(T_e+T_p)T_e^2}{X^2D_e^2a^2}Ls_0 \text{ (practical).}\end{aligned}\right\} \tag{66}$$

Since s_0 and J_0 are functions of L alone, these equations express n_0 as a function of i_z insofar as T_e, ξ, and D_e are constant.

Physically, the independent variable is the arc current. The corresponding dimensionless quantity in the mathematical theory is seen to be LJ_0 by Eq. (65). This quantity will, therefore be treated as the independent variable or parameter in the various plots below. It is the quantity which is denoted by G_2 in reference 6. Similarly Ls_0 corresponds to n_0.

It is of interest to find the variation of potential across the arc. This is most readily calculated and plotted in the form $\epsilon^{-\eta}$ which shows the charge distribution which would exist in the actual field if no magnetic forces were present. Elimination of u_p between Eqs. (15) and (15.5) gives (from the substitutions (54), (55) and (56))

$$\frac{d}{ds}\left[s\theta\frac{d\eta}{ds}-(T_p/T_e)s\frac{d\theta}{ds}\right]=\frac{T_e+T_p}{T_e}\theta. \tag{67}$$

Integrating once gives the function J in the right member. But by Eq. (60)

$$J=-\frac{sd\theta/ds}{1+L\theta}, \tag{68}$$

so that the integral of Eq. (67) becomes

$$d\eta/ds=(T_p/T_e)d\ln\theta/ds-\frac{T_e+T_p}{T_e}\frac{d\theta/ds}{\theta(1+L\theta)}.$$

A final integration and rearrangement gives

$$\epsilon^{-\eta}=\theta\left(\frac{1+L}{1+L\theta}\right)^{(T_e+T_p)/T_e}. \tag{69}$$

The T_p in the numerator of the exponent can easily be neglected, and this we shall do.

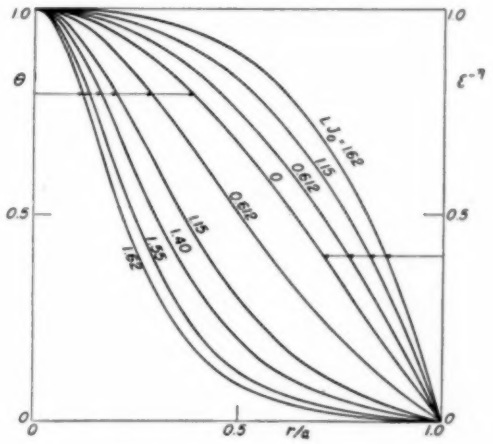

FIG. 4. Radial distributions of electrons (and ions) and potential in self-magnetic pinch effect. Lower left curves show relative electron concentrations with increasing arc current (LJ_0). Upper right curves show the distribution of the Boltzmann factor, exp $(-eV/kT_e)$.

The single quantity which is of primary importance in the magnetic effects is h'. Combining Eqs. (58) and (6) and comparing with Eq. (59) shows that

$$\left.\begin{aligned} h'&=\frac{T_e+T_p}{T_e\xi\gamma a}Ls_0^{\frac{1}{2}}Js^{-\frac{1}{2}},\\ h'&=1.15\times10^{-4}[(T_e+T_p)/(aX)]Ls_0^{\frac{1}{2}}Js^{-\frac{1}{2}}.\end{aligned}\right\} \tag{70}$$

Thus the quantity corresponding to h' is

$$LJ(s/s_0)^{\frac{1}{2}}.$$

It follows directly from Eq. (63) that the positive ion current density to the wall is

$$I_p=\tfrac{1}{2}ae\lambda n_0J_0/s_0$$

or by Eq. (54)

$$I_p=(2eD_p(T_e+T_p)/T_p)n_0J_0/a. \tag{71}$$

The calculations involved in the numerical solution of Eq. (60) were carried out by Mr. R. Beresford.

The calculated distributions of electron con-

centration are shown in Fig. 4 as plots of θ against fractional tube radius. The $LJ_0=0$ curve, corresponding to no magnetic effect, is one of the six curves of this group. The other five all lie below this one. The constriction of the arc is clearly seen. Each curve is labelled with the value of LJ_0 to which it corresponds.

Along with the peaking of the concentration goes a decrease of the plasma fields which is qualitatively the same effect as that found in Section III for the longitudinal field case. This is shown by the $\epsilon^{-\eta}$ curves also in Fig. 4. They appear above the $LJ_0=0$ curve. For $L=0$ the θ and $\epsilon^{-\eta}$ curves coincide, but the larger L the further they separate. Where the ion density is most greatly increased by magnetic concentration, the electric field drawing off the ions is most greatly decreased.

Table II shows further results of integrating Eq. (60). The mathematical quantities are listed in the first row, the numbers of the equations relating them to others in the second, their corresponding physical quantities in the third, and numerical values in the subsequent rows. The values of L used in the integrations are shown in the first column, and values of s and J at the tube walls are shown in columns 2 and 3. Column 4 contains the current-like quantity, column 5 the one corresponding to the axial concentration of electrons, and column 6 contains the ratio of axial to average electron concentration.

If there were no progressive concentration of the arc, $n_0/\bar{n}_e$ would be independent of arc current, but the increase of s_0/J_0 with increasing LJ_0 shows that a marked concentration of 4.5-fold takes place in the range of the table. This is shown in Fig. 5 where Ls_0 is plotted against LJ_0. This curve is rather well expressed by the

TABLE II. *Quantities involved in pinch effect.*

L Eq. (59)	s_0 Eq. (54)	J_0 Eq. (62)	LJ_0 Eq. (65) $\propto i$	Ls_0 Eq. (66) $\propto n_0$	s_0/J_0 Eq. (63) $n_0/\bar{n}_e$
0	1.441	0.623	0	0	2.32
2	0.948	0.306	0.612	1.90	3.10
10	0.545	0.1146	1.146	5.45	4.76
25	0.352	0.0558	1.396	8.81	6.31
50	0.258	0.0309	1.55	12.90	8.34
80	0.213	0.0203	1.62	17.0	10.46

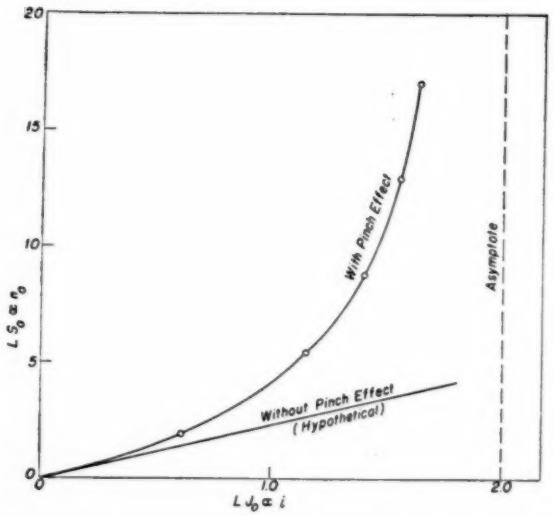

FIG. 5. Axial concentration of electrons (and ions) in self-magnetic pinch effect, as a function of arc current.

empirical equation

$$Ls_0=5LJ_0/(2.16-LJ_0). \tag{72}$$

It is rising more steeply than this hyperbola at $L=80$. Analysis of Eq. (60) for large values of L shows that 2 is an absolute upper limit for LJ_0 so that actually

$$LJ_0=2 \tag{73}$$

is the asymptote of the Ls_0 *vs.* LJ_0 curve.

Of course the value of n_0 (corresponding to Ls_0) cannot become infinite. With singly ionized atoms it cannot exceed n_a, the concentration of atoms. Thus this analysis predicts 100 percent ionization at the axis of an arc with currents far below those which, with a normal distribution in the cross section, would effect this. Steep increases in arc drop with current when a large diameter arc is already carrying a large current may well be due to this cause.

It is of interest to compare the critical current for the magnetic constriction with that arising from the transverse pressure effect.[6] For the former, Eqs. (65) and (73) give

$$i_{H\ \mathrm{crit}} \backsimeq 16c^2kT_e/3\pi e\gamma\xi D_e. \tag{74}$$

For the latter

$$I_{p\ \mathrm{crit}} \backsimeq 0.43\pi a^2 eD_e\xi n_0 \tag{75}$$

with $$n_0 \backsimeq (T_p/T_e)n_a. \quad (76)$$

Accordingly

$$\frac{i_{p\ \mathrm{crit}}}{i_{H\ \mathrm{crit}}} = 7.98\frac{\gamma a^2 e^2 D_e{}^2 \xi^2 T_p n_a}{c^2 k T_e{}^2}. \quad (77)$$

Now $D_e\xi$ is practically independent of n_a, but ξ varies oppositely from a though not as strongly as a^{-1}. Thus it appears that for larger radii and higher pressures the critical condition for blowing the gas out of the arc column lies at a higher value of current than does the critical condition for 100 percent ionization due to pinch effect. Putting in numerical values and using p for the gas pressure in bars, we have

$$i_{p\ \mathrm{crit}}/i_{H\ \mathrm{crit}} = 11 a^2 D_e{}^2 X^2 p/T_e{}^4 \text{ (practical)}. \quad (78)$$

AUGUST 15, 1939 PHYSICAL REVIEW VOLUME 56

Investigations of Ferromagnetic Impurities. I

F. W. CONSTANT AND J. M. FORMWALT
Duke University, Durham, North Carolina

(Received June 26, 1939)

A method has been developed whereby a permanent magnetic moment as small as 2×10^{-7} per cc may be measured in any small solid specimen. Various materials were tested by this method for ferromagnetic impurities. To remove surface impurities it was necessary to dissolve away part of the specimen. Most metals then showed some volume impurity. In aluminum, however, the volume impurity was nonmagnetic but could be dissolved out and deposited on the surface in a ferromagnetic state. Measurements were also made on the magnetic hardness and hysteresis curves of the impurities; part of the impurity was found to be very "hard," with saturation incomplete at several thousand gauss and a coercive force~100–200, and part quite "soft," with a relatively large initial susceptibility. Other properties of these impurities are being studied. The method was also extended to single crystals of dia- or paramagnetic materials whose magnetic anisotropy could be easily detected and measured.

AS previously reported,[1] an experimental method has been developed whereby very minute ferromagnetic impurities may be detected in various materials and some of the properties of these small impurities studied. The results of such studies should be of interest for several reasons. First, by such a method one may quickly detect and measure the amount of ferromagnetic impurity present in materials which are generally regarded as nonmagnetic and, in some cases, possibly estimate the kind and amount of impurity present. Then from a study of the properties of such impurities one may find how best to render a slightly magnetic material, brass, for example, less magnetic. Finally such studies should furnish further information as to the fundamental nature of ferromagnetism.

[1] F. W. Constant and J. M. Formwalt, Phys. Rev. **53**, 432 (1938).

EXPERIMENTAL METHOD

The method is quite simple. The specimen to be tested may have any shape, even be powdered if contained in a capsule, but small lumps or rods of about one gram were generally used. The specimen is first placed in a magnetic field of several thousand gauss, furnished by an electromagnet. This serves to magnetize all ferromagnetic impurities present in a common direction. Upon removing the specimen from this strong field such impurities will remain partially magnetized in this direction because of their remanent magnetization. The specimen is then placed in a light stirrup and suspended by a fairly strong quartz fiber in the center of a pair of Helmholtz coils, the direction of the remanent magnetization being perpendicular to the axis of the coils. A weak field of about 10 gauss is then applied and the resulting rotation measured by

means of a mirror, attached to the fiber, and a telescope and scale. The suspension was mounted inside a brass case with a glass window and was controlled by a torsion head at the top. The fiber was calibrated by measuring its period and was found to have a torsion constant of 0.0275 dyne centimeter per radian; it could support at least ten grams. The magnetic moment per cc is given by the formula $I=k\theta/VH$, where k is the torsion constant, θ the twist in a field H, and V the volume of the specimen. With the fiber used values of I as small as 2×10^{-7} could be measured, and with a finer suspension still greater sensitivity would be possible. Comparing this with the remanent magnetization of ordinary iron, about 500, shows that very minute impurities of the order of a millionth of one percent may be detected by this method provided they are ferromagnetic.

The volume of the specimen was either measured, or computed from its mass and density. The field of the Helmholtz coils was calibrated by means of a search coil and checked with the calculated value. The coils contained 400 turns each of No. 14 copper wire, mounted on circular frames 40 cm in diameter and 20 cm apart. The field at the center was then 18 gauss per ampere in the coils and it varied less than one percent within a 5-cm range.

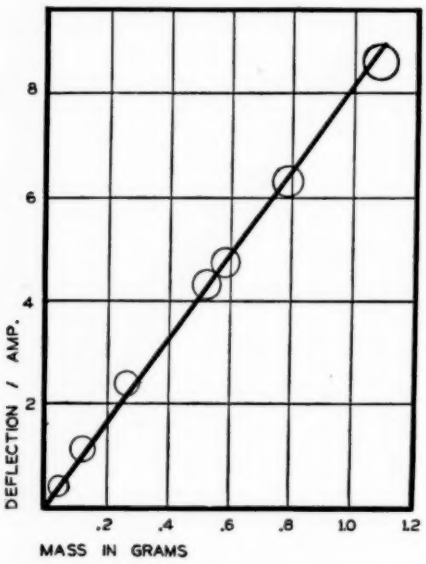

FIG. 1. Magnetic moment *vs.* mass for copper remaining after treatment in aqua regia.

TABLE I. *Volume impurities for four samples of sterling silver.*

SAMPLE	DEFLECTION/G OF SPECIMEN
a	23.05 cm
b	22.80
c	23.10
d	23.05
Mean	23.00±0.10
Mean magnetic moment/cc = 1.89×10^{-3}	

As explained later dia- or paramagnetic effects were generally too small to be measurable. However, in the case of soft ferromagnetic impurities the deflecting field would slightly magnetize the specimen in its direction and thereby give rise to a torque tending to twist the specimen in the direction of easiest magnetization, i.e., the direction for which the demagnetization factor was a minimum. Such effects were eliminated by reversing the field of the coils and taking the average of the two deflections since such a reversal also reversed the torque due to the permanent but not that due to the induced magnetization.

SURFACE AND VOLUME IMPURITIES

In measuring such minute impurities cleanliness was of the highest importance. Hence surface impurities had to be eliminated. The only effective method was to sandpaper the surface and then dissolve away 25 percent or more of the specimen. For metals nitric acid was generally used, although the choice of dissolving agent usually made little difference. Measurements of the magnetic impurity remaining were made as the specimen was gradually dissolved away in successive steps. It was found that after an abrupt initial decrease the magnetic moment then decreased linearly with the mass of the specimen thus indicating that the impurity was then a true volume one, distributed throughout the specimen. This linear relationship between total magnetic moment and mass in the case of a specimen of copper wire is shown in Fig. 1.

It was also found that different samples taken from the same spool of wire showed nearly the same magnetic moment per cc, again indicating a uniform volume impurity. In Table I are given

TABLE II. *Volume impurities for samples of copper.*

SOURCE	DEFLECTION/G OF SPECIMEN	$I \times 10^6$
No. 12 wire	9.5 cm	
No. 12 wire	11.9	
No. 12 wire	9.7	
Square wire	7.8	
Drawn rod	15.3	
Mean	10.8±2.2	38.
Eimer & Amend, (C.P., 0.000% Fe)		5.
National Bureau of Standards, (oxygen free)		0.6

the results for four samples of sterling silver wire, with the mean and mean deviation.

A sample of "chemically pure" silver foil, on the other hand, had a magnetic moment/cc $=3.3\times10^{-4}$.

In Table II are given the results for various samples of copper, the first three specimens being taken from the same spool of wire, the rest from other sources.

In the case of brass the variations from sample to sample were larger.

In Table III are summarized the results of measurements of the volume impurities of various substances, "no impurity" meaning a magnetic moment/cc less than about 10^{-6}.

The surface impurities were sometimes unimportant but often amounted to considerably more than the total volume impurity of the specimen.

In the case of aluminum, however, a different result was encountered. The surface impurity was removed from a cast specimen with HNO_3 and thereafter a very small volume impurity remained (see Table III) which decreased with the mass. When, however, a specimen was dissolved in HCl or aqua regia it rapidly became increasingly ferromagnetic. Apparently the aluminum contained a relatively large volume impurity which, being in solid solution, (microscopic study indicated $FeAl_3$), was not magnetic, but which upon solution became precipitated upon the surface as a ferromagnetic film. It is not surprising that aluminum was the only metal tested which showed this effect since it was the only one above iron in the electromotive series; but it is interesting that the film is ferromagnetic. Evidently the film could not appear when HNO_3 was used but could with HCl. This is attributed to the fact that HNO_3 is a stronger oxidizing agent. Mason[2] attempted to use such a film, formed by the action of NaOH on aluminum, to determine the percentage of iron present. In the present case a magnetic moment of approximately 0.1 was obtained for each cc of aluminum dissolved so that the aluminum originally must have contained a considerable iron impurity in a nonmagnetic state. However, an accurate estimate could not be made as there were indications that the film was very easily disturbed and so partly lost.

MAGNETIC CHARACTERISTICS OF THE IMPURITIES

As it was realized that only the remanent magnetization of the impurities was being measured an attempt was made to find out whether or not this was large and at the same time to study further the magnetic properties of such minute ferromagnetic impurities.

First it was observed that large fields (several thousand gauss) were necessary to reverse completely the remanent magnetization. To reduce it to zero the following fields in the opposite direction had to be applied: 90 gauss for silver, 200 for copper, 300 for bismuth and 500 for brass. This indicated that at least part of the ferromagnetic impurity was in a very "hard," prob-

TABLE III. *Volume impurities for various materials.*

MATERIAL	$I \times 10^9$
Brass	82.
Silver—sterling	1.9
—C.P.	0.33
Copper—magnet wire	0.38
—C.P., (0.000% Fe)	0.05
—National Bureau of Standards, (oxygen free)	0.006
Bismuth—extruded rod	0.14
—crystallized, C.P. 0.00% Fe)	0.01
Cadmium—C.P., (0.003% Fe)	0.014
Tin—C.P., (0.003% Fe)	0.002
Solder	0.07
Aluminum—drawn rod	0.003
—cast	0.001
Molybdenum	No impurity
Platinum	No impurity
Tungsten	No impurity
Potassium hydroxide	No impurity
Amber and paraffin	No impurity
Soft and Pyrex glass	No impurity

[2] R. B. Mason, Trans. Am. Electrochem. Soc. **56**, 45 (1929).

ably strained, state. The presence of such "hard" impurities assured sufficient remanent magnetization to make the present method practical.

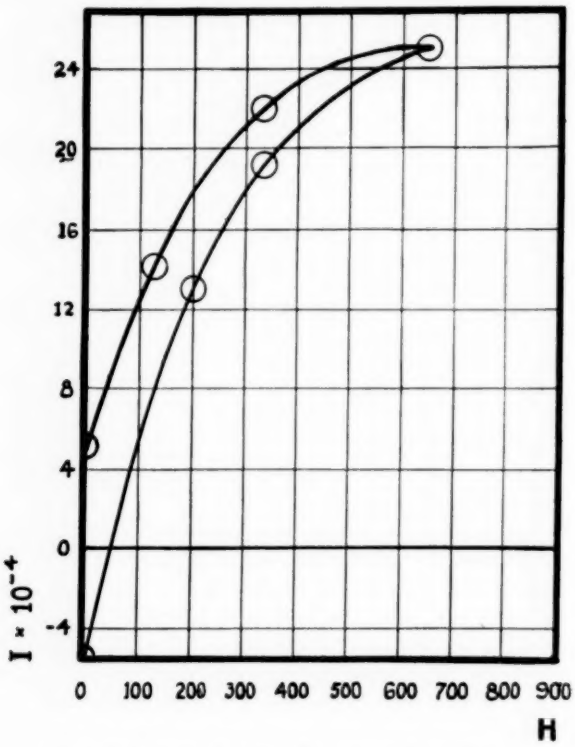

FIG. 2. Hysteresis curve for copper impurities.

Since the remanent magnetization might represent only a small fraction of the saturation magnetization and very "soft" impurities would not be detected at all by the above method the apparatus was modified so as to measure the magnetic moment of a specimen when the specimen was actually in a magnetizing field. For this purpose a second pair of coils of about 1700 turns each of No. 12 wire was mounted with its axis at right angles to that of the deflecting coils. The procedure was to mount the specimen with its length parallel to the axis of the large coils so that when their field was on the torsion fiber suffered no twist. Then the deflecting field was applied as before. Since, however, this latter field rotated the specimen out of line with the strong magnetizing field it was necessary to bring it back into its original position by twisting the torsion head. The strong magnetizing field then exerted no torque and the torque of the deflecting field, which was balanced by that given the fiber, was found by simultaneously cutting off both fields and noting the resultant rotation of the specimen as the fiber returned to an unstrained position. In this manner the magnetic moment of a specimen in fields up to 1000 gauss could be measured.

Figure 2 shows the hysteresis loop obtained for a specimen of copper wire, and Fig. 3 that for a sample of sterling silver wire. It will be observed that for copper the remanent magnetization is only about 20 percent of the magnetization in a field of 650 gauss and the coercive force, which is 50, is much less than the 200 gauss which was found earlier to be necessary to reduce the remanent magnetization to zero. This would indicate that the copper contains not only a very "hard" impurity whose magnetization does not approach saturation in fields up to 1000 gauss and whose coercive force is 200 or more, but also a considerably larger amount of "softer" impurity which has very little remanence and is magnetized in fields of 50 gauss, perhaps less. As stated above, indications of the "soft" impurity were noted when the deflecting field was reversed and unequal deflections in the two directions resulted. Probably the magnetic impurity actually exists in all degrees of strain and hardness throughout the specimen. In the case of silver the "hard" component appears

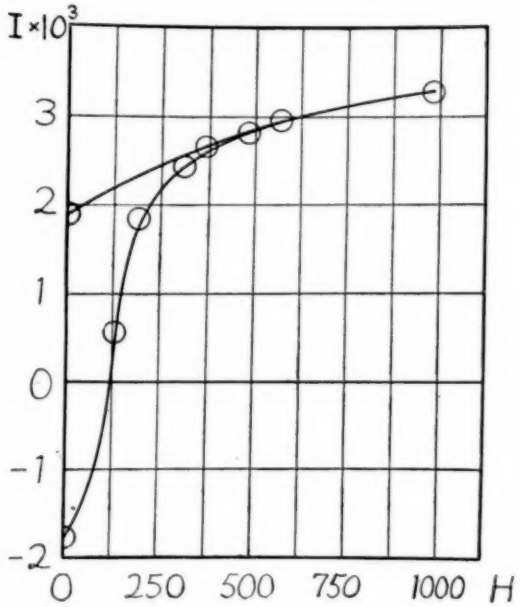

FIG. 3. Hysteresis curve for silver impurities.

more important, but again indications are that saturation is complete only in much larger fields.

The above results are in agreement with those of Bitter and Kaufmann,[3] who examined the magnetic behavior of known amounts of iron added to copper.

In the above measurements the probable error due to the instruments used and the necessary calibrations was estimated to be less than six percent for values of I greater than about 10^{-6}. To test the reproducibility of results a specimen was remagnetized and remounted eight times and the mean deviation in the deflection was less than one percent. However, it was important to remagnetize the specimen in the same direction since even in the field of the electromagnet saturation was not attained and the two sides of the hysteresis loops were not symmetrical.

Para- or Diamagnetic Effects

Calculations showed that dia- or paramagnetism of a specimen could cause rotation in the deflecting field only because of (1) different demagnetization factors in different directions when the specimen is not spherical, or (2) different susceptibilities in different directions, as for single crystals.

In the first case the torque per unit volume is given approximately by

$$L=H^2 \sin\theta \cos\theta K^2(N_1-N_2), \qquad (1)$$

where θ is the angle between the principal axis of the specimen and the field K is the susceptibility, N_1 and N_2 the demagnetization factors parallel and perpendicular to the principal axis. For the fields used this torque, being proportional to K^2, was negligibly small; the maximum possible deflection due to it was calculated to be about one-hundredth of a millimeter.

In the second case the torque per unit volume is given approximately by

$$L=H^2 \sin\theta \cos\theta\,(K_1-K_2), \qquad (2)$$

where K_1 and K_2 are the susceptibilities along the two principal horizontal axes. In this case the torque, being proportional to (K_1-K_2) rather than K^2, is of a much larger order of magnitude. For a single crystal of bismuth a maximum possible deflection of the order of 1 to 10 cm was computed. This torque, being proportional to H^2, would not be reversed upon reversing the field, whereas any torque due to a permanent ferromagnetic moment, M, would be reversed, since it is given by

$$L=MH \sin\theta \qquad (3)$$

and hence is proportional to H.

These calculations were verified experimentally. Platinum foil gave no deflection and an extruded bismuth rod,one which was completely reversed with the field. A crystallized specimen of bismuth, however, gave a deflection proportional to H^2, reaching a maximum of 3 cm, which was not reversed with the field. From this it may be seen that we have also a sensitive method for detecting and measuring magnetic anisotropy.

It is planned to give in a subsequent paper the results of further measurements on the properties of ferromagnetic impurities, in particular, the effect of temperature and heat treatment.

[3] F. Bitter and A. R. Kaufmann, Phys. Rev. **55**, 1142 (1939).

LETTERS TO THE EDITOR

Prompt publication of brief reports of important discoveries in physics may be secured by addressing them to this department. Closing dates for this department are, for the first issue of the month, the eighteenth of the preceding month, for the second issue, the third of the month. Because of the late closing dates for the section no proof can be shown to authors. The Board of Editors does not hold itself responsible for the opinions expressed by the correspondents.

Communications should not in general exceed 600 words in length.

Showers Produced by Penetrating Rays

For investigating showers we have used an apparatus involving the following: At the top there is a block of lead 20 cm square and 18 cm thick. Below this, and separated by spaces so as to cover a total length of 140 cm, there are four slabs of lead each 1 cm thick. Above the thick lead block, and at suitable distances above each of the other blocks, and beneath the lowest are trays, each containing 18 Geiger counters placed side by side. The counters are 1 cm in diameter and 20 cm long. Each is connected to an individual electroscope. The nature of the electrical arrangements is such that no electroscope is allowed to deflect unless at least one ray—and so a penetrating ray—has passed through all of the trays. Under these conditions, however, every counter which discharges is caused to record such discharge by means of a process in which spots of light reflected from the mirrors of all of the electroscopes are photographed.

We have used the above apparatus, among other studies, for the determination of the number of events which are accompanied by n additional rays for a range of n from 1 to 8. Results of two sets of experiments[1] are recorded in Table I together with the theoretical data given by H. J. Bhabha's[2] theory. In this table, E refers to the energy of a mesotron and m to its rest mass.

TABLE I. *Number of events which are accompanied by n additional rays E is the mesotron energy, m its rest mass.*

Theoretical

$E-mc^2$	$n=1$	2	3	4	5	6	7	8
10^8 ev	13.6	2.3	1.5	0.8	—	—	—	—
10^{10}	26.0	8.0	5.6	3.2	2.1	0.7	—	—
10^{12}	26.0	8.5	6.0	3.4	2.3	0.8	—	—

Experimental

Exp.	Thickness of Pb	$n=1$	2	3	4	5	6	7	8
1.	Below 18 cm Pb	11	5	1	2	1	1	1	1
	Below 19 cm Pb	13	4	3	0	3	0	0	0
2.	Below 18 cm Pb	7	3	0	0	0	1		
	Below 19 cm Pb	10	4	1	1	0	0		
	Below 20 cm Pb	12	2	1	0	0	0		
	Below 21 cm Pb	11	2	1	1	0	0		
	Below 22 cm Pb	9	1	0	1	0	0		
Averages for all data		10	3	1	0.7	0.6	0.3		
Final corrected averages		12.5	5	2	1.7	1.8	1.2		

The final averages given at the bottom of the table are corrected for counter inefficiency. It will be seen that these results agree very well with Bhabha's theory as regards the relative number of rays for mesotron energies between 10^{10} ev and 10^{12} ev. The actual number of rays found experimentally is about half that given by the theory and is more in accord with mesotron energies of 10^8 ev.

A complete description of these experiments and of other results from them will be published in a paper entitled "Showers Produced by Penetrating Rays and Allied Phenomena" by W. F. G. Swann, given as part of the "Symposium on Cosmic Rays" held at the University of Chicago, June 27–30, 1939.

W. F. G. SWANN
W. E. RAMSEY

Bartol Research Foundation of the Franklin Institute,
Swarthmore, Pennsylvania,
July 28, 1939.

[1] These two experiments differ in the fact that in the first there was a single 1-cm block of lead in addition to the 18-cm block, while in the second experiment there were four 1-cm blocks in addition to the 18-cm block. Moreover, in the second experiment certain precautions were taken to eliminate the effect of electron showers coming in from the side and operating the apparatus.

[2] H. J. Bhabha, Proc. Roy. Soc. **164**, 257 (1938).

Heavy Water Rochelle Salt

It has been found that replacing the water of crystallization of Rochelle salt by deuterium oxide by growing the crystals in heavy water raises the upper critical temperature and lowers the lower critical temperature at which abrupt changes in the dielectric and piezoelectric properties occur. The amount of the change of temperature depends upon the D_2O-H_2O ratio in the solution. With 99.5 percent D_2O the upper critical temperature is raised from 23.5°C to 34.5°C and the lower critical temperature is reduced from −19°C to −24°C. The values of the dielectric constant and the piezoelectric constant which exhibit the critical temperatures are reduced in the 99.5 percent D_2O crystal at temperatures between the Curie points to about 75 percent of the H_2O crystal values. Otherwise the elastic, dielectric, and piezoelectric properties are substantially unchanged. The results are reported in greater detail in a forthcoming paper by W. P. Mason and A. N. Holden.

A. N. HOLDEN
G. T. KOHMAN
W. P. MASON
S. O. MORGAN

Bell Telephone Laboratories,
463 West Street,
New York, New York,
July 31, 1939.

Ferromagnetism in Austenite

It is generally known that above 910°C iron is in the γ phase, consisting of a face-centered cubic lattice, while below this temperature it is in the α phase, which is body-centered cubic. Ferromagnetism can be detected only below 790°C so that γ-iron, or austenite as it is often called, is not ferromagnetic. Addition of alloying elements can lower considerably the temperature of the phase transformation, even below room temperature as in the case of austenitic stainless steel. But no matter how much this transformation may be lowered, it has always been found that the iron or steel remains nonferromagnetic as long as it is austenitic. For this reason the generally accepted viewpoint has been that the absence of ferromagnetism in austenite is one of its characteristic properties.

We have recently discovered that a steel containing 1.97 percent Ni, 0.86 Cr, 0.35 Mo and 0.28 C, is quite definitely ferromagnetic while in the austenitic condition and is thus an exception to the rule. The variation of magnetic intensity with temperature both on heating and on cooling in hydrogen is shown in Fig. 1. The measurements were made at 450 oersteds on a long rod so that the values shown are practically saturation values. On cooling the steel from 900°C at the rate of 6°C per minute, ferromagnetism first appeared at 750°C. The magnetic intensity at first increased rapidly and then leveled off around 600°C. That the steel was still austenitic was proved by dilatometric work on a sample cut from the same rod. It is well known that the $\gamma \rightarrow \alpha$ transformation in a rod is always accompanied by a very marked linear expansion. In the steel under discussion this break in the dilatometer curve started at 520°C and ended at 340°C, and it is the $\gamma \rightarrow \alpha$ transformation corresponding to this break that accounts for the sudden rise of the magnetic curve at 520°C.

Corroborating evidence that the steel was still austenitic above 520°C was found by microscopic examination of a sample quenched in water from 550°C. The structure was martensitic, showing that the steel could not have transformed previous to quenching. The cooling rate of 6°C per minute was great enough to prevent the transformation to ferrite and pearlite at 700°C or so. Unfortunately, it was impossible to prevent the transformation at 520°C so that we could not extend the study of magnetic austenite to room temperature.

It may be pointed out that the association of ferromagnetism with a face-centered lattice is nothing unusual since nickel and the iron-nickel alloys containing more than 30 percent Ni are ferromagnetic. But below 30 percent Ni, only the α phase alloys are ferromagnetic and the γ ones are not. The steel we have discussed falls in the low nickel group, for which the occurrence of ferromagnetism in austenite has not been previously reported. The composition range in which austenite can be ferromagnetic is quite narrow, as found by experiments on similar alloys.

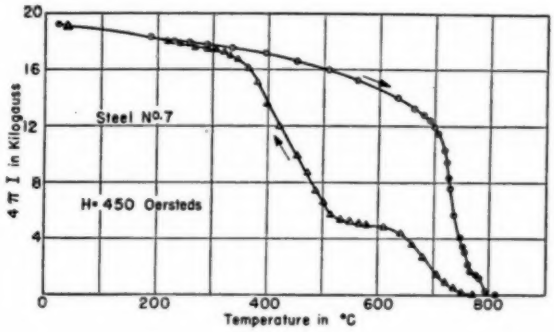

FIG. 1.

Complete details of this work will appear in the *Transactions of the American Society for Metals.*

L. P. TARASOV
E. R. PARKER

Research Laboratory,
General Electric Company,
Schenectady, New York,
July 25, 1939.

He^3 in Helium

We have used the 60″ cyclotron[1] as a mass spectrograph to show that He^3 is one of the stable isotopic constituents of ordinary helium. When the cyclotron was filled with helium, a linear amplifier chamber placed in the path of the ion beam was paralyzed at two values of the magnetic field, corresponding to the production of 8-Mev protons and 32-Mev alpha-particles. At a field midway between these two values, the amplifier showed the presence of a smaller, but quite definite, beam whose range was determined as 54 cm of air. He^{3++} is the only ion which satisfies the three criteria of e/m, v, and R measured in this way. Further weight is given to this view by the observation that this beam did not appear when the tank was evacuated, or filled with deuterium.

It was not possible to produce a steady beam of 24-Mev "light alpha-particles," because the cyclotron was "shimmed" for normal alphas and was therefore out of adjustment at lower fields. But it was possible to produce pulses of ions by lowering the magnetic field rapidly and letting the induced currents in the pole pieces increase the central magnetic field. We plan to shim the 37″ cyclotron for light alphas in the near future, to attempt to use the beam for disintegration experiments. The necessary intensity may be obtained by isotopic concentration or production of He^3 in the D−D reaction.

Because of the shimming differences noted above, it is impossible to measure the relative abundance of the helium isotopes; but the orders of magnitudes of the two beams may be of interest. There were approximately 10^{12} alpha-particles per sec. in the He^4 beam, and of the order of 10^3 per sec. in the He^3 beam. We looked for a beam at the He^5 magnetic field setting, but did not observe any effects.

We are indebted to Mr. William W. Farley for assistance in the experiment.

LUIS W. ALVAREZ
ROBERT CORNOG

Crocker Radiation Laboratory,
University of California,
Berkeley, California,
July 31, 1939.

[1] E. O. Lawrence, L. W. Alvarez, W. M. Brobeck, D. Cooksey, D. R. Corson, E. M. McMillan, W. W. Salisbury and R. L. Thornton, Phys. Rev. **56**, 124 (1939).

Coincidences Between Beta- and Gamma-Rays in Indium

Cloud chamber determinations of the beta-ray spectrum of In^{116} (54 min.) yielded an end point between 1.3 and 1.4 Mev.[1] It was pointed out by Brown and Mitchell that the use of a thick source would distort the shape of the distribution and prevent any possible resolution into groups. In an attempt to determine whether the spectrum is simple or complex, we have recorded gamma-gamma and beta-gamma coincidences produced in two fast and reliable Geiger-Mueller counters. The details of the experimental arrangement are described in another paper.[2]

The source, a 4.5×6.0 cm sheet of In 0.038 cm thick, after irradiation by slow neutrons from a paraffin bucket containing a 211-milligram source of radium mixed with beryllium, was mounted midway between the two counters. Aluminum of 0.60 cm thickness, sufficient to stop completely all beta-particles, was placed between the source and the gamma-ray counter. In order to obtain gamma-gamma coincidences, a similar thickness was placed between the source and the beta-ray counter. Beta-gamma coincidences were obtained as a function of the beta-ray energy, by performing experiments with different thicknesses of absorber between the source and the beta-ray counter. Corrections were made for decay, for gamma-rays recorded by the beta-ray counter, and for chance coincidences. The resolving time of the apparatus for coincidences is 0.56×10^{-7} min.

The experiments on gamma-gamma coincidences yielded a value of 0.65 ± 0.06 per 1000 gamma-rays recorded. The existence of gamma-gamma coincidences, of course, demands that there be more than one gamma-ray emitted per disintegration.

In Fig. 1, the number of beta-gamma coincidences per beta-particle recorded is plotted against the thickness of the beta-absorber, and therefore as a function of the beta-ray energy. It will be noted that, within the experimental error, the value of the ordinate remains constant. There is, therefore, no indication of a complex spectrum such as was found by the authors for the 148-min. period of manganese.[2]

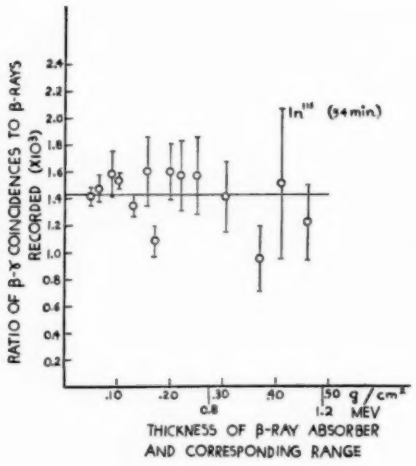

FIG. 1. Beta-gamma coincidence measurements.

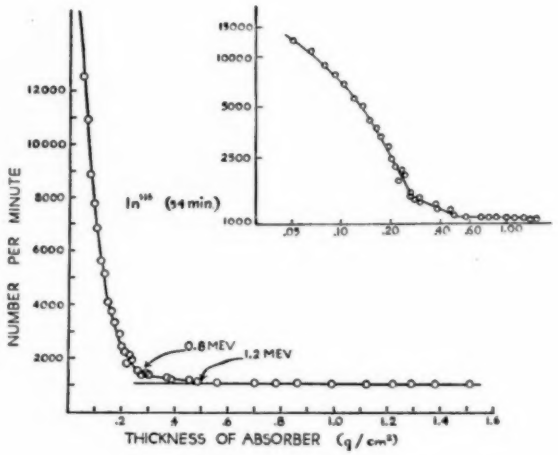

FIG. 2. Absorption in aluminum.

Recently, some question has arisen as to the value of the beta-ray end point. It has been suggested that the true end point is about 0.8 Mev and that the higher energy electrons recorded in the cloud chamber experiments were due to recoil electrons from the gamma-rays. With this in mind, a careful study was made of the absorption of the total radiation in aluminum. A typical run is shown plotted in Fig. 2. It will be noted that there appear to be two discontinuities, one at 0.8 Mev, and the other at 1.2 Mev. These discontinuities are demonstrated more clearly in the logarithm *vs.* logarithm plot shown in the insert. It is interesting to note, also in this connection, that, as shown in Fig. 1, the numerical value of the coincidences per particle detected remains constant out to an absorption thickness corresponding to the 1.2-Mev end point. One may still argue that the coincidences obtained for thicknesses of absorber corresponding to energies above 0.8 Mev are due to Compton electron-gamma coincidences, and that the numerical value of the Compton-gamma per Compton ratio is fortuitous. To test this point, an attempt was made to repeat the experiment with a different geometrical arrangement. However, the loss of intensity due to this change prevented our coming to any definite conclusions on this point.

If one makes the plausible assumption that the sensitivities of the counter to the different gamma-rays emitted per disintegration are not very different from an average sensitivity (including solid angle), S_γ, one may calculate K, the average number of gamma-rays per disintegration. Let N_β and N_γ be the number of beta- and gamma-rays emitted by the source, and let $N_\beta S_\beta$ and $N_\gamma S_\gamma$ be the respective number recorded, then

$$N_{\beta\gamma}/N_\beta S_\beta = S_\gamma K = 1.4\times10^{-3}, \quad (1)$$

$$N_{\gamma\gamma}/N_\gamma S_\gamma = \tfrac{1}{2}S_\gamma K(K-1) = 0.65\times10^{-3}; \quad (2)$$

therefore,

$$K = 1.9. \quad (3)$$

It appears then that the disintegration from In^{116} to Sn^{116} is, for the 54-min. isomer, a simple beta-transition

followed on the average by two gamma-rays. It follows also that the disintegration leads to an excited state of Sn^{116}.

The authors wish to express their thanks to the Penrose Fund of the American Philosophical Society for a grant.

LAWRENCE M. LANGER
ALLAN C. G. MITCHELL
PAUL W. MCDANIEL

Department of Physics,
Indiana University,
Bloomington, Indiana,
July 26, 1939.

[1] M. V. Brown and A. C. G. Mitchell, Phys. Rev. **50**, 593 (1936). Gaerttner, Turin and Crane, Phys. Rev. **49**, 793 (1936).
[2] Langer, Mitchell and McDaniel, Phys. Rev. In press.

Raman Effect in Samarium Nitrate Solutions

Rasetti[1] has adduced evidence for the possibility of an electronic Raman effect in the case of the diatomic *molecule* NO, where the Raman band corresponds to the transition $^2\Pi_{1/2}-{}^2\Pi_{3/2}$. While all attempts at discovering an electronic Raman effect in *atoms* by one of us (L. Sibaiya) in thallium vapor (after a suggestion by Jevons[2]) failed, it was surmised that samarium *ion*, Sm^{+++}, with a ground state ^6H, was perhaps more suitable for the study of such an effect because of the ease with which the ions could be had at high concentrations in solution. But the examination of the Raman spectrum (Fig. 1*A*) of a dilute solution of samarium nitrate (about 8 percent) revealed no new features except the nitrate frequency at 1047 cm^{-1}, the water bands and the characteristic fluorescent bands of samarium with intensity maxima at λλ5600, 5950, 6030 and 6390A (Fig. 2). When the investigation was, however, repeated at a higher concentration (about 40 percent), three entirely new bands made their appearance (Fig. 1*B*). Since even the Raman band of water arising from λ4047A is here completely absent due to the strong absorption of the solution for this radiation, the three new bands have to be ascribed to the incident radiation λ4358A. As no trace of these bands is seen in the dilute solution, it follows first, that the new bands do not arise from fluorescence and second, that they appear because of the increased concentration of samarium ions in solution. No such effect arising from an increased concentration of the nitrate ion in the case of potassium nitrate, for instance, could be observed. The new bands therefore with approximate frequency shifts of 950, 680 and 2770 cm^{-1} at their maxima from the incident line λ4358A have been *tentatively* ascribed to an electronic Raman effect in samarium ions. A calculation

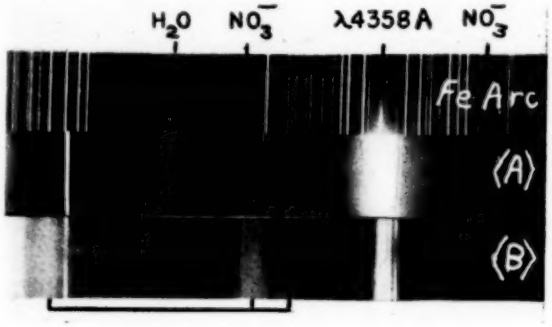

FIG. 1.

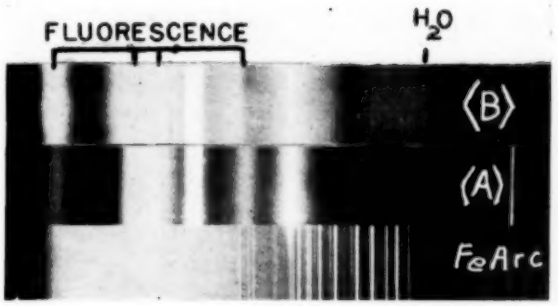

FIG. 2.

of the frequency separation between $^6H_{5/2}$ and $^6H_{7/2}$ from Goudsmit's formula yields a value 932 cm^{-1}, which agrees fairly satisfactorily with the observed Raman shift of 950 cm^{-1}; the band at 2770 cm^{-1} requires the assumption of a transition from $^6H_{7/2}$ to $^6H_{11/2}$. The width of these bands, however, remains to be explained. An analysis of the absorption spectrum of samarium salts at low temperatures by Spedding and Bear[3] has shown that the ground level $^6H_{5/2}$ is a close group of about five levels with a total separation of about 250 cm^{-1}. Frank[4] concludes that the ground level can split only into a doublet in an ionic field with cubic symmetry; this possibly explains the existence of another band at 680 cm^{-1}. If it is assumed that the larger number of low lying levels postulated by Spedding and Bear is correct, Van Vleck[5] sees no other possibility of explaining them but as an interaction between vibration and electronic states. The sharpness of these close levels observed at such low temperatures as 20°K−78°K cannot obtain at ordinary temperatures and to this cause is traced the bandlike appearance of what ought to have been Raman "lines." The provisional explanation here put forth for the new bands observed at greater concentration of samarium ions is being tested with other salts of samarium and europium. In Fig. 2 the Raman band of water in concentrated solution (*B*) is seen to be widened out as compared with the same band in dilute solution (*A*); this possibly arises from an interaction of the ionic fields with the OH bond.

Another very interesting feature in Fig. 1 is the rotational wing accompanying the incident radiation λ4358A present only in the Raman spectrum of the dilute solution and entirely absent in the spectrum of the concentrated solution brought about by an enormous increase of fluid viscosity. Attention to this point has been recently drawn by Raman and Venkateswaran[6] who have worked with four liquids of increasing viscosity; we have in the present instance a case where the increase in concentration of the same solution suppresses the wings on account of enhanced viscosity.

L. SIBAIYA
H. S. VENKATARAMIAH

Department of Physics,
University of Mysore,
Central College, Bangalore,
June 26, 1939.

[1] F. Rasetti, N. Cimento, **7**, 261 (1930).
[2] Jevons, *Report on Band-Spectra of Diatomic Molecules* (1932), p. 246.
[3] F. H. Spedding and R. S. Bear, Phys. Rev. **46**, 975 (1934).
[4] A. Frank, Phys. Rev. **48**, 765 (1935).
[5] J. H. Van Vleck, J. Phys. Chem. **41**, 67 (1937).
[6] Raman and Venkateswaran, Nature **143**, 798 (1939).

The Fission of Protactinium*

(Element 91)

In view of the demonstration of the fission of $_{92}$U and $_{90}$Th, it has seemed desirable to investigate the possible fission of the intermediate element $_{91}$Pa, atomic weight 231.

This rare element was available in the form of a preparation of 130 mg containing 9.0 percent Pa_2O_5, 90 percent ZrO_2, and 1 percent HfO_2.[1] The sample was carefully purified to remove all possible natural radioactive isotopes by separation of Ba, La, Pb, Bi, Th and U.

Observation of fission

In order to observe the fissions directly, 0.06 mg of Pa was deposited on one electrode of an ionization chamber connected to a linear amplifier. By using high collecting fields and increasing the resolving power of the amplifier-recording system, it was easily possible to detect ionization pulses due to fissions of Pa over the background produced by 80,000 alpha-particles per second.

Figure 1 is an oscillograph record showing a typical Pa fission having an amplitude about twice the background, the sample being bombarded with fast neutrons from the cyclotron. Comparative tests were made of Pa, Th and U with Be^9+H^1 neutrons from the cyclotron, Rn-Be neutrons, Ra-Be photoneutrons and D-D neutrons (through the kindness of W. H. Zinn), as well as thermal neutrons. Pa does not undergo fission with thermal neutrons or photoneutrons. Its threshold is probably ~1 Mev, appreciably lower than Th, and possibly about the same as for the fast neutron fission of U. That no fissions are observed with slow neutrons shows that the observed fissions were not due to U impurity. The number of fissions observed from a given amount of Pa is approximately thirty to forty times the number observed from the same amount of Th when irradiated with fast neutrons from the cyclotron (about 2 Mev maximum under the conditions used), hence a Th impurity could not have been responsible for the fissions observed with Pa. No marked difference was observed in the magnitude of the ionization pulses from Th, Pa and U.

Chemical separation of fission products

By chemical separation it was possible to determine two of the fission products of Pa to be radioactive Rb and Cs, with half-periods of 18′ and 30′, respectively. Eight milligrams of Pa were bombarded with fast neutrons directly behind the Be target in the cyclotron for 45 minutes. The irradiated preparation was melted with about 50 mg each of $RbHSO_4$ and $CsHSO_4$, the melt dissolved in water, and the Pa-Zr precipitated hot with a slight excess of ammonia. To the filtrate a few mg of Sr, Ba and Zr salts were added and precipitated with H_2SO_4 and NH_3, respectively. The $Zr(OH)_4$ took down any possible trace of Pa. In the second filtrate, containing only alkali metals, the Rb was precipitated by sodium-bitartrate and the Cs filtrate evaporated to dryness.

The counter measurements were begun 40 minutes after irradiation. The Rb-Cs separation was checked spectroscopically after the counts were made. The initial activities of the two products were about 200 and 400 counts per minute, respectively above background.

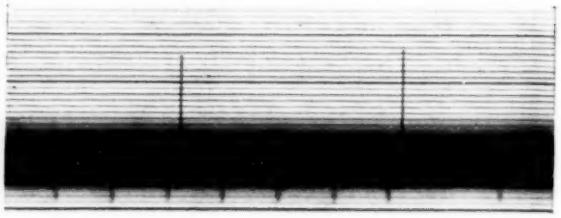

FIG. 1.

Parallel experiments with Th and U, and data from the literature[2–4] indicate that the same Rb and Cs periods result from the fission of these elements.

	$_{90}$Th	$_{91}$Pa	$_{92}$U
Rb	17′	18′	19′
Cs	33′	30′	30′

The relative intensities are in first approximation also equal.

The presence of Cs (30 minutes) and Rb (18 minutes) in approximately equal ratios among the fission products of U, Pa and Th, emphasizes a considerable similarity in the decay of the excited fission fragments from the three processes. This is particularly striking when compared to the great differences between the natural decay series of these elements. The data strongly suggest that while the distribution of types of fission fragments may be statistical,[5] nevertheless a considerable fraction of the fragments follow certain preferred disintegration processes, at least after the initial more or less instantaneous emission of neutrons, beta- and gamma-rays.

$_{91}Pa^{231}$ is of particular interest since it is formed from $_{92}U^{235}$ (actino-uranium) by the emission of one alpha- and one beta-particle. Since $_{92}U^{235}$ is commonly believed to be the isotope responsible for the slow neutron fission of U, it has been suggested from nuclear stability arguments[6] that Pa would have a low threshold and undergo fission with slow neutrons. These experiments show that this is not the case, and that while the threshold is lower than for $_{90}Th^{232}$, it is probably not far different from the threshold for U fission with fast neutrons. These results further emphasize the importance of direct experimental investigation of fission of the separated isotopes of U.

A. v. GROSSE

Department of Chemistry,
University of Chicago,
Chicago, Illinois.

E. T. BOOTH
J. R. DUNNING

Pupin Physics Laboratories,
Columbia University,
New York, New York,
July 15, 1939.

* Publication assisted by the Ernest Kempton Adams Fund for Physical Research of Columbia University.

[1] See A. v. Grosse, Science **80**, 2984 (1934).
[2] Hahn and Strassman, Naturwiss. **27**, 163 (1939).
[3] G. N. Glasoe and J. Steigman, Phys. Rev. **55**, 982 (1939).
[4] Heyn, Aten and Bakker, Nature **143**, 517 (1939); **143**, 679 (1939).
[5] N. Bohr, Phys. Rev. **55**, 418 (1939).
[6] John A. Wheeler, Princeton Meeting, June (1939).

Cross Section for the Reaction $H^2+H^2 \rightarrow H^1+H^3$ With a Gas Target

The absolute cross section for the reaction $H^2+H^2 \rightarrow H^1+H^3$ has been determined for bombarding energies from 50 to 390 electron kilovolts and with a target of *deuterium gas* at 0.1 mm pressure. The magnetically analyzed beam of deuterons enters the target chamber through a 12 cm long canal comprising 5 defining holes of diameters 1 to 2 mm, traverses the target volume, then passes through an exit canal into a Faraday cup. No foils are used. Satisfactory vacuum conditions in the accelerating tube and Faraday cup are maintained by fast pumps.

Results of preliminary measurements are tabulated below:

Bombarding Energy, E	50	100	200	330	390 Kev
Total Cross Section, $\sigma \times 10^{26}$	1.4	1.6	2.5	3.8	4.9 cm^2

Subject to the next paragraph, the probable error in each value is estimated at 6 to 8 percent due to all causes except contamination of the beam with light hydrogen. The extent of this contamination is not known, but the relative intensities of the mass 1, 2, 3, and 4 spots make it seem very unlikely that it exceeds 20 percent. The tabulated cross sections are low by the corresponding amount.

Recombination of the ions in the beam in passage through the target would result in a spuriously low beam measurement. The best experimental evidence on this point at present is that no change in beam current is observed when gas is admitted to the target chamber to raise the pressure from 0.005 mm to 0.1 mm. Since, however, about a minute is required for this operation and since it is difficult to maintain a steady, focused beam of the necessary intensity ($\sim 1\mu$a) through the narrow entrance canal, this observation is insensitive to changes of 10 to 20 percent.

A direct check on the recombination is now being made by passing the beam, after it emerges from the exit canal, between the faces of a deflecting electromagnet, then onto a solid deuterium target. If there are neutral deuterium atoms in the emerging beam, the corresponding proton yield from bombardment of the solid target will persist when the magnet is on.

J. A. Van Allen
A. Ellett
D. S. Bayley

Department of Physics,
State University of Iowa,
Iowa City, Iowa,
July 28, 1939.

The Normal Modes of Oscillation of the Long Chain Paraffin Hydrocarbons

E. J. Routh[1] describes a method of finding the normal modes of vibration of a finite chain of similar systems. The authors have applied this to the vibrations of the members of the methane series (C_nH_{2n+2}). The model assumed consisted of N carbon atoms lying in a plane with the tetrahedral angle between their bonds and the hydrogen atoms in planes through the carbon atoms at right angles to this plane, the angle between the C−H bonds was also assumed to be the tetrahedral angle. The Lagrangian was set up by considering only the nth CH_2 group and its interaction with the four neighboring CH_2 groups. The forces were assumed to be simple harmonic and along the lines joining the particles. The following interactions were considered: H_n-C_n, H_n-H_n', C_n-C_{n+1}, C_n-C_{n+2}, H_n-C_{n+1}, H_n-H_{n+2}, H_n-C_{n+2}, and $H_n-H'_{n+2}$ together with the analagous interactions of the other atoms. Here H_n and H_n' indicate the two hydrogens and C_n the carbon atoms of a single CH_2 group. The force constants K_1, K_3, K_4, K_6, K_8, K_9, K_{10}, K_{11}, respectively, are taken with the interactions above.

The elongations and Lagrangian were expressed in terms of X_n, Y_n, Z_n, x_n, y_n, z_n, x_n', y_n', z_n', the coordinates of the C, H, and H′, atoms so taken that a rotation through 180 degrees and a translation along the C−C bond leads to the coordinates of the adjacent CH_2 group. The equations of motion obtained from the Lagrangian are satisfied by solutions of the form $X_n=A\exp i(\omega t-\lambda n)$, $Y_n=B\exp i(\omega t-\lambda n)$, etc., where A, B, etc. are constant amplitudes, ω the angular velocity, and λ the phase angle between the vibration of successive CH_2 groups. There thus results a set of nine simultaneous linear equations in A, B, C, a, b, c, a', b', and c', which have solutions only if the ninth-order determinant of the coefficients vanishes. This ninth-order determinant can be diagonalized into one fifth- and one fourth-order determinant. These then form two equations in ω and λ whose roots in ω for a given λ give the nine fundamental frequencies of oscillation of the molecule.

Explicit solutions of these for ω in terms of λ, the dimensions and the force constants, cannot be obtained. However, roots may be obtained easily when $\lambda=0$ and $\lambda=\pi$ for in this case the fifth-order determinant further simplifies to a quadratic and a cubic and the fourth-order determinant to a cubic and a single root. For $\lambda=0$ there is one zero root and for $\lambda=\pi$ there are two corresponding to translations along the three coordinate axes.

In order to determine the dependence of the normal frequencies on the phase angle, λ, the authors have applied this work to the infra-red spectrum of undecane ($C_{11}H_{24}$) as measured in this laboratory with a NaCl prism spectrograph in the region from 1μ to 15μ. The potential energy constants K_1, K_3, K_4, K_8 were determined from four intense bands and it was assumed that K_{10} was equal to K_8 and that K_6, K_9, and K_{11} were negligible. Using the constants thus determined the normal frequencies for $\lambda=0$, 5, 45, 90, 135, 175, and 180 degrees were determined. It was found that the variation of the frequency with the phase was in most cases very slight and that accordingly the phase could be neglected. The nine fundamental frequencies, their overtones and simple combination bands were found to account for all of the observed bands within seven percent which is well within the accuracy of the constants and dimensions used.

A paper covering the development of the equations and the calculations will be presented later for publication.

L. H. Thomas
S. E. Whitcomb

Ohio State University,
Columbus, Ohio,
July 24, 1939.

[1] E. J. Routh, *Advanced Rigid Dynamics* (Macmillan, 1930), p. 276.

Deviation From the Coulomb Law for a Proton*

Fröhlich, Heitler and Kahn[1] have recently discussed the possibility of a short range deviation from Coulomb's law between an electron and a proton, on the basis of a quantized wave field theory of the mesotron type. They considered the interaction of the electron with the charge distribution about the proton. This is just the influence of the electric field of the electron on the self-energy that the proton has due to its interaction with the mesotron field. They concluded that it was possible to obtain a proton-electron force which became repulsive at short distances, and hoped thereby to account for some recently noted[2] anomalies in the fine structure of hydrogen. They emphasize, moreover, that it is for this essential to obtain a repulsion and not just a reduction of the Coulomb attraction as would, for example, result from merely spreading the charge of the proton over a small volume. I wish to point out, however, that despite the indications of the above calculations, no mesotron theory which is not radically different than those considered at present can possibly give such a short range repulsion between a proton and an electron.

According to such theories, the charge density about a proton has the form

$$\rho(\mathbf{r})=e(1-\alpha)\delta(\mathbf{r})+e\rho_1(\mathbf{r}), \tag{1}$$

where

$$\alpha=\int\rho_1(\mathbf{r})d\mathbf{r} \tag{2}$$

plays the role of the probability[3] that the proton is found dissociated into a neutron and a positive mesotron distributed about it with a charge density $e\rho_1(\mathbf{r})$. The proton-electron potential[4] is then given by

$$V(\mathbf{R})=-\frac{e^2}{R}(1-\alpha)-e\int d\mathbf{r}\rho_1(\mathbf{r})/(|\mathbf{R}-\mathbf{r}|), \tag{3}$$

so that, if as is the case with present field theoretic calculations, $\rho_1(\mathbf{r})$ is everywhere positive, one has the inequality

$$V(\mathbf{R})<-\frac{e^2}{R}(1-\alpha). \tag{4}$$

Thus $V(\mathbf{R})$ may become repulsive only if $\alpha>1$, an occurrence which is not physically sensible since the proton cannot be a neutron more than 100 percent of the time or give more of its charge to mesotrons than it has initially.

Although with their theory, α was divergent, the authors were able to obtain convergent integrals for $V(\mathbf{R})$, which could apparently be positive. To show how this is related to the value of α, we write

$$V(R)=-\frac{e^2}{R}+e^2\int_R^\infty 4\pi r^2\left\{\frac{1}{R}-\frac{1}{r}\right\}\rho_1(r)dr, \tag{5}$$

which follows from Eqs. (3) and (2) in the case of spherical symmetry. The integral converges for $R\neq 0$ if $\rho_1(r)$ is finite for $r\neq 0$. According to the scalar mesotron theory,[5]

$$\rho_1(r)\sim c/r^3 \quad \text{for} \quad r\to 0,$$

so that for $R\to 0$,

$$V(R)\sim-\frac{e^2}{R}+\frac{4\pi ce^2}{R}\log(b/R)-4\pi e^2c\left(\frac{1}{R}-\frac{1}{a}\right),$$

where a, b, c are positive constants. The logarithmic term seems to make $V(R)$ positive for small R. As we have seen above, however, this must mean that $\alpha>1$, in fact α is infinite, since $\rho_1(r)$ is not integrable. A similar result is obtained in the vector mesotron theory, where the divergence of α is stronger.

It must be noted, however, that even if the field theory were not divergent, one could erroneously obtain a value of α larger than unity in a perturbation calculation which stopped at a finite order (as the present calculations necessarily do!). One would simply need to make the coupling of the field with the heavy particles large enough.

One sees then how the apparent result that there may be a repulsion in the electron-proton interaction on the basis of current mesotron theories is based, not so much on the inherent inconsistencies of field theories, as on the nonconvergence of the perturbation methods used.

W. E. Lamb, Jr.

Columbia University,
New York, New York,
July 24, 1939.

* Publication assisted by the Ernest Kempton Adams Fund for Physical Research of Columbia University.

[1] H. Fröhlich, W. Heitler and B. Kahn, Proc. Roy. Soc. **171**, 269 (1939).

[2] See S. Pasternack, Phys. Rev. **54**, 1113 (1938).

[3] While the formalism does permit one to use the concept of a dissociation probability to the extent that it is in the text, it does not permit one to use this concept to deduce more complicated properties of the heavy particles such as magnetic moments. Several erroneous estimates involving α and the magnetic moment of a free mesotron have appeared in the literature.

[4] According to the field theories, Eq. (3) is valid if a polarization of the mesotron cloud by the electron is neglected, since no exchange terms enter due to the distinguishability of electron and mesotron.

[5] W. E. Lamb, Jr., and L. I. Schiff, Phys. Rev. **53**, 651 (1938).

Virtual State of He^5 and Meson Forces

Experiments by Staub and Stephens[1] on the breakup of He^5 indicate a virtual level of this nucleus at about 0.8 Mev. If, as seems probable, it is the ground state of He^5 that is involved here, and if one assumes that the general features of the Hartree method remain applicable, then the added neutron may be said to be in a P state. The states of the system that may result are a $^2P_{1/2}$ or a $^2P_{3/2}$.

Chief among the forces which might be expected to contribute to a splitting of this pair of states is the spin orbit force

$$V(r^{ij})(\boldsymbol{\sigma}^i\cdot\mathbf{r}^{ij})(\boldsymbol{\sigma}^j\cdot\mathbf{r}^{ij}), \tag{1}$$

which arises in the meson theory of nuclear forces; the observed value of the quadrupole moment of the deuteron indicates that terms such as (1) are an important part of the nuclear Hamiltonian.

A perturbation calculation was undertaken in order to estimate the amount of separation that this type of force might bring about. The use of perturbation theory in this apparently unfavorable case will be justified because higher order perturbations will be shown to fall off even though the perturbing potential is large.

The diagonal matrix elements of the term (1) were found to be equal for the states $^2P_{1/2}$ and $^2P_{3/2}$ without introducing explicitly the radial dependance of V and of the wave functions; hence to first order the splitting vanishes. The result was found to follow directly from the fact that the configuration being considered consists of a single particle outside a closed shell.

The treatment of the second-order splitting is simplified by the fact that there are no low lying states which combine with the two being considered. The configuration which gives rise to the $^2P_{1/2}$ and $^2P_{3/2}$ may be written S^4P. Other possible configurations are

(a) S^4D or S^4S', (b) S^4F,
(c) S^2P^2, (d) S^3DP or $S^3S'P$.
(e) S^2PD^2.

Here S' represents a neutron or proton in an excited S state. Of these possible intermediate states (a) and (c) are excluded on grounds of parity; (b) has a total angular momentum of 7/2 or 5/2 and is hence noncombining. We are therefore restricted to such states as (d), (e), etc., which have odd parity and whose reduction yields components with angular momentum 3/2 and 1/2. These configurations involve the breaking up of the alpha-particle core and therefore lie perhaps 15 or 20 Mev higher than the ground state. Considering then the magnitude of the energy denominators and the probable nonoverlapping of the wave functions, it seems certain that second and higher order perturbations will be greatly reduced.

Under these circumstances an important factor in the splitting of the two states will be the relativistic (Thomas) splitting described by Inglis and estimated by him for the case of Li^7. From the order of magnitude of his result, as well as from a rough evaluation, one would put the Thomas splitting for the ^2P state of He^5 at one or two hundred thousand volts. The second-order meson splitting should not exceed this magnitude. The sign of the resultant splitting will be more difficult to predict, since the Thomas doublet is inverted.[2]

I am indebted to Dr. Gaerttner for the information that new work at Pasadena on the structure of the He^5 level reveals it to be a doublet with a splitting of about 150–175 kev, in satisfactory agreement with theoretical expectations.

Thanks are due Professor J. R. Oppenheimer and Dr. L. I. Schiff for valuable suggestions and criticism.

S. M. DANCOFF

Department of Physics,
University of California,
Berkeley, California,
July 31, 1939.

[1] W. E. Stephens and H. Staub, Phys. Rev. **54**, 237 (1938).
[2] D. R. Inglis, Phys. Rev. **50**, 783 (1936).

Erratum: The Interaction of Configurations: $sd-p^2$

(Phys. Rev. **43**, 264 (1933))

An error was made in the evaluation of the radial integral R_e. Using the Rydberg constant ($R_\infty = 109{,}737$) and correcting this error we obtain $R_e = 21{,}387$ cm^{-1} in place of 25,620 cm^{-1}. The $sd\ ^1D$ is now calculated to be at -4272 cm^{-1} (observed -3592 cm^{-1}) from the center of sd configuration and $p^2\ ^1D$ at 21,353 cm^{-1}. The $sd\ ^1D$ appears below the ^3D (as before) due to the inclusion of the interconfiguration matrix elements, but the numerical agreement between theory and experiment is markedly improved. The $sd\ ^1D$ is now calculated to be 2234 cm^{-1} below ^3D (previously 4164 cm^{-1}) whereas it is observed at 1554 cm^{-1} below ^3D.

The writer is greatly indebted to Dr. J. P. Vinti for directing his attention to this integral.

R. F. BACHER

Cornell University,
Ithaca, New York,
July 21, 1939.

Erratum: The Paschen-Back Effect. VI. The Spectrum of Neon

(Phys. Rev. **56**, 54 (1939))

In the article with the above title the upper halves of Figs. 2*C* and 3*B* have been interchanged.

J. B. GREEN

Ohio State University,
Columbus, Ohio,

J. A. PEOPLES, JR.

Lehigh University,
Bethlehem, Pennsylvania,
July 17, 1939.

Velocity of Radio Waves in Air

(Phys. Rev. **55**, 1100 (1939))

In the discussion "Velocity of Radio Waves in Air" by G. H. Brown, which appeared in the "Letter to the Editor" section in the *Physical Review*, we note that the captions of Figs. 1 and 2 have been interchanged. Fig. 2 should read "Intensity pattern when the velocity is 80 percent of that of light."

G. H. BROWN

RCA Manufacturing Company,
Camden, New Jersey,
July 31, 1939.

THE AMERICAN INSTITUTE OF PHYSICS

INCORPORATED

ADMINISTRATIVE STAFF

HENRY A. BARTON, *Director*

MADELINE M. MITCHELL, *Publications Manager*

Office: 175 Fifth Avenue, New York, New York

JOURNALS

THE PHYSICAL REVIEW

REVIEWS OF MODERN PHYSICS

JOHN T. TATE, *Editor*

J. W. BUCHTA, *Assistant Editor*

JOURNAL OF APPLIED PHYSICS

ELMER HUTCHISSON, *Editor*

THE JOURNAL OF THE OPTICAL SOCIETY OF AMERICA

THE REVIEW OF SCIENTIFIC INSTRUMENTS

F. K. RICHTMYER, *Editor*

JOURNAL OF THE ACOUSTICAL SOCIETY OF AMERICA

FLOYD A. FIRESTONE, *Editor*

THE JOURNAL OF CHEMICAL PHYSICS

HAROLD C. UREY, *Editor*

JOSEPH E. MAYER, *Assistant Editor*

THE AMERICAN PHYSICS TEACHER

DUANE ROLLER, *Editor*

GOVERNING BOARD

For The American Physical Society:

JOHN T. TATE, *Chairman*
University of Minnesota

GEORGE B. PEGRAM, *Secretary*
Columbia University

KARL T. COMPTON
Massachusetts Institute of Technology

For The Optical Society of America:

E. C. CRITTENDEN
National Bureau of Standards

A. C. HARDY
Massachusetts Institute of Technology

W. B. RAYTON
Bausch & Lomb Optical Company

For The Acoustical Society of America:

FLOYD A. FIRESTONE
University of Michigan

HARVEY FLETCHER
Bell Telephone Laboratories

WALLACE WATERFALL
The Celotex Corporation

For The Society of Rheology:

WHEELER P. DAVEY
Pennsylvania State College

MELVIN MOONEY
United States Rubber Products, Inc.

R. L. PEEK, JR.
Bell Telephone Laboratories

For The American Association of Physics Teachers:

PAUL E. KLOPSTEG
Central Scientific Company

FREDERIC PALMER, JR.
Haverford College

F. K. RICHTMYER
Cornell University

The American Institute of Physics is a membership corporation of which five societies are the founding members. These five societies are the principal national societies devoted to pure and applied physics in America. Their names, and those of their representatives who form the Governing Board of the Institute, are given above. The principal work of the Institute is the publication of journals sponsored by the societies or by itself. The names and the editors of the journals are also listed above.

The broad purpose of the Institute is to represent, in all matters of wide or common interest, the five thousand or more members and subscribers associated with the Founder Societies and the journals. It aims to advance the science and profession of physics, and to promote cooperation between pure research, the applied sciences and the industries. To achieve these aims, it is greatly in need of an endowment and is empowered by law to administer grants and funds of any kind.

CONTENTS

PHYS. REV. 56 (1939) AUGUST 15

Induced Radioactivity in Cadmium and Indium . . . . . J. M. CORK AND J. L. LAWSON 291

X-Ray Resonance Absorption Lines in the Argon *K* Spectrum . . . . . LYMAN G. PARRATT 295

Nuclear Energy Levels in F^{19} . P. GERALD KRUGER, F. W. STALLMANN AND W. E. SCHOUPP 297

Nuclear Spin and Magnetic Moment of $_{13}Al^{27}$ . . . . . S. MILLMAN AND P. KUSCH 303

Absorption Spectrum of Aluminum Fluoride (AlF) . . . . . GEORGE D. ROCHESTER 305

On Diffraction and Radiation of Electromagnetic Waves . . . . . S. A. SCHELKUNOFF 308

Note: On Diffraction and Radiation of Electromagnetic Waves . J. A. STRATTON AND L. J. CHU 316

On the Surface States Associated with a Periodic Potential . . . . . WILLIAM SHOCKLEY 317

Use of Surface States to Explain Activated Adsorption . . . . . W. G. POLLARD 324

Structure of Liquid Potassium . . . . . NEWELL S. GINGRICH AND C. N. WALL 336

Forces in Molecules . . . . . R. P. FEYNMAN 340

Intercrystalline Thermal Currents as a Source of Internal Friction . . . . . R. H. RANDALL, F. C. ROSE AND C. ZENER 343

Dielectric Breakdown in Ionic Crystals . . . . . H. FRÖHLICH 349

Remarks on the Dielectric Breakdown . . . . . R. J. SEEGER AND E. TELLER 352

Normal Modes of Vibration of a Body-Centered Cubic Lattice . . . . PAUL CHARLES FINE 355

Theory of Magnetic Effects in the Plasma of an Arc . . . . . L. TONKS 360

Investigations of Ferromagnetic Impurities. I . . . F. W. CONSTANT AND J. M. FORMWALT 373

Letters to the Editor:

Showers Produced by Penetrating Rays . . . . . W. F. G. SWANN AND W. E. RAMSEY 378

Heavy Water Rochelle Salt . A. N. HOLDEN, G. T. KOHMAN, W. P. MASON AND S. O. MORGAN 378

Ferromagnetism in Austenite . . . . . L. P. TARASOV AND E. R. PARKER 379

He^3 in Helium . . . . . LUIS W. ALVAREZ AND ROBERT CORNOG 379

Coincidences Between Beta- and Gamma-Rays in Indium . . . . . LAWRENCE M. LANGER, ALLAN C. G. MITCHELL AND PAUL W. MCDANIEL 380

Raman Effect in Samarium Nitrate Solutions . . . . L. SIBAIYA AND H. S. VENKATARAMAIAH 381

Photon of Protactinium . . . . . A. V. GROSSE, E. T. BOOTH AND J. R. DUNNING 382

Cross Sections for the Reaction $H^2+H^2 \rightarrow H^1+H^3$ With a Gas Target . . . . . J. A. VAN ALLEN, A. ELLETT AND D. S. BAYLEY 383

Normal Modes of Oscillation of the Long Chain Paraffin Hydrocarbons . . . . . L. H. THOMAS AND S. E. WHITCOMB 383

Deviation From the Coulomb Law for a Proton . . . . . W. E. LAMB, JR. 384

Virtual State of He^2 and Meson Forces . . . . . S. M. DANCOFF 384

Erratum: The Interaction of Configurations: $sd-p^2$ . . . . . E. F. BACHER 385

Erratum: The Paschen-Back Effect. VI. The Spectrum of Neon . . . . . J. B. GREEN AND J. A. PEARLMAN, JR. 385

Velocity of Radio Waves in Air . . . . . G. H. BROWN 385

LANCASTER PRESS, INC., LANCASTER, PA.